CHALMERS

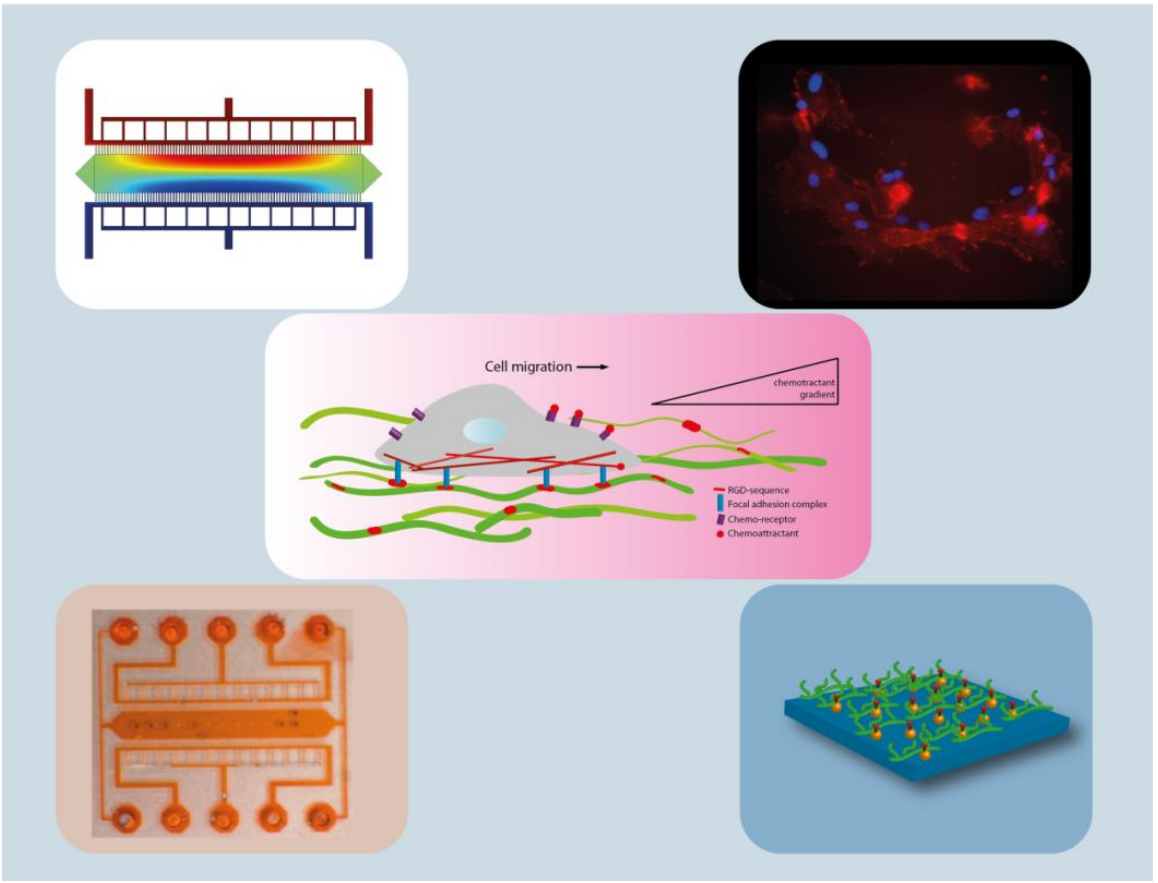

Development of a Microfluidic Platform for Cell Migration Studies along Gradients

Master of Science Thesis in the Master Degree Program Biotechnology

ELIN BERNSON

Department of Applied Physics

Division of Biological Physics

CHALMERS UNIVERSITY OF TECHNOLOGY

Gothenburg, Sweden, 2012

Development of a Microfluidic Platform for Cell Migration Studies along Gradients

ELIN BERNSON

Department of Applied Physics
Division of Biological Physics
CHALMERS UNIVERSITY OF TECHNOLOGY
Göteborg, Sweden 2012

Development of a Microfluidic Platform for Cell Migration Studies along Gradients

ELIN BERNSON

Department of Applied Physics

Division of Biological Physics

Chalmers University of Technology

SE-412 96 Göteborg

Sweden

Telephone +46 (0)31-772 1000

The research leading to these results has received funding from the EU 7th Framework Programme (FP7/2007-2013) under grant agreement NMP3-SL-2009-229294 NanoCARD, and from Vinnova under contract no: 2009-00227.

Cover: Collage of images presented in the report; upper left: simulation result of concentration profile in the developed microfluidic chip, lower left: the developed microfluidic chip, middle: sketch of cell migration, upper right: cells seeded in the developed microfluidic chip, lower right: sketch of surface modifications used in the project.

Chalmers Reproservice

Göteborg, Sweden 2012

Preface

When I studied my last year in high school, my biology teacher took the class to a company working with stem cells and tissue engineering. That evening, I told my parents that I would be a researcher in the stem cell field and work with tissue engineering in the future. After five years in the Biotechnology program at Chalmers, I have finally got the opportunity to perform research in the field during the writing of my Master's thesis. I believe that the area of tissue engineering and regenerative medicine holds a great potential for future medical applications. Already today there are products on the market and continuous research will hopefully lead to both improved and more easy to use products as well as new applications that can cure diseases to which we today are defenseless. The basic research that was performed in this thesis focused on fundamental cell processes, research that can generate better understanding of basic cell biology. This type of research is in my eyes very important in order to be able to control cells in cultures and for tissue engineering purposes.

During this thesis I have got an insight in how research is performed on an academic level and I have achieved experience in planning experiments and writing a scientific report. The thesis work has provided a deeper knowledge in a design and production process as well as in techniques as computer simulation, cell culturing, image analysis and surface chemistry. I also got the opportunity to design and present a poster based on my thesis project which was a great experience (the poster is included in the thesis as Appendix B).

There are some people that should be specially acknowledged. First I want to thank my supervisor Patric Wallin for all his exceptional guidance and coaching during the project. Patric has always taken his time to discuss questions or problems and been very helpful whenever help was needed. I also want to thank Francesco Mazzotta who put a lot of time and energy into producing the master for the microfluidic channel. The Au nanopatterned surfaces that played a big part in this project were kindly provided by Joachim Spat's group at Max Planck Institute for Intelligent Systems, Stuttgart, Germany. Vera Hirshfeld-Warneken and Yvonne Schön should be specially acknowledged for the production of the surfaces. The examiner of this thesis, Assoc. Prof. Julie Gold, I want to thank for her time and worthwhile comments during our discussions. It has been a privilege to work at the department of Applied Physics, and last I want to send a great thanks to the all the staff who made the days a little funnier!

Development of a Microfluidic Platform for Cell Migration Studies along Gradients

ELIN BERNSON
Department of Applied Physics
Division of Biological Physics
Chalmers University of Technology

Abstract

Cell migration is a cellular fate process essential for embryogenesis, tissue regeneration and wound healing. *In vivo* cell migration is promoted by soluble chemoattractants which stimulate cell movement, a process called chemotaxis. Migration is also controlled by cell surface interactions where focal adhesions are formed between cell integrins and attachment peptides, such as RGD (Arginine-Glycine-Aspartic acid), in the extra cellular matrix. It has been shown that by varying the spacing of these attachment peptides on a surface, cell attachment, spreading and focal adhesion formation can be controlled. In addition, varying the spacing of attachment peptides is known to influence cell fate processes, such as apoptosis, proliferation and differentiation.

The hypothesis that we wish to investigate is that cell migration is affected by the spacing of attachment peptides. The aim of this project was to design and evaluate an experimental system that could monitor cell migration as a function of attachment peptide spacing by simultaneously exposing cells to a chemotactic gradient in the culture media. Therefore, Au nano-patterned surfaces, with Au nano-dots placed in hexagonal pattern with an inter-particle spacing increasing gradient-wise from 65 to 85 nm over 6 mm (Spatz group, MPI Intelligent Systems, Stuttgart) were used to control the spacing of a cyclic RGD attachment peptide, which preferentially binds to the Au nano-dots. These surfaces were combined with a microfluidic network capable of generating stable concentration gradients of chemoattractants. The microfluidic chip was designed and evaluated with help of a finite element method (Comsol, Stockholm, Sweden) where simulations were performed and concentration gradient formation, velocity, and flow and shear stress profiles were investigated. Several designs were tested and parameters such as placing of inlets and outlets, channel dimensions and connections, were evaluated. Based on the simulation data, the final microfluidic chip was designed, produced and experimentally characterized.

The design is a diffusion based gradient generator capable of generating a concentration gradient inside a flow-free cell culture chamber, ensuring no shear stress induced migration in the main cell culture channel. The microfluidic chip was further combined with the cRGD functionalized surfaces and it was shown that Human Umbilical Vein Endothelial Cells (HUVECs) attach and spread and that they can be cultured in the system for at least five days during static conditions (longest time evaluated). The developed system is able to generate relevant concentration gradients of a chemoattractant factor, the microfluidic channel can be combined with an Au nano-dot patterned substrate, and cells can be cultured and monitored *in situ*, both in live and fixed/stained states, using bright field, phase contrast and fluorescent microscopy. In conclusion, a microfluidic platform was developed in which it is possible to study the effect of attachment peptide spacing during directed cell migration.

Keywords: Cell surface interactions, cRGD attachment peptide spacing, Microfluidics, Cell migration

Table of Contents

Introduction

Tissue regeneration is a fundamental process for life and is a very interesting area in biology. The term regeneration can be described as "*reproduction or reconstitution of a lost or injured part*" or "*a form of asexual reproduction*" (Stedman's medical dictionary). (1) As a result of better understanding the underlying processes of tissue regeneration new doors have opened within the fields of tissue engineering and regenerative medicine, techniques that aim to generate new tissue or organs using cells and biological promoting materials. (2) The cellular fate processes migration, differentiation, proliferation and apoptosis are important factors in tissue regeneration and therefore also in the field of tissue engineering and regenerative medicine. In a stem cell niche these processes are controlled and maintained by the surrounding environment consisting of the extracellular matrix (ECM), secreted factors and other niche cells. At the event of cell culturing this environment and thereby the control of the fate processes is lost. Cell surface interactions as well as the liquid composition around cells have been shown to play a major role in determining cellular fate. Migration is a key process *in vivo* for tissue formation where cells are guided to specific sites and is usually a response to an extracellular chemical signal leading to a process called chemotaxis. Cell migration has been stimulated *in vitro* with concentration gradients of chemoattractants, such as vascular endothelial growth factor (VEGF). (3) It has also been shown that the concentration, or spacing, between attachment peptides in the extracellular matrix (ECM) plays an important role for initial cell attachment and migration through the matrix. The cell binds to attachment peptides in the ECM with integrins and forms focal adhesion complexes. Through focal adhesions the cell senses the environment and signals from the binding event can lead to actions as cell migration. The amino acid sequence RGD (Arginine, Glycine, Aspartic acid) is a very important and well-studied binding site present in many molecules of the ECM, where it functions as a site for cell attachment as it is recognized and bound by integrins on the cell. Creating concentration gradients and present defined spacing of attachments molecules *in vitro* in a single model system would bring the opportunity to study the complexity of cell migration with respect of combinatorial effects from the surface chemistry and the strength of cell attachment in more detail.

A possibility to precisely control the liquid environment around cells is presented in the microfluidic technique. Microfluidic systems allow precise control of the microenvironment around cells and have the ability to form stable concentration gradients over a micrometer scale, very similar to *in vivo* dimensions. The technique can be used to form concentration gradients of chemoattractants, inducing cell migration. A technique that allows an exact control of surface patterning is the use of Au nanopatterned surfaces. These are surfaces patterned with Au nanoparticles with precisely controlled spacing. The technique is used to create controlled density gradients where the surfaces are functionalized by attaching molecules on top the Au nano dot gradient, creating a nanopatterned surface with a density gradient with chemical and structural properties. With the use of Au nanopatterned surfaces it is possible to create and control spacing and gradients of molecules, for example the cell attachment peptide cyclic RGD (cRGD), on a surface in a precise manner. Several experiments have been performed on cell attachment over varying RGD surface densities and distributions in which it has been concluded that cell attachment depends on RGD surface density. Responses as cell spreading, focal contact formation, cell survival and proliferation have also been investigated. (4) As focal contact formations depend on the RGD surface properties one can assume that also cell migration induced by a chemoattractant will be affected by the RGD spacing on the cell culture substrate,

something that to our knowledge has not been investigated before. A combination of the two techniques microfluidics and functionalized Au nanopatterned surfaces is able to bring new insights of the effect of the spacing of attachment peptides during migration along concentration gradients. This can be important for future research within the area of tissue engineering and regenerative medicine, as new insights in the cellular fate processes can lead to better understanding tissue regeneration.

Purpose

The aim of the thesis is to develop a platform where the effect of attachment molecule spacing on cell migration can be investigated. This will be done by designing and producing a microfluidic device that allows formation of a soluble gradient that is used to stimulate cell migration, in this study the design will focus on gradient formation of Vascular Endothelial Growth Factor (VEGF) that induces Human Umbilical Vein Endothelial Cell (HUVEC) migration. The formation of a concentration gradient will be investigated in simulations using the simulation software Comsol, and by experimentally analysis. The microfluidic design will be combined with a modified surface that presents a precise density gradient of attachment molecules to the cells. The purpose is to develop a surface modification that allows specific cell attachment of the attachment peptide cyclic RGD (cRGD). Cell culture experiments of HUVECs will be used to confirm the success of the microfluidic design and surface modifications.

Objective

The objective with the design that will be developed in this project is to study migration of HUVECs along a gradient of VEGF and investigate what effect different concentrations of cRGD have on the migration. The opportunity to study cell migration with cell-surface interactions and the effect of the spacing of attachment peptides in a microfluidic device is a novel design. This could be used to screen different types of cells and examine how they respond to different surface molecule concentrations and how cell migration can be promoted or inhibited. The results could be used for future applications such as coating of a tissue engineering scaffold where one could design areas enhancing migration of different types of cells, thereby guide different types of cells into the different areas of the scaffold.

Scope

The limited time of this thesis results in the following restrictions:

- Only one microfluidic chip device will be designed and produced
- Only cRGD will be used as attachment peptide
- Only Human umbilical cord endothelial cells (HUVECs) will be studied
- Amount of cell experiments depends on success of design fabrication and characterization

Background

1.1. Tissue engineering

Tissue engineering is an area of research that holds a great potential for future medical applications. Robert Langer, a world leading researcher in the field describes tissue engineering as it "*generally involves the use of materials and cells with the goal of trying to understand tissue function and some day enabling virtually any tissue or organ on the body to be made de novo*" (Robert Langer, (2)). The use of material has been investigated from various angles where both natural and artificial materials have been used for cell cultures and cells have been cultured in bioreactors with designs promoting cell growth and differentiation. One major challenge today lies in how all cells in a large cell culture should be nourished and how to remove waste products as there is a limit of how big cell constructs can be grown. That limit could be moved far up, if there was a technique to vascularize cell constructs in vitro, meaning to form a vascular system circulating nutrients as well as removing waste products. Several approaches to create vascularized tissue have been explored, for example to get endothelial cells to grow into scaffolds and form blood vessels, or to co-culture endothelial cells with for example fibroblasts or hepatocytes thereby get the endothelial cells to form new vessels within the cell culture. (2) Yet today there is no technique for vascularization that fully works. The possibility to study cellular fate processes as cell migration could be a key for finding new solutions to this obstacle and mimicking the *in vivo* environment would open up for new opportunities to study cell migration.

1.1.1. Angiogenesis

The presence of a vascular system in a tissue is essential for cell survival and function. The vascular system provides the tissue with oxygen, nutrition and transport of soluble factors as hormones to the cells and waste products away from the cells. (2) Vascularization is often required for tissue regeneration and *in vivo* angiogenesis is connected to the processes regeneration, proliferation and differentiation of a tissue or organ. Angiogenesis is the process where endothelial cells form vascular sprouts from already existing vessels. This process can be compared to vasculogenesis where a vascular network is formed without any existing vessels. (1) These two processes, vasculogenesis and angiogenesis, are driven by different growth factors where vasculogenesis is promoted by platelet derived growth factor (PDGF) and angiogenesis is induced by vascular endothelial growth factor (VEGF). At the event of tissue damage cells in the area send out the chemoattractant VEGF which binds to a VEGF receptor (VEGFR2) expressed principally on all endothelial cells causing the cells to proliferate, migrate and differentiate forming new sprouts thereby vascularizing the repaired tissue. The migration is directed towards the damage area as the concentration of the soluble VEGF is decreasing gradient-wise with the distance from that area, and cells can sense the gradient and migrate in that direction. (1) The concentration has a sever effect on cellular fate process and steers cells in certain directions. Cells that have migrated into an area of higher VEGF concentration will at some saturation concentration stop to migrate and start to proliferate instead. (5) *In vitro* this saturation concentration has been determined to be approximately 100 ng/ml. (6) Based on knowledge of angiogenesis *in vivo* VEGF has been proposed to be an important factor for vascularization of tissues in the field of tissue engineering and regenerative medicine and models for controlled release strategies of VEGF have been developed and investigated. (2)

1.1.2. The extracellular matrix

Cells *in vivo* are surrounded by a three dimensional matrix, called the extracellular matrix (ECM), consisting of a mixture of proteins, glycoproteins, glycosaminoglycans and small molecules (see fig. 1). The organization of the ECM is unique for each tissue and determines both the structural properties, such as elasticity, and functional properties, such as cell-extracellular signaling events, in a tissue. (2)The ECM molecules are produced and secreted by the cells themselves and the ECM is constantly undergoing changes and reconstructions.

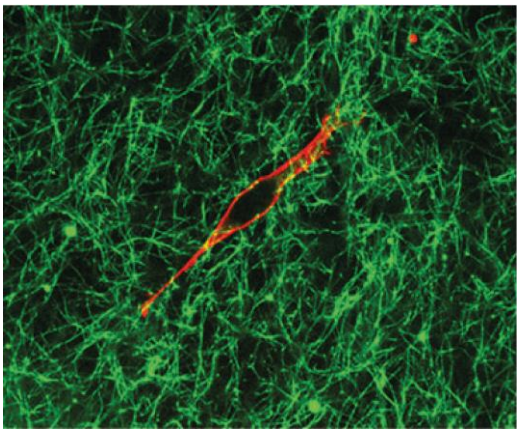

Figure 1. Cell (F-actin stained in red, MDA-MB-231 breast cancer cell) surrounded by ECM (fibronectin stained in green). Image: Nicolas O. Deakin, SUNY Upstate Medical University, Molecular biology of the cell, February 1, 2011; 22(3), cover page.

Cells adhere to the ECM through focal adhesions were transmembrane proteins, mainly integrins, attach to certain attachment peptide sequences present on the ECM molecules (fig. 2). Integrins are heterodimeric proteins that consist of α- and β-subunits, each existing in several conformations (18 and 8 respectively), giving a range of heterodimers (24) with varying affinities. (7) Of these 24 integrins, approximately 12 are shown to bind to the attachment peptide sequence Arginine-Glycine-Aspartic acid (RGD), being one of the broadest cell adhesion sequences in terms of integrin binding. (4) The RGD sequence is abundant on many ECM molecules, for example collagen, laminin and fibronectin. (2) The event of growth factor signaling, such as the one described above with VEGF, can affect the affinity of the integrin – attachment peptide binding. Byzova *et al.* (2000) showed that presence of VEGF in HUEVC culture stimulated the activation of the $\alpha_v\beta_3$ integrin, which plays an important role in angiogenesis. (8) When several integrins bind to attachment peptides such as RGD sequences they form so called focal adhesion complexes. Through focal adhesions cells signal in two ways: inside-out signaling and outside-in signaling. The first type is signaling from the inside of the cell that affects the extracellular attachment peptide – integrin binding such as changing the affinity of the binding, while the other signaling comes from the integrin binding event and sends signals into the cell. (4) Intracellular the focal adhesion is connected, through a signaling pathway, to the cytoskeleton where it plays an important role in cell-extracellular signaling and cell fate processes such as cell adhesion and migration. Cell migration is one example of outside-in signaling where actin filaments and new focal adhesions are formed in the protruding part of the cell, acting as anchoring points, while the actin filaments in the retracting part are degraded and reorganized. Focal adhesion are also important for cell survival as some cell types that are not able to adhere or form focal adhesions with the surrounding environment can undergo apoptosis. (4)

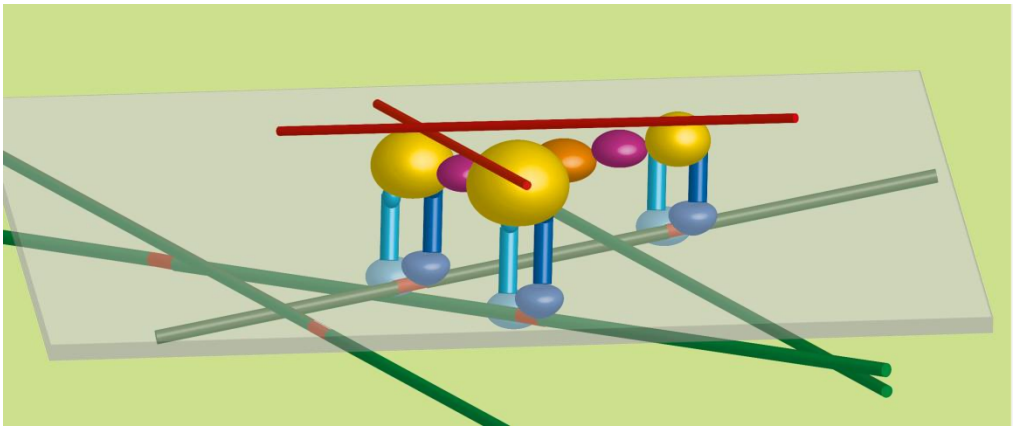

Figure 2. Cell integrins (blue) attach to an attachment peptide (red) at the ECM molecules (green). Together the interactions form a focal adhesion site as illustrated by the pink, yellow and orange bubbles (note that this is just a schematically sketch). Signaling occurs through the integrins to the cytoskeleton (outside-in signaling) and the other way around (inside-out signaling).

1.1.3. Cell migration

Cell migration is a key process for tissue formation and regeneration as well as for immune responses. The process depends on extracellular signals like chemicals released from other cells, adhesive molecules in the ECM or on other cells, or mechanical and structural features of the surrounding environment. A migrating cell goes through four stages; polarization, protrusion, traction and disassembly. Polarization occurs as a response to extracellular stimuli and the cell rearranges its organelles and cytoskeleton to form an anterior and a posterior part. At the protrusion stage the anterior part becomes the leading edge where focal adhesion are formed with the ECM attachment peptides and connected to the actin skeleton. This connection generates cell movement forward as the cytoskeleton is rearranged, called the protrusion stage. In the disassembling stage focal adhesions at the rear part are disassembled as new focal adhesions are formed at the leading edge. (7) An extracellular stimulus that induces cell migration is described in the angiogenesis process (section 1.1.1), where endothelial cells migrate in a concentration gradient of the chemoattractant VEGF, a process is called chemotaxis (fig. 3). (1) In order for a cell to migrate, it must sense the concentrations gradient applied over it as the chemo-receptors on the cell binds to the chemoattractant. This means that if a cell is approximately 30 µm long (between the leading and retracting part) the applied concentration must change enough over that distance for the cell to sense a difference in concentration. It has been shown that endothelial cells need a gradient steepness of at least 14 ng of change in concentration per mm in order to migrate in the direction of high concentration *in vitro*. (3) It is important that a migrating cell has attachment peptides to form focal adhesion with. It has been shown by Maheshwari *et al.* (2000) that random fibroblast cell migration depends on attachment peptide (RGD) density where a higher density generated both larger amount of cells attached and higher migration speed, indicating that RGD peptide density is highly affecting cell migration events. (9)

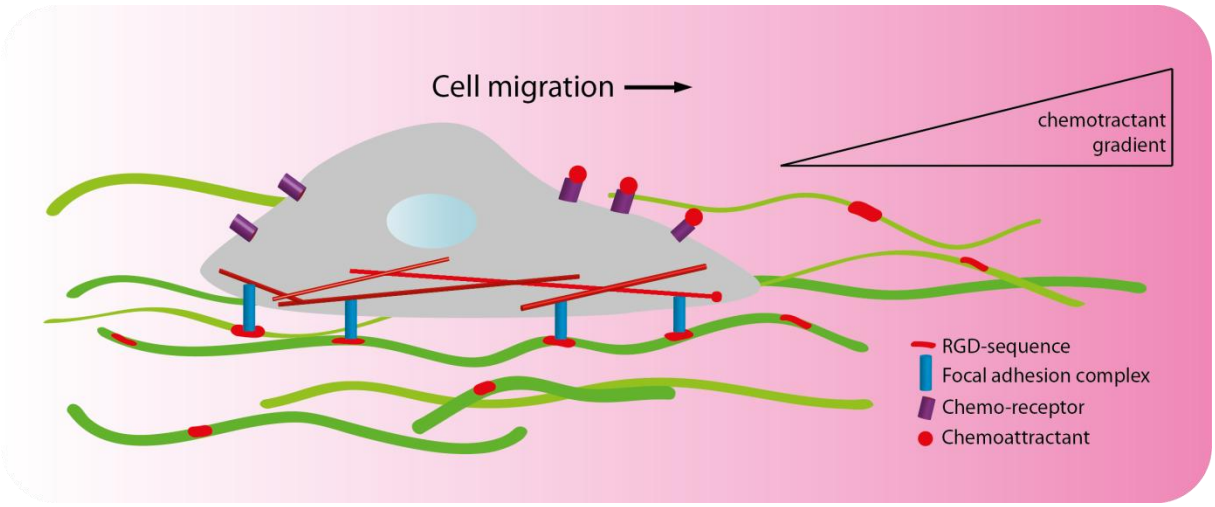

Figure 3. Chemotaxis, cell migration due to chemoattractant gradient, is induced by an applied concentration difference over the cell. Chemo-receptors bind to the chemoattractant and signal to the cell to migrate. Focal adhesions are formed between cell integrins and attachment peptides in the ECM and act as anchoring point during the migration.

1.1.4. HUVECs

Human Umbilical Vein Endothelial Cells (HUVECs) are used as model system in this project. The cells are taken from human umbilical veins, the cord from newborns. Endothelial cells express the VRGFR2 receptor and are known to migrate in VEGF gradients *in vivo* during angiogenesis and it has also been shown that HUVEC chemotaxis can be induced by a microfluidic generated VEGF gradient *in vitro*. (3) The cells express, amongst others, the $\alpha_v\beta_3$ integrin known to bind to RGD attachment peptides in the ECM. (10)

1.2. Microfluidics

Microfluidics is described as "*manipulation of fluids in channels with dimensions of tens of micrometers*" Whitesides (2006) and is a technique that has been emerging fast during the last decades. The technique has a wide area of use, from chemical reactions and information technology to biological analysis. (11) The fact that very small volumes are handled brings many advantages; among them that the flow is always laminar leading to the fact that mixing is only occurring by diffusion. As the volume of the channels is very small, little amounts of substrates are needed and there is low energy consumption leading to lowered overall costs. Changes in media and temperature can also be fast. The technique allows control of single cells and many cells can therefore be studied in parallel in the exact same environment. Some disadvantages are slow diffusive mixing and difficulties in handling very small volumes. (12) In this project microfluidic networks were used to generate a concentration gradient of a chemoattractant on the micrometer scale similar to the *in vivo* environment, which is able to induce cell migration.

1.2.1. Laminar flow

Fluid flows in smooth layers with no turbulence within the liquid leads to laminar flow. Due to shear forces, and the "no-slip condition" meaning that the flow velocity is zero at the walls, the flow velocity profile has a parabolic shape (see fig. 4). (13) Mathematically the velocity profile in the x-direction inside a pipe can be described as:

$$v_x = v_{max}\left[1 - \left(\frac{r}{R}\right)^2\right] \qquad \text{(Eq. 1)}$$

where R is the radius of the pipe, r the distance from the center of the pipe and v_{max} the maximum velocity. (13) The equation tells us that at the walls of the pipe, where r=R, the velocity will be zero. This creates so called "dead zones" at the walls of the pipe where there is no flow, an important property to consider in experimental applications. One way of determining whether a flow will be laminar or turbulent is using the dimensionless Reynold's number which is the ratio between the inertial forces and the viscous forces. For flow in a pipe Reynold's number can be calculated as

$$Re = \frac{Dv_{avg}}{\nu} \qquad \text{(Eq. 2)}$$

where D is the pipe diameter, v_{avg} the average velocity and ν the kinematic viscosity. For Re<2300 the flow is said to be laminar and for Re>3000 the flow is fully turbulent. In microfluidics, due to the very small dimensions of the channels with low inertial forces, the flow is always laminar. Studying equation 2, this result is indicative as D will be very small, generating a low Reynold´s number. As the velocity profile of the flow is straight, mixing in the y-direction only occurs by diffusion. (13)

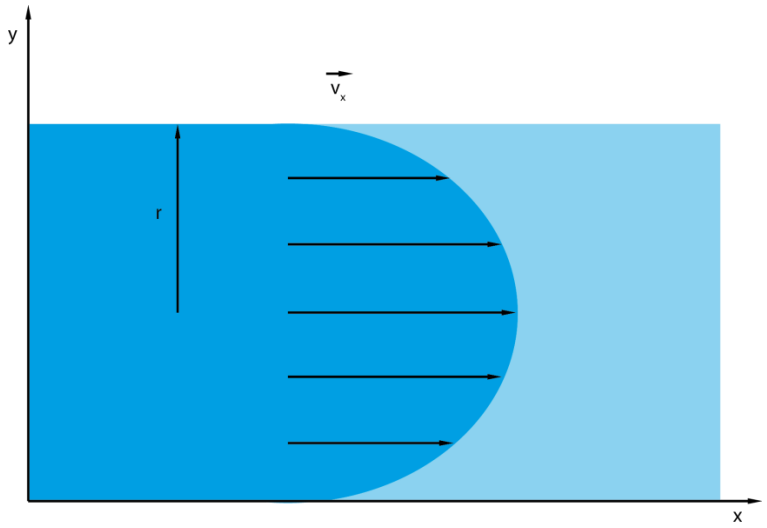

Figure 4. Laminar flow profile of flow in a pipe. The velocity profile has a parabolic shape with the highest velocity in the middle of the channel and no velocity at the walls.

1.2.2. Shear stress

Shear stress in laminar flow is the result of the microscopic actions of the molecules between the layers in the flow, and can be described as

$$\tau = \mu \frac{dv}{dy} \qquad \text{(Eq. 3)}$$

where μ is the dynamic viscosity of the liquid, v the fluid velocity and y the position in y-direction. This means that the shear stress profile is proportional to the derivative of the velocity profile. Studying fig. 4, we see that the change in velocity is largest at the outer ends of the flow profile and zero at the site of maximum velocity and hence the shear stress profile will look as illustrated in fig. 5. (13) When an object is placed on a surface with flow above, it will be subjected to shear stress. For a hemispherical object, for example a cell, the shear stress applied on it can be approximated as

$$\tau = \frac{3\mu U}{2a} \qquad \text{(Eq. 4)}$$

where U is the fluid velocity, μ is the fluid viscosity, and a is the average diameter of the object. (14) It has been shown that shear stress can affect cell migration and shear stresses at 3dyn/cm^2 or higher can drive migration in the direction of flow. (15) It is therefore important to consider shear stress when designing microfluidic devices for cell applications.

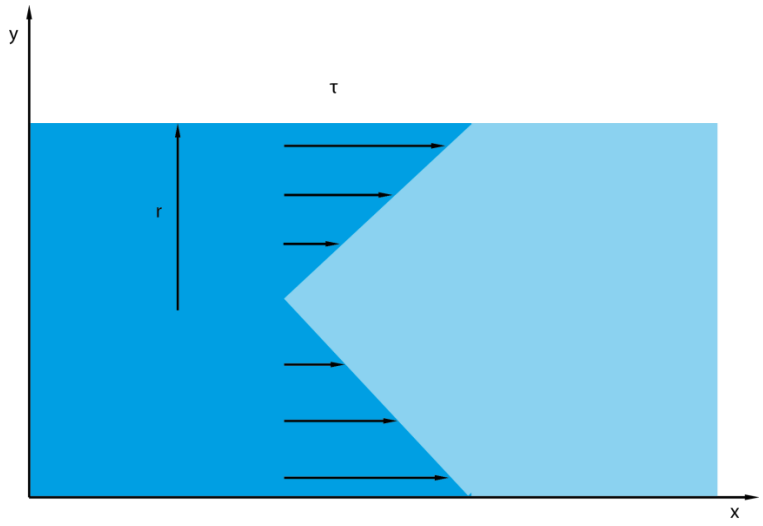

Figure 5. Shear stress profile of flow in a pipe. The shear stress is largest at the walls and smallest in the middle of the pipe.

1.2.3. Concentration gradient formation

As mentioned earlier mixing only occurs through diffusion in laminar flow. In microfluidics this means that concentration gradients over extremely short distances can be achieved by flowing two streams with different concentrations next to each other. One example is shown in fig. 6, which demonstrates a microfluidic device that was designed to generate a concentration gradient over a distance on the cellular level. (16) This property makes it possible to mimic the *in vivo* environment with gradients at the µm scale. For the purpose of generating a concentration gradient it is important to consider what molecule should be investigated as the rate of diffusion diverges between different molecules depending on their molecular weight. The diffusion coefficient for a molecule A trough a substance B is calculated as:

$$D_{AB} = \frac{0{,}001858T^{3/2}\left[\frac{1}{M_A}+\frac{1}{M_B}\right]^{1/2}}{P\sigma_{AB}^2\Omega_D} \qquad \text{(Eq. 5)}$$

Where T is the absolute temperature in Kelvin, M_A, M_B are the molecular weights of A and B respectively, P is the absolute pressure, σ_{AB} is the collision diameter and Ω_D is the collision integral for molecular diffusion. (13) Equation 5 shows that a smaller molecule diffuses faster than a larger molecule. In this project, the aim was to achieve a concentration gradient of the molecule VEGF inside a microfluidic device. The diffusion coefficient for VEGF is D=9,4e-7 m^2/s. (17)

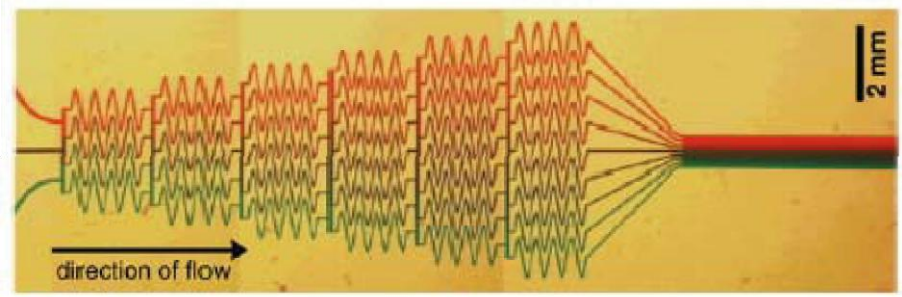

Figure 6. A diffusion-based concentration gradeint generating microfluidic device. (16)

1.2.4. Multiphysics simulation software

Computer simulations of problems including different physical phenomena are a useful tool during product design and development. In this project the software COMSOL Multiphysics © (Stockholm, Sweden) was used to solve multiphysic problems of fluid flow and transport of diluted species, where the transport of diluted species is dependent on the velocity distribution. The software is compatible with the design software AutoCAD© (Autodesk, San Rafael, CA, USA) and drawings can be imported directly into COMSOL Multiphysics ©. From defined input data, as for this project velocity, start concentration and other boundary conditions, and defined what physics to solve for the software uses the finite element method (FEM) to solve for partial differential equations (PDEs) or ordinary differential equations (ODEs). (18) The FEM solver divides the continuous system into a finite number of elements with finite size, a process called discretization. For each element a solution is obtained and all these solutions together return a solution of the system. Depending on how the discretization is defined, solutions will be calculated in different nodes or points of the discrete elements. The generation of discrete elements is done in the software by setting a mesh of which the size and shape can be defined by the user. A smaller mesh size means that the solver generates a solution with higher resolution than with a mesh with larger mesh size. Solving a model with a coarser mesh decreases the solution time, but when using a coarse mesh, it is important to conclude mesh independency. This means that it has to be excluded that a finer mesh would generate a systematically different solution than the one obtained with the coarse mesh size.

Simulations can be performed in either stationary or time dependent conditions. A stationary solver only returns the final, stationary solution while a time dependent solver returns solutions for all different time points. It is the physical problem that determines which solver to use. For the physics of fluid flow, for example, only the stable, stationary solution might be of interest, while the solution for transport of diluted species is interesting in a time dependent manner. The solution time is usually much longer when using a time dependent solver, why a stationary solver often is chosen if possible.

1.2.5. Production of a microfluidic chip

Production of microfluidic devices is today quite straight forward using photolithography and soft-lithography, illustrated in fig. 7. For the photolithography process, a positive Cr mask where the channel structure is transparent is first produced from a drawing of the desired structure using electron beam lithography. SU-8 photoresist is spin coated on a wafer and the thickness of the SU-8 can be controlled by the spinning speed and acceleration, as well as different SU-8 compositions that differ in viscosity. The wafer is then exposed to UV-light through a mask, which selectively exposes a pattern of the photoresist. The UV light cross-links the SU-8 and upon addition of an organic solution, a so called developer, the non-exposed photoresist becomes soluble while the exposed SU-8 is insoluble. This allows only the un-exposed photoresist to be removed by the developer. To solidify the remaining photoresist the wafer is hard baked at 150°C for approximately 5 minutes. (Protocol developed at the department of Applied Physics, Chalmers, Sweden)

The wafer, also called master, can now be used in a soft-lithography process where microfluidic channels are produced. The pre-polymer poly-di-methyl siloxane (PDMS) is molded onto the master, and after curing it is peeled off and bonded onto a glass cover slip. The microfluidic channels are created due to the pattern created from the master (see fig. 9) and one master can be reused to produce many channels. PDMS has many advantageous properties for the purpose

of microfluidics; it can be molded into microfluidic structures with integrated fluidic valves, it is transparent, non-autofluorescent, biocompatible and permeable to gas. Some drawbacks are that the permeability can lead to that the sample is dried out as water vapor is diffusing which makes it important to control the humidity of sample, and small hydrophobic molecules can absorb to the PDMS and disturb the sample results. PDMS monomers can also contaminate the samples. (12)

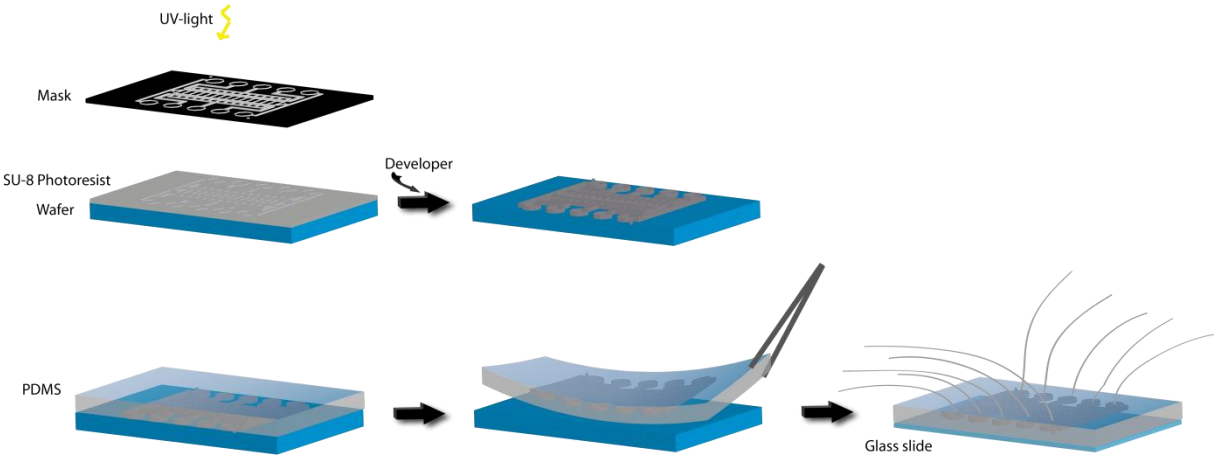

Figure 7. Microfluidic channel production. A master is produced using a photolithography method where the channel structure is formed on a wafer. PDMS is molded onto the channel structure and is, after curing, peeled off and placed onto a glass slide. Tubing can now be connected to the channels to apply flow.

1.3. Au nanopatterned surfaces

The technique of patterning a surface with Au nanoparticles and produce so called Au nanopatterned surfaces opens up for new possibilities in precisely controlling surface densities. Using the combined techniques of diblock copolymer self-assembly and electron beam lithographic techniques the Au nanoparticles are self-assembling on a glass surface in a hexagonal pattern, and the spacing between the particles can be very precisely controlled by controlling concentrations and speed of the included dip-coating process. It is also possible to produce Au nanopatterned surface that has particles put down in a gradient manner, ranging from a higher to a lower inter-particle spacing. SEM images of a glass surface with a gradient spacing of Au nanoparticles are shown in fig. 8. The Au nanoparticles can subsequently be functionalized with a molecule of interest, creating a surface with precisely controlled molecular density. Hirschfeld-Warneken *et al.* (2008) produced a functionalized surface with defined attachment peptide spacing, on which cell attachment as a function of attachment peptide spacing was studied. The attachment peptide they used was a cRGD peptide which is bound by the cell integrins. The size of the Au nanoparticles is 5-8 nm and a cell integrin is approximately 8-12 nm, which allows only one integrin to bind to each functionalized Au nanoparticle. (19)

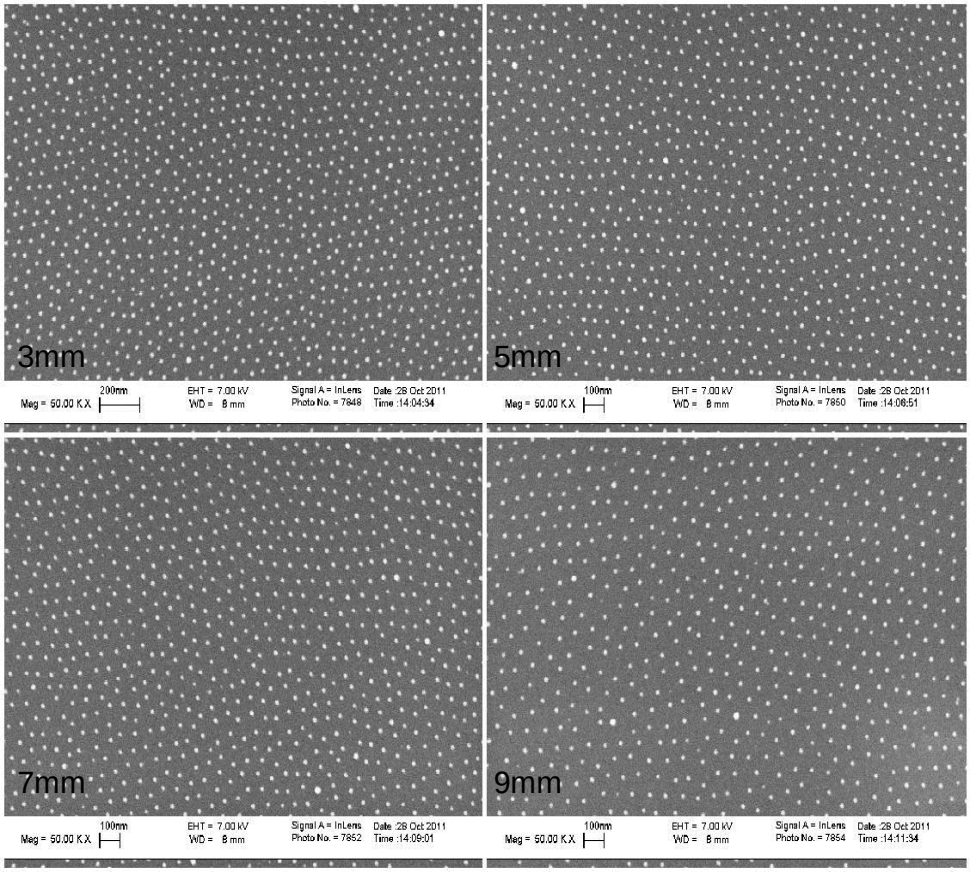

Figure 8. SEM image of a Au nanopatterned surface. This surface has a spacing changing in a gradient manner from 65-85 nm and the four images are taken at four positions from the dipping edge of the surface.

1.3.1. The peptide sequence RGD as a biomaterial coating

As mentioned earlier, attachment peptides are key factors in cell fate processes such as attachment and migration. Attempts to coat surfaces of implants or tissue engineered constructs for medical applications with ECM molecules containing attachment peptides, such as laminin, fibronectin or collagen, have been to increase and facilitate cell attachment. Using these large protein structures has some disadvantages as they have to be isolated directly from organisms which can lead to infections and increased immune response at the site of implantation. It is also difficult to control the amount of attachment sites at these surfaces. (4) The possibility to immobilize RGD peptides directly on a surface and thereby being able to precisely control the spacing would open up for a new generation of surface modified implants or tissue engineered constructs.

1.3.2. Impact of ligand spacing on cell migration and attachment

Au nanopatterned surfaces can be used to investigate the effect of attachment peptide spacing on cell fate processes. Arnold *et al.* (2004) showed that integrin clustering and activation is affected by attachment peptide spacing and concluded that a spacing of 58-73 nm of attachment peptides is a universal length scale for this process as spacing above 73 nm decreased focal adhesion formation. The study was performed on osteoblasts, fibroblasts and melanocytes. (19) Spreading behavior of cells is also affected by attachment peptide spacing where a spacing of 58 nm promotes good adhesion and spreading while cells on 110 nm spacing remain round and do not spread. (20) Migration in the direction of adhesion cues, so called haptotaxis, was shown to occur in attachment peptide spacing gradients where the spacing changed at least 15 nm per 1 mm in the direction towards areas with lower spacing. (21) It remains yet uninvestigated how attachment peptide spacing affects chemotactic cell migration.

1.3.3. Production process

Au nanopatterned surfaces are produced by a combination of diblock copolymer self-assembly and electron beam lithographic techniques. (22) When diblock copolymers such as polystyrene(x)-*block*-poly(2-vinylpyridine)(y) (PS(x)-*b*-P(2VP)(y)) are put in Toluene they self-assemble into uniform micelles where the soluble PS forms an outer layer around the less soluble P2VP. If mixed with an Au salt solution the metal ions are dissolved in the core of the micelles. A glass slide is then dip-coated in a solution with diblock copolymers containing Au particles in the core and a mono-micellar layer is formed at the surface. The substrate is treated with hydrogen plasma in order to remove remaining polymers. The treatment also deposits the Au particles firmly onto the glass surface. An Au nano-pattern is formed which is mechanically stabile and not removed from the surface by soft tissue or O_2 plasma treatment. The spacing of the Au nanopattern is controlled by the composition of the diblock copolymer micelles. (22) Another way of controlling the spacing is by altering the speed in the dip-coating process, an approach that can be used to produce surfaces with Au nanoparticle spacing changing in a gradient manner.

1.3.4. Surface functionalization

Au nanopatterned surfaces can be functionalized to promote cell adhesion by coating them with an attachment peptide. For attachment peptide experiments the cyclic RGD (cRGD) peptide is commonly used. It is bound, amongst others, by the $\alpha_v\beta_3$ integrin present on endothelial cells. (9) cRGDs are stable against enzymatic degradation and would therefore be stable *in vivo*, a property that is very important for medical purposes. To be able to attach the peptide to the Au nanoparticles the cRGD peptide can be attached to a thiol group via a linker-sequence (fig. 9a)).

The thiol group binds to the Au nanoparticles by breaking its sulfur-hydrogen bond and forms a covalent bond between the sulfur and gold atom. The linker can consist of polyethylene glycol (PEG) which acts as a spacer that separates the cRGD peptide from the Au nanoparticle, the space depending on the length of the PEG-linker. Fig. 9b) illustrates schematically how the cRGD-thiol molecule binds to the Au nanoparticle.

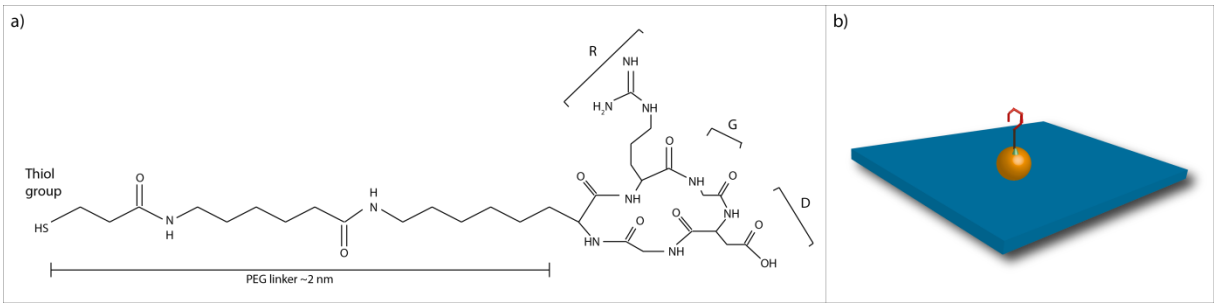

Figure 9. a) Molecular structure of thiol-cRGD peptide, with a PEG linker in between. b)Au nanoparticles are functionalized with cRGD. A thiol group (light blue) binds to the Au nanoparticle. The cRGD peptide (red) and the thiol group are separated by a PEG linker (brown).

1.3.5. Passivation with PLL-PEG

To passivate surfaces and prevent protein adsorption and cell attachment, Poly-L-lysine – Polyethylene glycol (PLL-PEG) can be used (fig. 10a)). The positively charged backbone chain PLL is interacting by Coulomb forces with a negatively charged surface, while he hydrophilic PEG chain grafted onto the PLL are sticking up, preventing protein adsorption and cell adhesion, see fig. 10b). The mechanism of passivation assumes steric hindrance of protein adsorption as the inert hydrated PEG layer shields the proteins from the surface. (23) A layer with PLL(20)-3,5-PEG(2) will have a wet thickness of about 5 nm. (23)

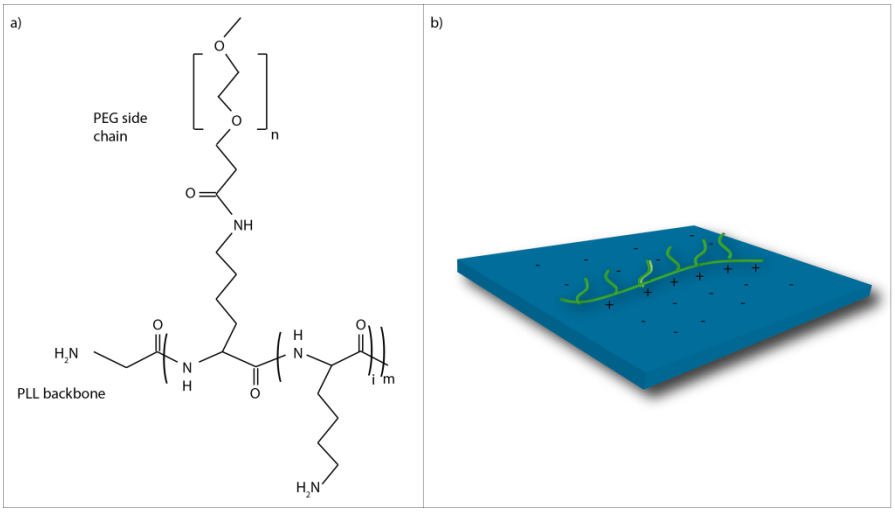

Figure 10. a) Molecular structure of PLL-PEG. b) The positively charged PLL main chain binds electrostatically to the negatively charged glass surface. The main chain is grafted with PEG side chains that form an inert layer shielding the surface from protein and cell attachment.

1.3.6. Protein adsorption experiments with QCM-D

Quartz Crystal Microbalance with Dissipation monitoring (QCM-D) is a technique that uses the piezoelectric property of quartz, which means that the material is deformed when exposed to an electrical potential. Upon an alternating potential, a quartz crystal will oscillate with a frequency described as:

$$f_n = \frac{nv_q}{2*t_q} = \frac{nv_q}{\lambda} \qquad \text{(Eq. 6)}$$

Where n is the overtone number (1, 3, 5 etc.), t_q is the thickness of the quartz crystal, v_q is the speed of sound in quartz (3340 m/s) and λ is the wavelength. From the equation we can see that the frequency of the oscillation depends on the thickness of the crystal in an inverted proportional manner. When an adsorbed layer is coupled to the surface of a crystal the frequency changes as a function of the adsorbed mass. By exposing the sample to a liquid containing a molecule that is absorbed onto the surface, the mass of the crystal will increase, and thereby the frequency decreases. The QCM-D instrument collects the frequency data and gives an indication of whether a solution adsorbs onto a surface or not. (24) This technique can therefore be used to monitor changes in adsorbed material on a surface, for example in the case of an interaction between the surface and the injected compound. In this project, QCM-D technique was used to validate surface adsorption of PLL-PEG and passivation of the same. The D in QCM-D stands for dissipation. By measuring the energy dissipation, properties of the density of the adsorbed layer can be achieved. A rigid layer would result in lower energy dissipation than a soft, for example hydrated layer. (25) In summary, with the ability to measure both frequency shifts and dissipation shifts at a surface exposed to continuous flow, it is possible to study surface adsorption and interactions.

2. Materials and Methods

2.1. Design and simulation of a microfluidic platform

The microfluidic platform was designed in AutoCAD© (Autodesk, San Rafael, CA, USA). It was evaluated with a finite element model (Comsol, Stockholm, Sweden) where equations for fluid flow and transport of diluted species were solved and generation of a concentration gradient simulated. Equations assumed stationary conditions for the fluid flow as:

$$\rho(\boldsymbol{u} * \nabla)\boldsymbol{u} = \nabla * \left[-p\boldsymbol{I} + \mu(\nabla\boldsymbol{u} + \nabla\boldsymbol{u})^T - \frac{2}{3}\mu(\nabla * \boldsymbol{u})\boldsymbol{I}\right] + \boldsymbol{F} \quad \text{(Eq. 7a))}$$

$$\nabla * (\rho\boldsymbol{u}) = 0 \quad \text{(Eq. 7b))}$$

For transport of diluted species, equations were used for either stationary conditions:

$$\nabla * \left(-D_j \nabla c_j\right) + \boldsymbol{u} * \nabla c_j = R_j \quad \text{(Eq. 8a))}$$

$$\boldsymbol{N}_j = -D_j \nabla c_j + \boldsymbol{u} c_j \quad \text{(Eq. 8b))}$$

Or for time dependent conditions:

$$\frac{\partial c_j}{\partial t} + \nabla * \left(-D_j \nabla c_j\right) + \boldsymbol{u} * \nabla c_j = R_j \quad \text{(Eq. 9a))}$$

$$\boldsymbol{N}_j = -D_j \nabla c_j + \boldsymbol{u} c_j \quad \text{(Eq. 9b))}$$

where ρ is the density, u is the velocity field, p is the pressure, I is the unit matrix , μ is the dynamic viscosity, F is the volume force field, D_j is the diffusion coefficient, c_j is the concentration, R_j is the reaction rate, N_j is the flux and t is the time.

Several models were tested were parameters such as width and height of the different channels, the number of and placing of inlets and outlets, as well as connections between inlets and outlets, source and sink channels, capillaries and cell culture chamber were evaluated. Data of concentration formation data was exported to Matlab where it was analyzed and plots were generated. The goal was to obtain a concentration gradient in the cell culture chamber (10000x2000 μm) that was steep enough (>14ng/ml/mm, see section 1.1.3) and uniform over at least 6 mm (the width of the functionalized Au-nanopatterned gradient).

2.2. Microfluidic chip production and characterization

2.2.1. Mask production

The chrome photo-mask was produced in the cleanroom at MC2 microtechnology and nanoscience by electron beam lithography (JEOL JBX-5DII, Japan).

2.2.2. Master production

The master was produced using the photolithographic method described in section 1.2.5. In short, a photoresist of SU-8 was spin coated onto a wafer, exposed to UV light through a mask and the un-exposed SU-8 removed by a developer. The sample was then hard baked to harden the remaining SU-8. In the microfluidic design the capillaries were lower than the rest of the channels. To obtain this difference in height he production process was divided in two steps; the first layer was produced using a mask with included capillaries, while the mask for the second layer did not include capillaries. The master could then be used repeatedly for PDMS molding.

2.2.3. PDMS chip production

Poly(dimethylsiloxane) (PDMS) prepolymer (Sylgard® 184, Dow Corning, Midland, MI) and curing agent were carefully mixed in a 10:1 ratio and placed in vacuum for 30 minutes. The solution was casted over the master, placed under vacuum for additional 30 minutes to remove all air bubbles and placed in oven at 90 °C for 2h. To separate the cured PDMS from the master it was peeled of, and inlets and outlets were created using a biopsy punch with inner diameter of 1,4 mm. The channel and a glass slide were activated in an air plasma cleaner (PDC-32G 18W Harrick Plasma, USA) for 30 s, after which they were put together and placed in oven (90 °C, 5 min).

To achieve a more stable PDMS layer over the inlets and outlets, a second layer of PDMS was produced on a flat master by the same method. Before attaching the PDMS channel and the glass slide, the second layer of PDMS was bonded on top of the microfluidic network containing PDMS part by air plasma activation, as described before.

To attach the PDMS channel over an Au nanopatterned surface, the same procure as described above was used, except from that the Au nanopatterned surface was activated for 5 min in the plasma cleaner. This was necessary to achieve proper bonding.

2.2.4. Microfluidic chip characterization and concentration gradient formation

Tubes (outer ø 1,6 mm, inner ø 0,5 mm) connected to pumps (milliGAT LF, GlobalFIA, Fow Island, WA, USA) were attached to the two inlets (see Appendix A). To the four outlets tubes were attached and allowed free out-flow. Cell chamber inlets were plugged to avoid flow through the cell culture chamber. To avoid bubble formation, the channel was first flushed with ethanol (70%) to pre-wet the channel, and then washed with milliQ.

To analyze gradient formation, color dye (Direct Red 80, Sigma-Aldrich, St. Louis, MO, USA) (concentration, dissolved in milliQ water) was introduced through inlet x and water through inlet x. Images was taken with stereomicroscope (MZ12.5, Leica, USA) and digital camera (Olympus C5060 Wide zoom) attached via the ocular lens ports (eyepiece). Flow rates between 1nl-1µl/s, controlled by software Labview program (developed by PhD. student Patric Wallin, Chalmers University of Technology), were investigated.

To analyze gradient concentration of a molecule similar in size to VEGF (MW = 38,2 kDa), FITC-CM-Dextran (MW = 40 kDa, 10 µM in PBS, Sigma-Aldrich, St. Louis, MO, USA) was introduced through the source channel. Imaging was done with an inverted fluorescent microscope (Axiovert 200, Zeiss, Germany) and CCD camera (AxioCam MRn, Zeiss, Germany) with 10x magnification, at flow rates 1, 4, 40 and 400 nl/s.

2.3. Au nanopatterned surfaces

Substrates were sterilized with ethanol and cleaned in air plasma for 30 s prior to surface modifications.

2.3.1. Surface functionalization with cRGD

Au nanopatterned substrates aimed for petri dish experiments were immersed in RGD-thiol-water solution (c[RGDFK(AXH-MPA)], 25 μmol) for 24 h (kindly provided by Benjamin Geiger, Weizman Institute, Israel). The substrates were then rinsed with milliQ water in a shaker for 24 h with several water exchanges.

Au nanopatterned substrates aimed for microfluidic experiments were modified after bonding the PDMS channel to the Au nanopatterned surface. Channels were filled with RGD-thiol-water solution (c[RGDFK(AXH-MPA)], 25 μmol) and incubated for 24 h. Channels were then flushed and then filled with milliQ water with several water exchanges for 24 h.

2.3.2. Surface passivation with PLL-PEG

The functionalized substrates were passivated by immersing them in a PLL-PEG solution (PLL(20)-g[3,5]-PEG(2), 10 μg/ml in PBS, SuSoS, Germany) for 1 h.

2.3.3. Validation of protein adsorption with QCM-D

To test the ability of PLL-PEG to inhibit protein adsorption, protein interaction studies were performed in QCM-D. Measurement was performed on an E4 Q-Sense instrument with four parallel flow modules that allowed four measurements to be done simultaneously. Four surfaces were prepared: 1) clean SiO_2, 2) fresh 55 nm spaced Au particles on SiO_2, 3) SiO_2 incubated with milliQ for 2 days, and 4) 55 nm spaced Au particles on SiO_2 functionalized with cRGD, prepared as in section 2.3.1. Samples were mounted in the instrument and flushed with PBS (50μl/min) 30 min (baseline stabilization) followed by PLL-PEG injection (50 μl/min) for 30 min. After PLL-PEG was immobilized the system was rinsed with PBS (45 min, 50 μl/min) and subsequently complete media with serum (10 % fetal bovine serum, Thermo Fisher Scientific, Waltham, USA) was injected for 10 min (50 μl/min). The flow was turned off for 1 h to let proteins adsorb and PBS was then injected to remove unbound proteins (2 h). Frequency shifts were normalized with division of the overtone number from baseline measurement. The 7^{th} overtone is shown in the result as the variation of frequency shifts was small between the overtone signals.

2.4. HUVEC culture

Human Umbilical Vein Endothelial Cells (HUVEC (S200-05n) (Pre-Screened) Cell Applications Inc., San Diego, USA) were cultured in Endothelial Cell Growth Medium (Cell Applications Inc., San Diego, USA). Cell media was exchanged every third day and cells were kept at 37°C in a humidified, 5 % CO_2 atmosphere.

2.4.1. Thawing

HUEVCs were kept in gas phase of liquid nitrogen tank until use. They were thawed fast under warm water and added to a flask with 7,5 ml pre-warmed Endothelial Cell Growth Medium.

2.4.2. Passaging

Cells were passaged before reaching 80 % confluency and only cells in passage 3-7 were used in the project. HUVECs were trypsinated with 1 ml Trypsin-EDTA 1X solution (L11-004, PAA, Pasching, Austria) for 1 min. The trypsination was then stopped with 3 ml trypsin inhibitor from Glycine max (T6414, Sigma-Aldrich, St. Louis, MO, USA).

2.4.3. Cell culture in petri dishes

Cells were seeded in petri dishes at a concentration of 100 000 cells/ml (1 ml) together with 3 ml Endothelial Cell Growth Medium. Dishes were incubated at 37°C in a humidified, 5 % CO_2 environment for 24 h.

2.4.4. Cell culture in microfluidic system

Cells were introduced through cell culture chamber inlets (see appendix 1) at high concentration (520 000 cells/ml). Channels were placed in 37°C, humidified, 5 % CO_2 environment for 24 h. Cell culture was performed under static conditions without flow in the channels, and to avoid dehydration of the channel additional cell media was placed as a droplet over the channel and a lid was placed above the sample. To examine cell viability for longer time, one channel was placed in 37°C, humidified, 5 % CO_2 environment for 5 days. Cells were investigated under microscope (DM4000 M, Leica, USA) every 24 h, after which a new droplet of cell media was placed on top of the channel.

2.5. Fluorescence microscopy

2.5.1. Cell staining

After 24 h substrates were washed with PBS and cells were fixed with 4 % formalin (Formalin 10 % phosphor-buffered pH 7.0, Oy Chemicals Ab, Haukipudas, Finland) for 30 min in 4°C. Substrates were washed with PBS and cells were stained with 6-diamidino-2-phenylindole (DAPI) (Excitation/Emission 364/454 nm when bound to DNA) for staining the nucleus and fluorescence-conjugated Phalloidin (Alexa Fluor® 555 Phalloidin, Excitation/Emission 555/565 nm, Life technologies, Carlsbad, CA, USA) for staining F-actin (DAPI 1:500, Phalloidin 1:200, 0,1 % Triton-X in PBS) in darkness for 30 min and then washed and stored in PBS.

2.5.2. Cell imaging

Stained cell samples were imaged in a fluorescent microscope (Axioplan 2, Zeiss, Germany) and images were taken with CCD camera (AxioCam, Zeiss, Germany) at 10x, 20x and 40x magnification.

Bright field microscope (DM4000 M, Leica, USA) was used to image live cells during cell culturing.

2.6. Image analysis

2.6.1. Quantitative data, ImageJ

Images of gradient formation with color dye (Direct Red 80) were analyzed in ImageJ. Intensity line profile plots (20 pixels wide) were generated over the length of the cell culture chamber every 1 mm. Plot values for each line were analyzed in Matlab and a relative intensity plot generated for each flow rate.

Concentration gradient formation of FITC-Dextran was imaged with 10x magnification, which did not cover the whole channel. Images taken at the middle of the channel with 1 mm in between were analyzed in ImageJ and line profile plots (100 pixels wide) made for each image. Plot values for each line were analyzed in Matlab and a relative intensity plot generated for flow rate 4 nl/s.

Images randomly taken with x10 magnification on stained cells were used to analyze number of cells attached onto a surface. The blue channel (DAPI) of the image was imported to ImageJ, it was made binary and the threshold was adjusted. Number of cells per image was measured using "particle analysis – nucleus counter" (particle size 20-600 pixels).

2.6.2. Qualitative data

Images of stained cells were adjusted for contrast and brightness individually in each color channel in AxioVision software (Rel 4.8, Zeiss, Germany), to increase the clarity of images. No further image processing was applied and images are representative for each surface.

2.7. Statistical analysis

Statistical data was analyzed using Welch's *t*-test (unequal sample sizes and unequal variance) with significance level p=0,05. The error is represented as the standard error of the mean for each population.

3. Results

3.1. Design and simulation of a microfluidic platform

The microfluidic chip consisted of a cell culture chamber in which the cells were cultured and where a concentration gradient should be formed. In order to avoid having the cells exposed to shear stress and thereby avoid shear stress induced migration, the channel was designed with a flow-free cell culture chamber. The cell culture chamber was instead connected to a source channel into which a high concentration of the molecule of interest was introduced, and sink channel that had a zero concentration of the molecule, see fig. 12. Between the source and sink channels and the cell culture chamber, smaller capillaries served as connecting channels, hydrodynamically decoupling the source and sink channels from the cell culture chamber. By applying flow in the source and sink channels a concentration gradient was generates in the cell culture chamber based solitary on diffusion. The coordinate system used for the channel is shown in fig. 12.

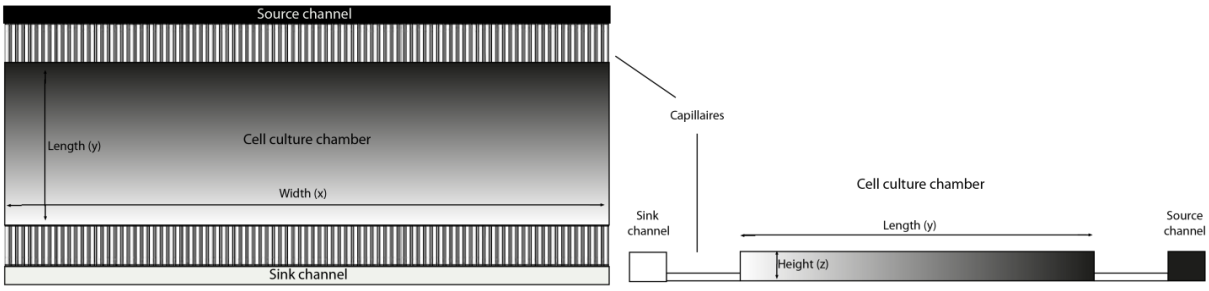

Figure 12. The microfluidic chip contained a cell culture chamber in which a concentration gradient was generated. In the source and sink channel there was flow of high and no concentration of the molecule of interest, and they were connected to the cell culture chamber through capillaries. The side view illustrates that the capillaries were lower than the rest of the channels. Coordinates and nomination of them (length, width and height) are illustrated and the terms will be used in the following text.

With the goal to generate a concentration gradient optimized for this study several models were created in AutoCAD and evaluated in Comsol. The results for fluid flow and transport of diluted species in different models were compared and parameters as width, height and length of channels, as well as the amount and placing of inlets and outlets were evaluated. Furthermore, the effect of flow rate on concentration gradient formation was investigated to find optimal flow rates. Flow rate in the text is specified as the flow rate applied at each inlet.

3.1.1. Flow of cell media through cell culture chamber

In the beginning of the design process, one idea was to apply a very slow flow of cell media directly to the cell culture chamber. The idea was to avoid problems of nourishment depletion in the cell culture chamber as the volume is much smaller than that of a petri dish or standard cell culture. As seen in fig. 13, even a very slow flow through the cell culture chamber disturbed the concentration gradient formation and the idea was therefore discarded.

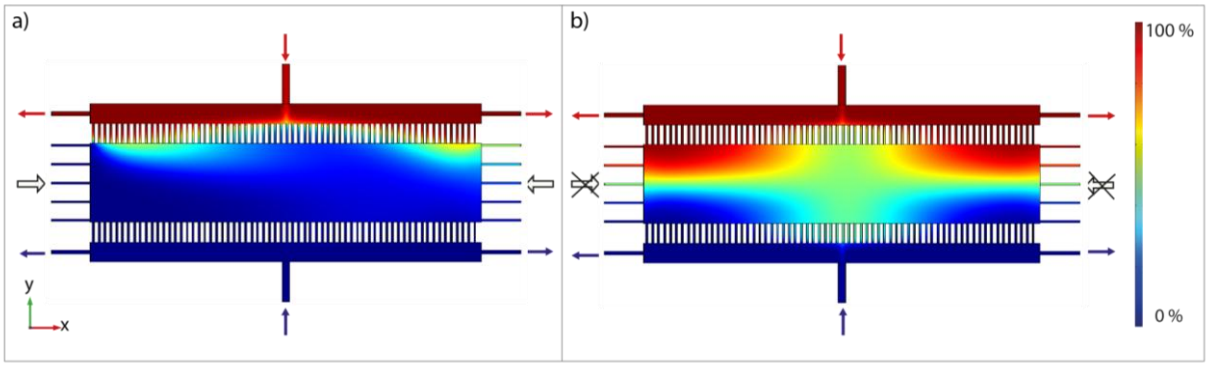

Figure 13. Concentration gradient formation: a) With a slow flow (0,02 nl/s, white arrows) through the cell culture chamber. As can be seen the gradient was completely disrupted by the flow as the concentration in the cell culture chamber is zero at almost all positions. b) Without flow through the cell culture chamber there is a concentration gradient formed in the cell culture chamber.

3.1.2. Placing of inlets and outlets

Several models were designed to test the effect of different inlet and outlet configurations on the gradient formation. The first model had only inlets at one side of the source and sink channels (fig. 14a)), and the gradient is only stable at one third of the cell culture chamber. The second model had instead inlets at both sides and an outlet in the middle (fig. 14b)). This generated a concentration gradient that was smeared in the center of the cell culture chamber. A third model was designed with two inlets that divided into several channels before they reached the source and sink channels, and three outlets. The idea was to achieve a more uniform concentration throughout the entire cell culture chamber but as can be seen in fig. 14c), the shape of the concentration gradient was not improved and unsatisfying in the center of the channel. To overcome this problem, the flow direction was reversed with inlets in the middle and outlets at the sides of the source and sink channel. As shown in fig. 14d) the concentration gradient was now much more evenly distributed throughout the cell culture chamber.

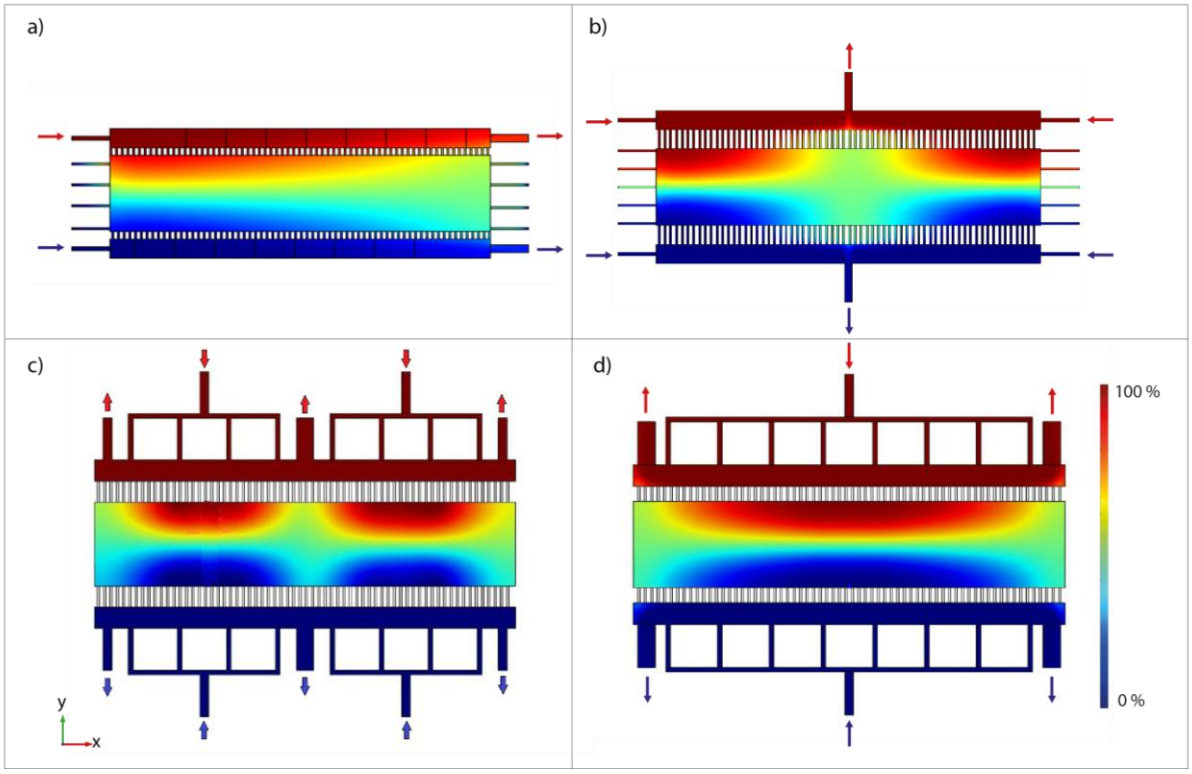

Figure 14. Concentration gradient formation in four different models that were tested. a) Inlet from one side generated a gradient that was stable in only one third of the channel. b), c) Concentration gradient was smeared as sites of outlet placement. d) When outlets were placed at the sides of the chip and with inlet channels dividing into several channels before reaching the source and sink channels, a uniform concentration gradient was generated in the middle of the cell culture chamber.

3.1.3. Length of cell culture chamber

The concentration gradient achieved in fig. 14d) was generally satisfying, but it was not uniform over a 6 mm width. Therefore, a longer model was designed with cell culture chamber dimensions of 14 000 x 2 000 x 200 µm (width x length x height). Comparison between a shorter and a longer model is shown in fig. 15a) and b) where the longer model generated a uniform gradient over a wider area than the shorter. The concentration gradient generated in the longer model was uniform over a 6 mm width (c) and d)), shown by plotting concentration gradient profiles at four positions inside the cell culture chamber, as indicated in the figure.

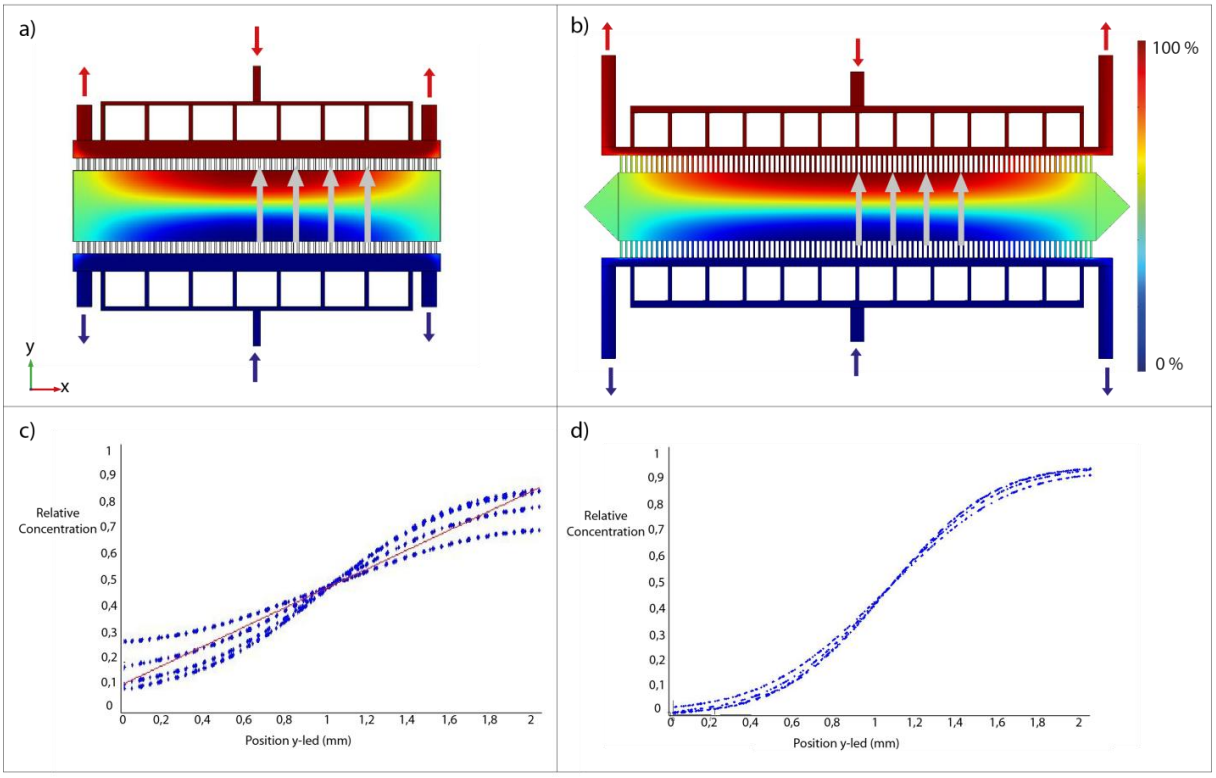

Figure 15. Cell culture chamber a) 10 000 µm and b) 14 000 µm wide. A wider cell culture chamber allowed for a uniform concentration gradient formation over a wider area. c) and d) shows concentration line profile plot at the center and 1, 2 and 3 mm from the center of the cell culture chamber. The difference in concentration between the center and 3 mm from the center was higher in (c) where it was approximately 20 % than in (d) where it is approximately 5 %.

3.1.4. Design of source and sink channels

Several inlets to the source and sink channels led to an increasing velocity at the ends of the sink and source channels as more liquid was added after each inlet. An additional model was developed (fig 16a)) were triangular shaped source and sink channels should equal out the increasing liquid volume and generate a uniform velocity within the channels. Simulation data showed that the concentration gradient formation was not improved in the new model compared to the model with equal sized source and sink channels as the concentration gradient still was lost at the ends of the cell culture chamber (see fig. 16).

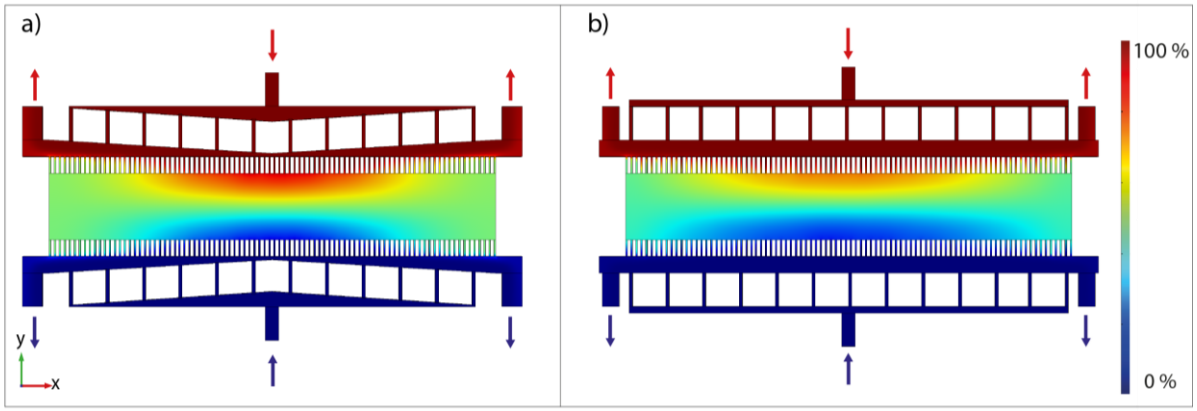

Figure 16. a) Triangular sink and source channels were compared to rectangular ones (b) to receive a more uniform velocity distribution in the source and sink channels. Concentration profiles in a) and b) shows that the gradient formation did not differ between the two models. The flow rate was 4 nl/s.

3.1.5. Size of source and sink channels

The size of the source and sink channel was investigated. Fig. 17 shows simulation data with a channel width of 500 µm and 250 µm respectively and it was concluded that a lower size of the source and sink channels generated a steeper concentration gradient. This means that a design like that in fig. 17b) would demand a lower flow rate and therefore less reagents to achieve a similar concentration gradient.

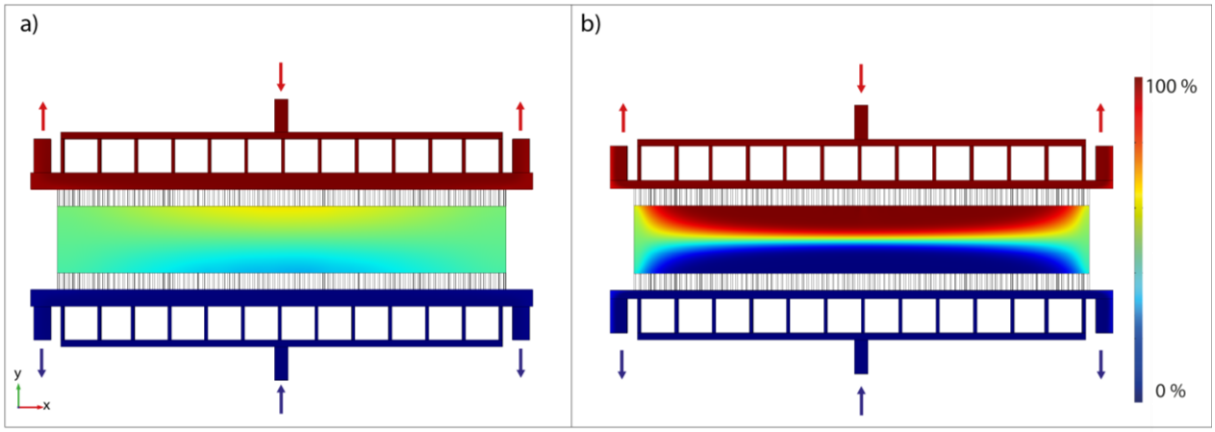

Figure 17. Same model with varying width of source and sink channels a) 500 µm and b) 250 µm. The simulation data shows that narrower source and sink channels generated a steeper concentration gradient. Flow rate was 20 nl/s.

3.1.6. Height of capillaries

From the source and sink channel molecules in the flowing liquid diffuse through the capillaries and into the cell culture chamber and form a gradient. Therefore, the size of the capillaries was an important factor as it limits the amount of diffusing molecules. In fig. 18 simulation data from two designs with capillary heights of 25 and 50 µm (a) and b) respectively) were compared. The data demonstrated that higher capillaries generated a steeper concentration gradient.

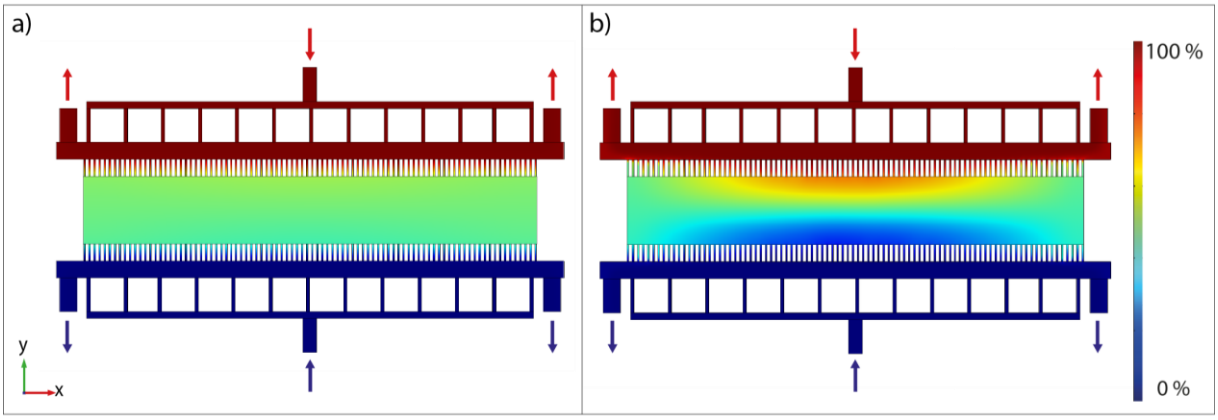

Figure 18. Same chip with height of capillaries a) 25 µm and b) 50 µm. Higher capillaries generated a steeper gradient.

3.1.7. Length of capillaries

The length of the capillaries was investigated by perform simulations on two models with 250 µm and 350 µm long capillaries, respectively. Simulation data, fig. 19, show that shorter capillaries generate a steeper gradient than longer capillaries.

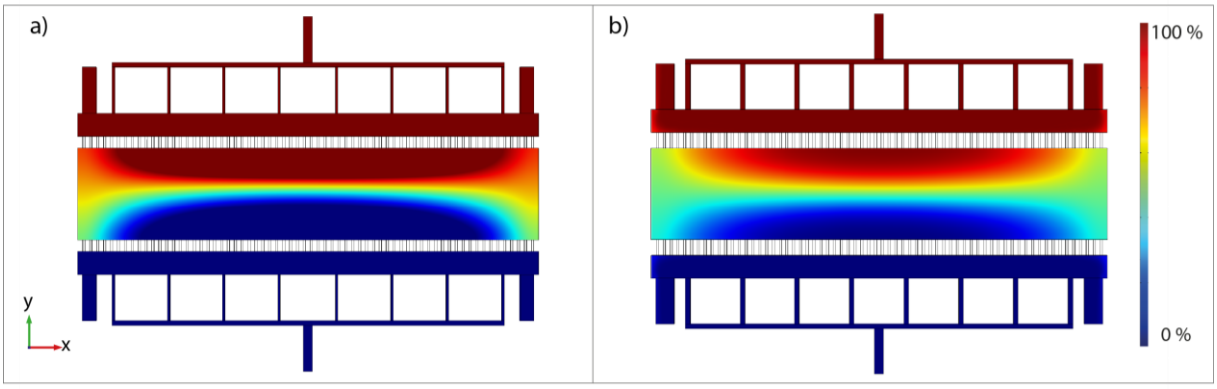

Figure 19. a) A model with 250 µm long capillaries generated a steeper gradient than a model with 350 µm long capillaries (b).

3.1.8. Effect of molecular weight on channel clearance

Due to variances in size, and thereby diffusion coefficients, different molecules in the cell media will be exchanged in the cell culture chamber at various rates. The total clearance of a molecule, meaning the time it takes to completely clear the cell culture chamber from the molecule, will therefore also depend on molecular weight. Simulations were performed for three different sized molecules; a small molecule, glucose, a medium sized molecule, VEGF, and a large molecule, hyaluronan, see table 1 for molecular weights and diffusion coefficients. At t=0, the cell culture chamber had an initial concentration of 100 % of the studied molecule, and flow with 0 % concentration (flow rate 4 nl/s) was applied in the source and sink channels. The small glucose molecule diffused fastest and was cleared after approximately 2,3 h (fig. 20a)), while it took 2,8 h for the medium sized VEGF to be cleared from the cell culture chamber (fig 20a) and b)). For the large hyaluronan molecule, it was never cleared over the time of the study (3,5 h) (fig 20c)).

Table 1. Molecular weights and diffusion coefficients for three different sized molecules.

Molecule	Molecular weight (Da)	Diffusion coefficient (m^2/s)
Glucose	180	$5{,}2*10^{-10}$ [1]
VEGF	38 200	$9{,}4*10^{-11}$ [2]
Hyaluronan	3 000 000	$5{,}6*10^{-14}$ [3]

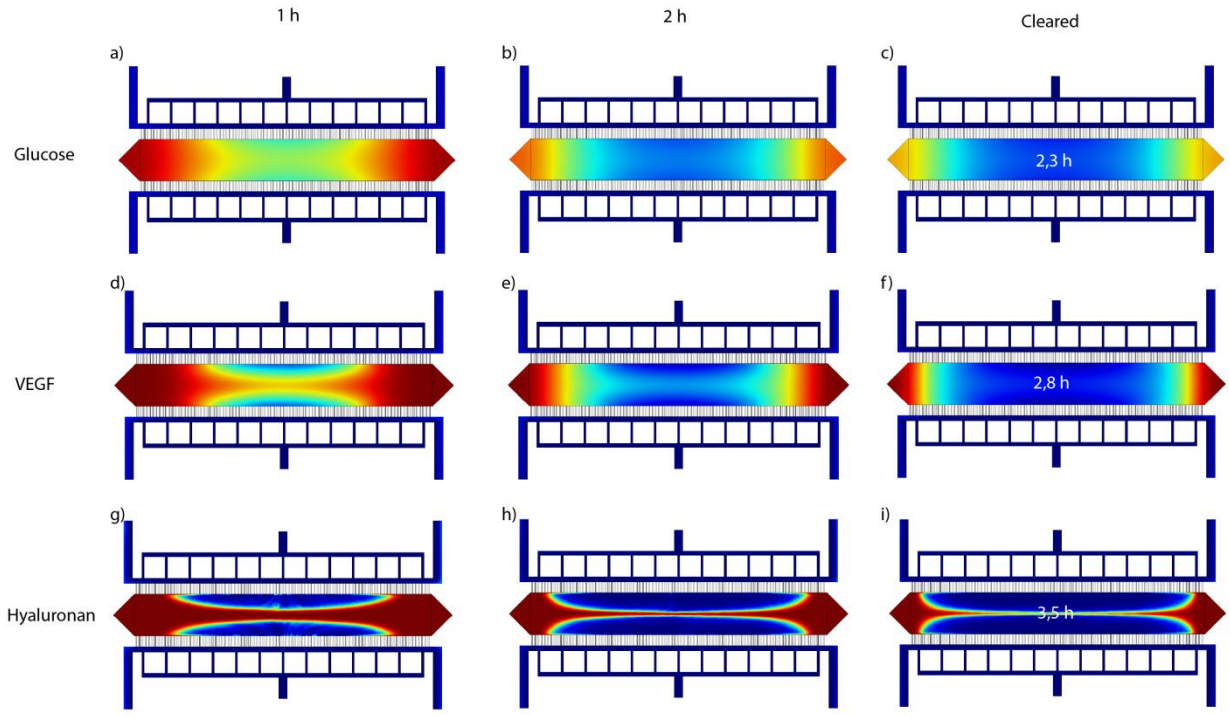

Figure 20. Simulation data for clearance of the cell culture chamber. a, b, c) The small molecule diffuse fast and was cleared from the chamber after 2,3 h. d, e, f) The larger molecule VEGF diffused slower and was cleared after 2,8 h. g, h, i) The very large molecule hyaluronan diffused very slow and was never cleared from the chamber even after 3,5 h.

[1] Grigoriev, I. S., and E. Z. Meylikhov (editors). 1991. Physical Values Handbook. EnergoAtomIzdat, Moscow

[2] Mac Gabhann, F., Popel, A.S. *Differential binding of VEGF isoforms to VEGF receptor 2 in the presence of neuropilin-1: a computational model.* Am. J. Physiol. Heart Circ. Physiol., 2005(288) pp. H2851-H2860.

[3] Garg, H.G., Hales, C.A. Chemistry and biology of hyaluronan, 2004, Elsevier.

3.1.9. The selected design

The design that was selected based on the various simulations and optimizations is shown in fig. 21 and 22. The dimensions of the cell culture chamber are 2000 x 14000 x 200 µm (length x width x height). The volume of the cell culture chamber is subsequently 5,6 µl. The capillaries were 50 µm high, 50 µm wide and 500 µm long and were placed 100 µm apart (see Appendix A for detailed drawing and dimensions). The inlets were divided into 13 channels, connecting to the source and sink channel, in order to generate an even concentration distribution throughout the cell culture chamber. In order to support the PDMS gel, thirteen pillars are placed 1000 µm apart in the cell cultured chamber. In addition to support they also provide guidelines for imaging of the cell culture chamber. The design also took care of all over dimensions so that three channels could be placed onto one master. Having multiple channels on one master simplifies the PDMS molding process as three channels could be produced in parallel.

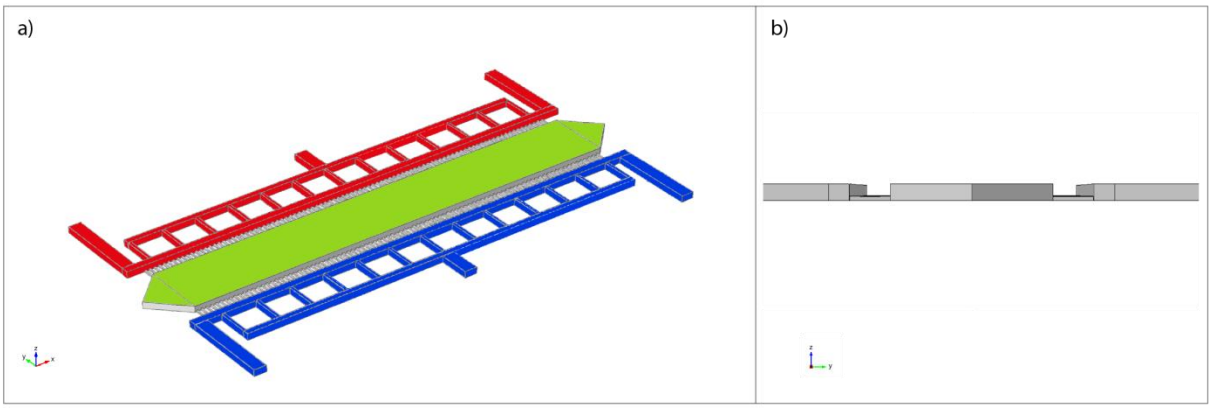

Figure 21. a) Microfluidic device seen from top. Red: source channel, blue: sink channel, green: cell culture chamber. b) Side view of the microfluidic device. The capillaries were lower than the rest of the channels.

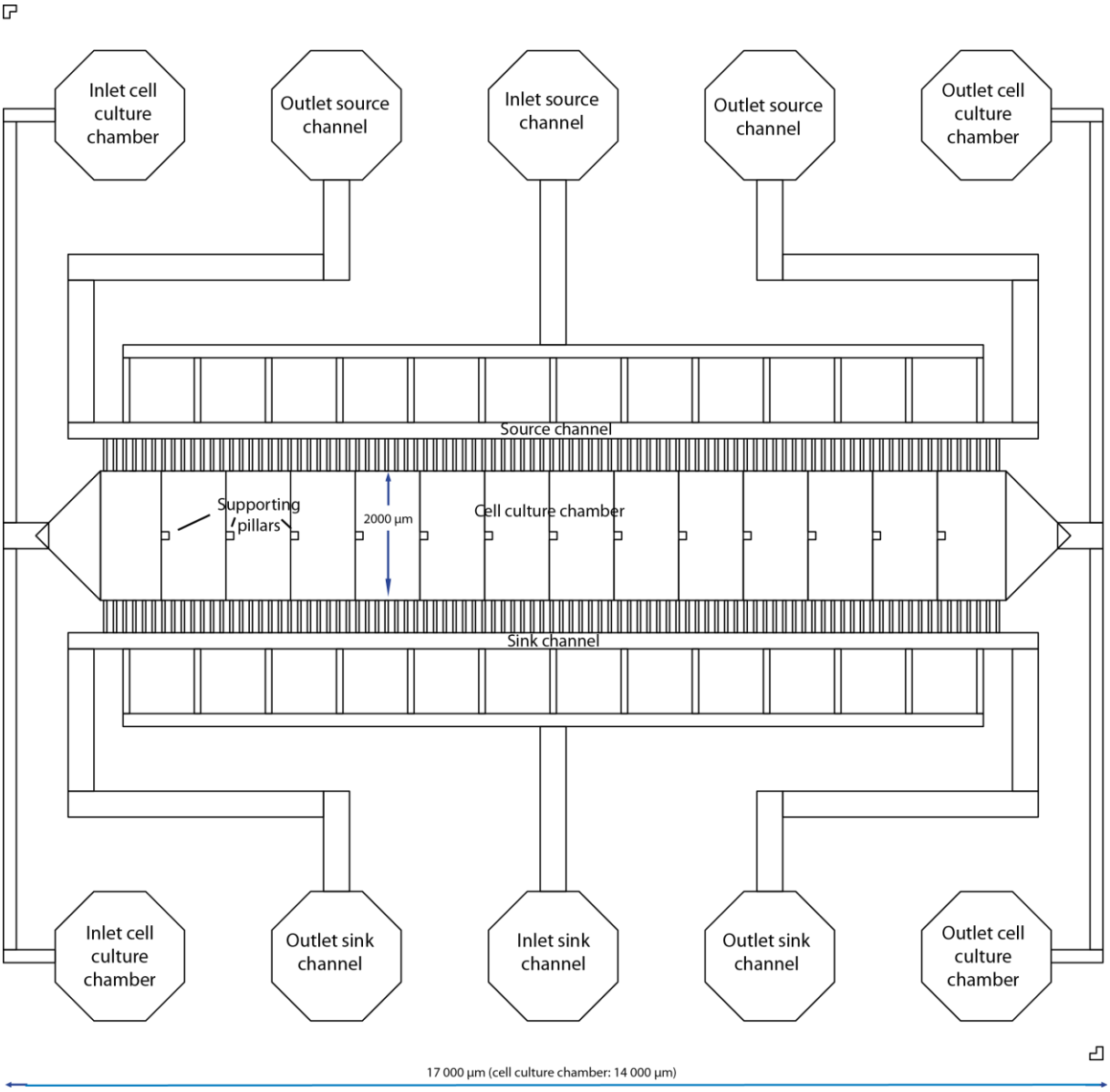

Figure 22. CAD-drawing containing the whole design of the microfluidic chip, including inlets and outlets. For a larger and more detailed image, see Appendix A.

3.1.10. Flow rate

The flow rate was one of the most important parameters when examining the formation of a concentration gradient. The impact of the flow rate can be seen in fig. 23 were simulation data of concentration gradient formation as a function of flow rate is shown for four different flow rates. The result shows that higher flow rates generate steeper gradients than lower flow rates. The diffusion coefficient used in the simulation was based on VEGF (table 1). A parametric sweep over 100 flow rates ranging between 1,6-80 nl/s was done to investigate this relation further, result is shown in fig. 24 where it can be seen that higher flow rates generate steeper gradients that are linear over a shorter distance than for slower flow rates. Fig 25 further illustrates the dependence of flow rate on gradient formation. Fig 25a) and c) demonstrates how the steepness of the gradient increases with the flow rate while the second derivative in fig. 25b) and d) show that the length of the linear gradient decreases with an increasing flow rate. Flow rates around 4,8 nl/s were found generate the most linear concentration gradient throughout the whole length of the cell culture chamber. The concentration gradient generated at this flow rate was further characterized at four positions in the cell culture chamber and as demonstrated by the plot data in fig. 26b), the gradient was nearly uniform over a 6 mm wide area.

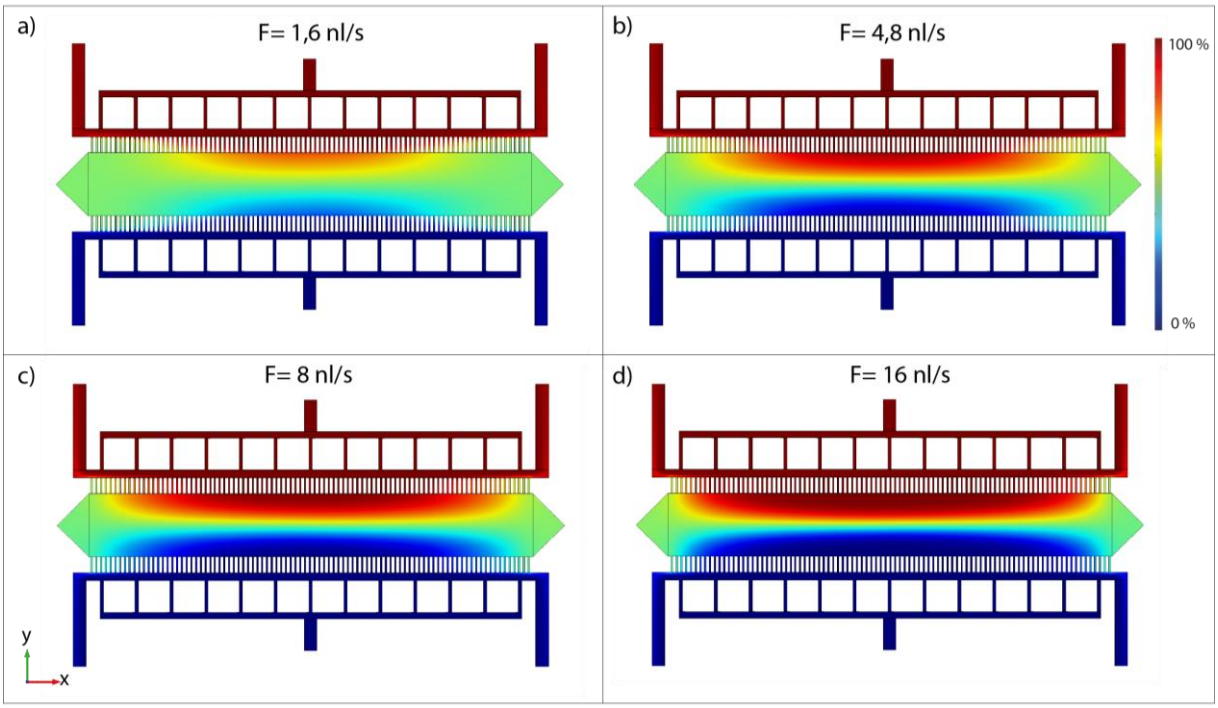

Figure 23. Simulation data of concentration gradient formation flow rates of a) 1,6 nl/s, b) 4,8 nl/s, c) 8 nl/s and d) 16 nl/s. a) A low flow rate do not generate a steep enough gradient. d) Too high flow rates generate too steep concentration gradients. Flow rate 4,8 nl/s (b) was found to be optimal for concentration gradient formation in this study.

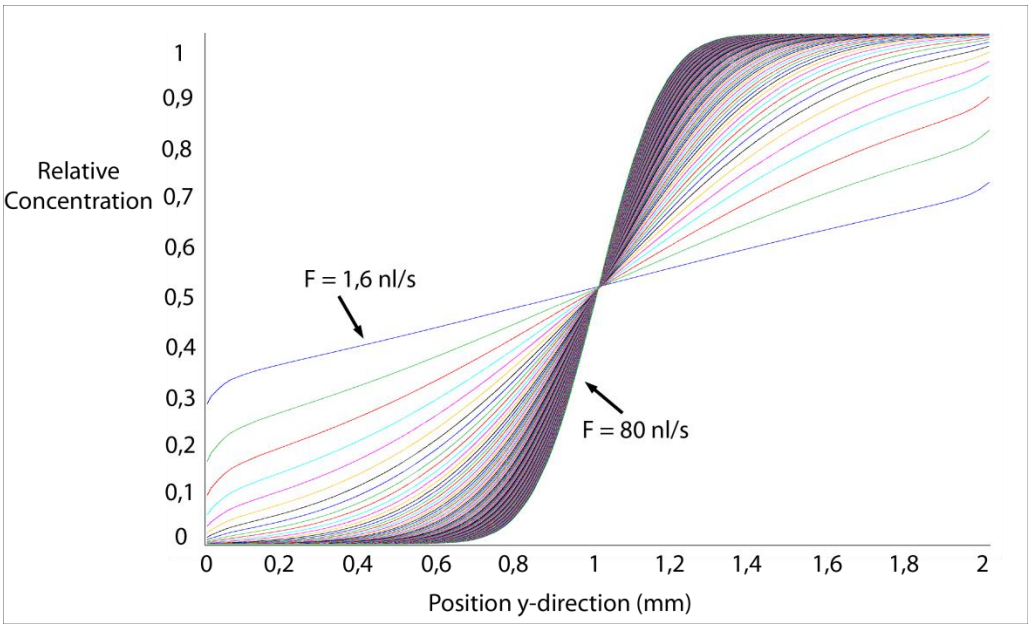

Figure 24. Concentration gradient formation at the center of cell culture chamber for 100 flow rates ranging from 1,6 nl/s to 80 nl/s. Higher flow rates generate steeper gradients.

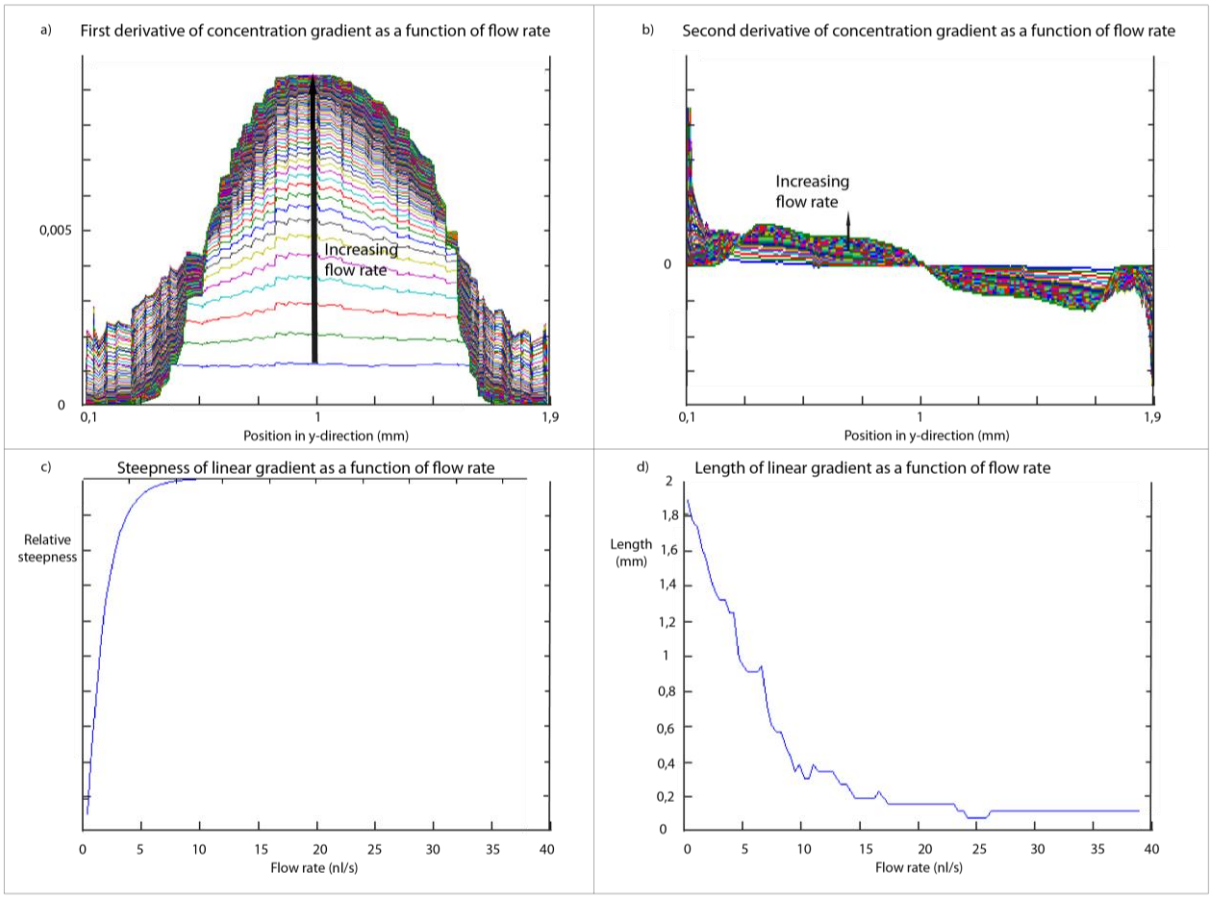

Figure 25. a) First derivative of concentration gradient as a function of flow rate where the highest derivatives is generated at the highest flow rates. b) Second derivate of concentration gradient as a function of flow rate. c) The steepness of the generated concentration gradient increases with the flow rate and is saturated after approximately 10 nl/s. d) The linear region of the generated gradient seems to decrease exponentially as the flow rate increases.

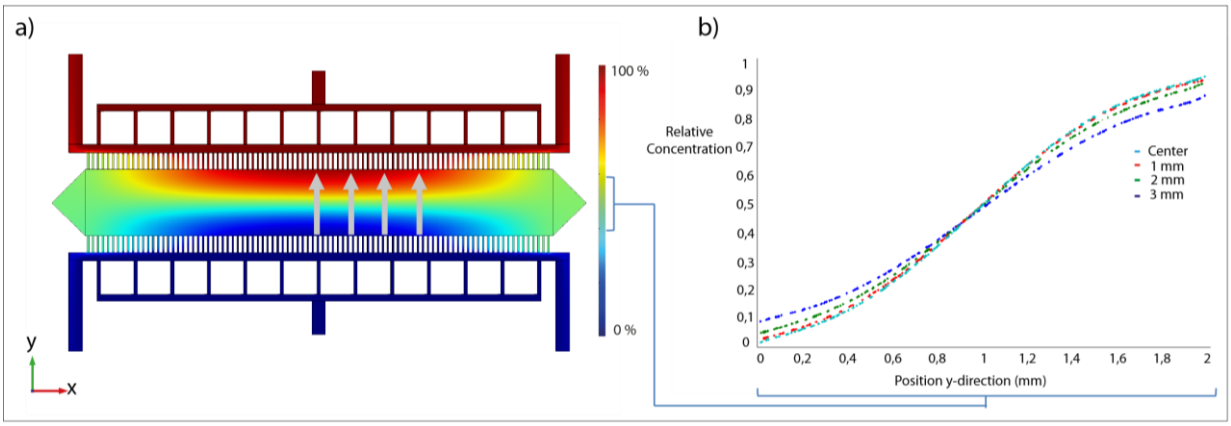

Figure 26. a) Concentration gradient formation at a flow rate of 4,8 nl/s. b) Concentration gradient line profile plot in the center of the channel and 1, 2 and 3 mm from the center (marked by arrows in (a)). The concentration gradient was uniform in the channel and showed a nearly linear behavior between y=0,4-1,6 mm.

3.1.11. Time dependent gradient formation

As the concentration gradient formation depends only on diffusion, it takes time to build up a gradient within the cell culture chamber. To investigate how long time it would take to establish a stable gradient based on the diffusion coefficient for VEGF a time dependent simulation was performed. Fig. 27 demonstrates the concentration gradient profile at four different time points. The gradient was fully developed after 7,5 h, and did not change afterwards (24h).

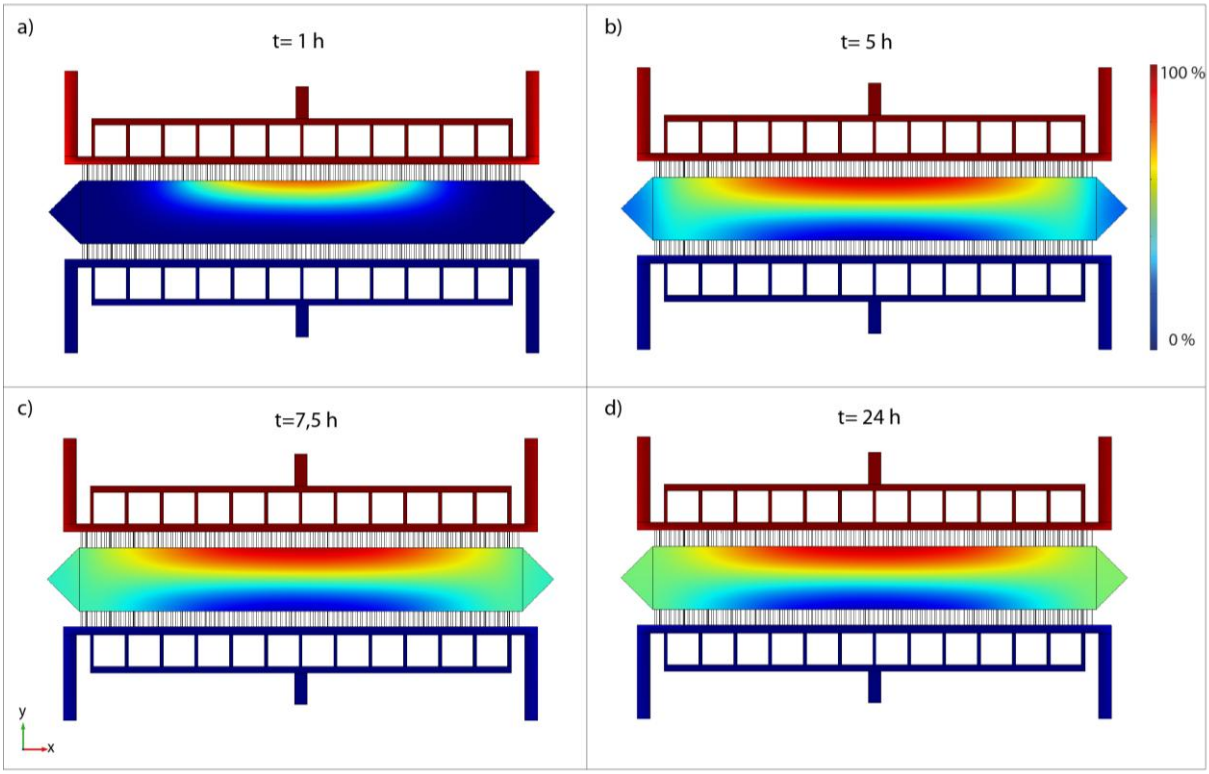

Figure 27. Time dependent concentration gradient formation at F=4,8 nl/s. a) After 1 h, the investigated molecule (VEGF) had started to diffuse into the cell culture chamber. b) After 5 h, a gradient was mainly formed and c) after 7,5 h, the gradient was fully developed. d) The gradient was still unchanged after 24 h.

3.1.12. Characteristics of the chosen design

The velocity profile inside the cell culture chamber showed a distribution as shown in fig. 28a) and b), where a very slow flow can be seen inside the cell culture chamber. The resulting shear force in fig. 28c) shows that no shear force was applied at the surface inside the cell culture chamber. Fig. 28d) illustrates the pressure drop which was evenly distributed throughout the microfluidic channels.

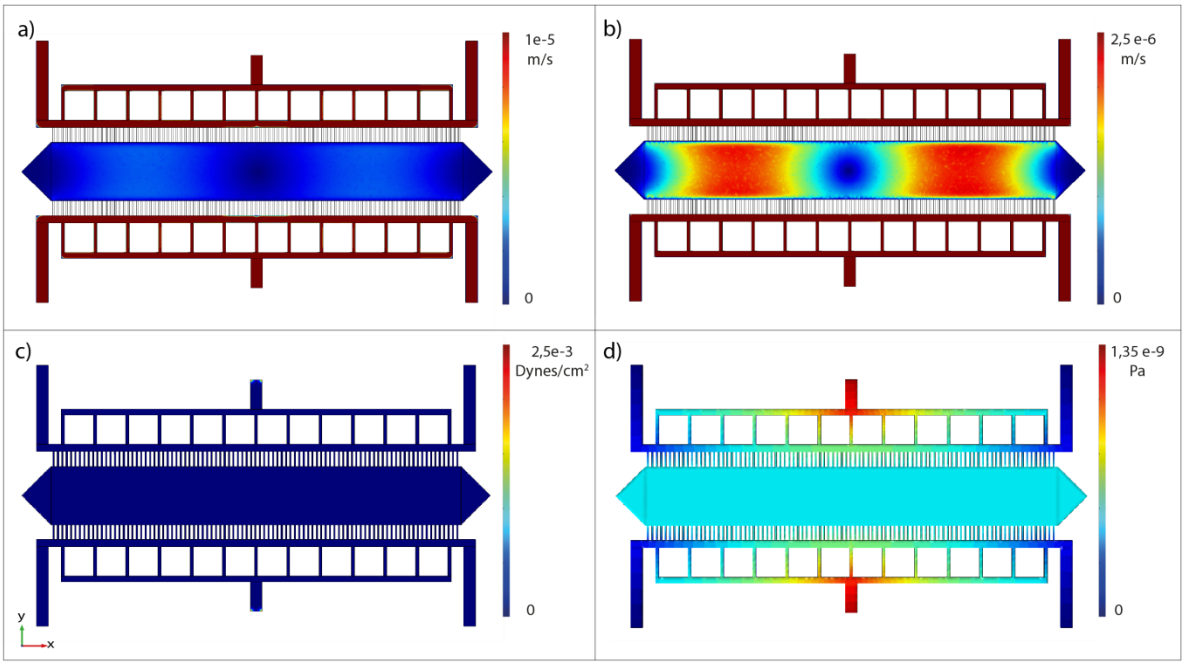

Figure 28. a) Velocity distribution inside the microfluidic channel, where red corresponds to 1e-5 and blueto 0 m/s. b) Velocity distribution (dark red > 2,5 e-6 m/s). A very slow velocity is found inside the cell culture chamber. c) Shear stress profile at the surface shows that no shear stress was present inside the cell culture chamber. d) Pressure inside the microfluidic channel. The pressure dropped evenly throughout the channel and there was no pressure inside the cell culture chamber. Flow rate was 4,8 nl/s.

3.2. Microfluidic chip production and characterization

3.2.1. PDMS chip production

The microfluidic chip was successfully produced in PDMS and could be bonded to both glass slides and an Au nanopatterned surface. Fig. 29 shows a chip filled with color dye to visualize o all connections and channels.

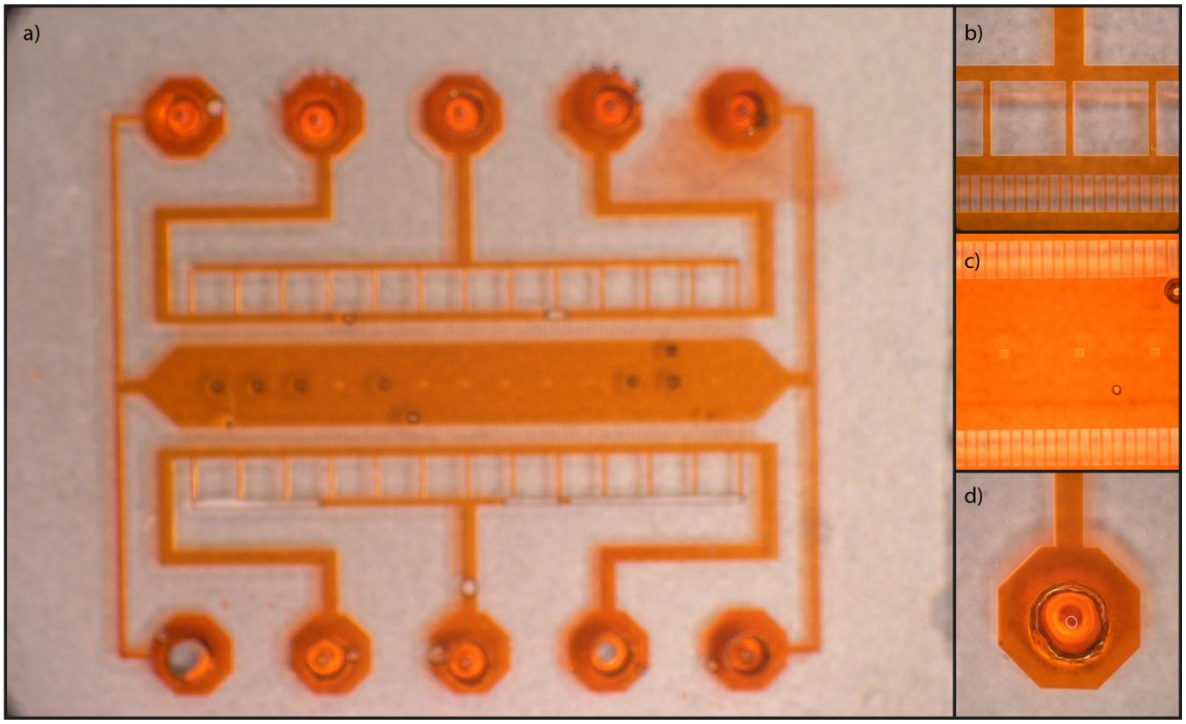

Figure 29. a) The microfluidic chip produced in PDMS, channels filled with color dye. b) The inlet channels split into several channels joining the source and sink channels. c) Part of the cell culture chamber with the connecting capillaries. d) Holes for inlets and outlets were punched through the PDMS.

3.2.2. Microfluidic chip characterization

Simulation data of concentration gradient formation was compared with experimental results. A red color dye (Direct Red 80) was introduced to the source channel, images were analyzed and intensity line profiles were plotted. To be able to compare simulation and experimental data, simulations were performed with the diffusion coefficient of the color dye, which is $D=3*10^{-10}$ m^2/s. Fig. 30 shows that experimental data correlates well to simulation data as a uniform gradient of color dye was formed in the cell culture chamber over a 6 mm wide area in both experiments. The gradient from the simulation data is S-shaped while the gradient from experimental data is more linear, even though the curves are slightly S-shaped (fig. 31).

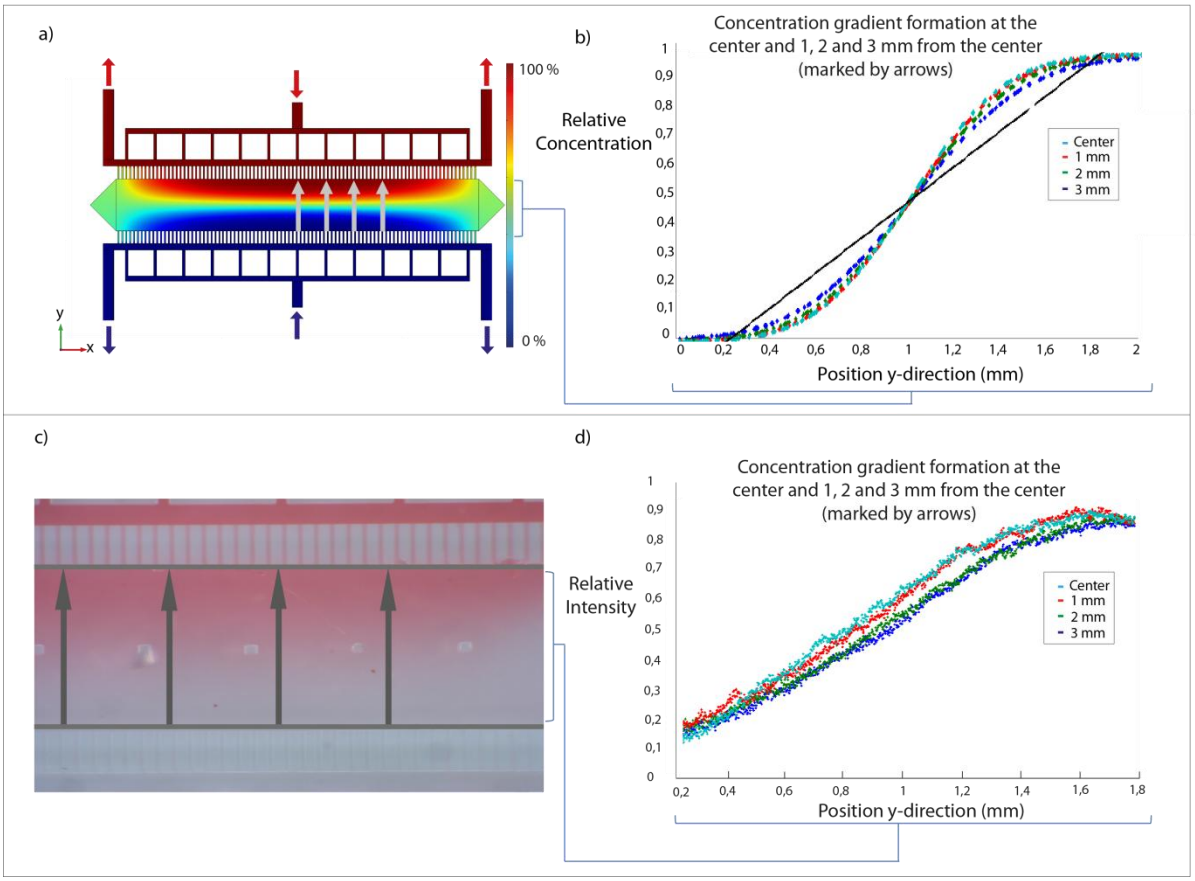

Figure 30. a) Concentration gradient formation from simulation data for color dye (Direct Red 80, $D=3*10^{-10}$ m^2/s) and b) intensity line profiles at the center and 1, 2 and 3 mm from the center of the cell culture chamber (marked by arrows) show a uniform concentration gradient formation in the cell culture chamber. A linear regression line was produced for the four plot values and the gradient curve is clearly S-shaped. c) Concentration gradient formation in the microfluidic cell culture chamber with color dye (Direct Red 80) and d) intensity line profiles show that a similar but slightly more linear concentration gradient than in b) was produced. Flow rate was 1 nl/s.

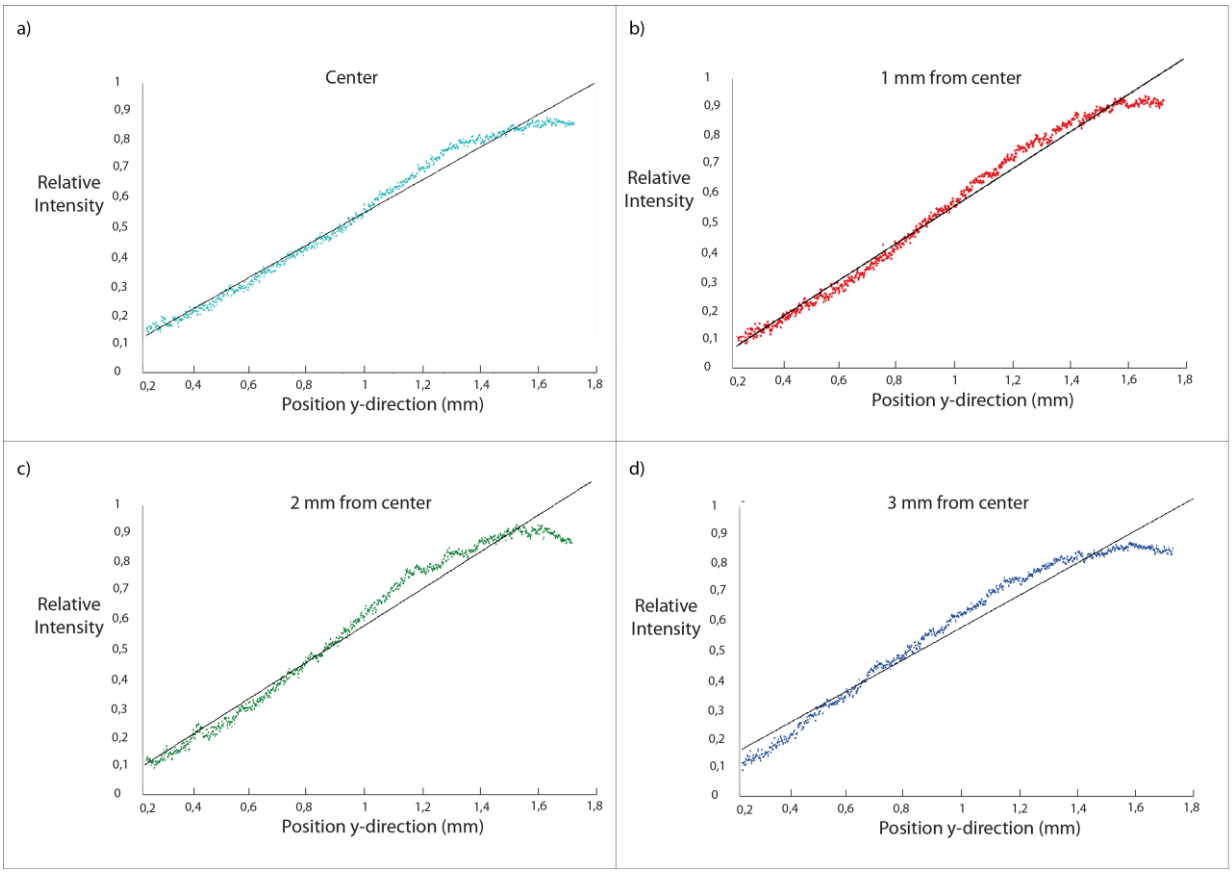

Figure 31. Linear regression lines generated for each data set at a) center, b) 1 mm, c) 2 mm and d) 3 mm from center of the microfluidic cell culture chamber. a), b), c) The curves are slightly S-shaped. d)The concentration gradient at 3 mm from the center does not show the S-shape but is more linear with a drop off at y=1,4 mm.

To experimentally investigate concentration gradient formation with a molecule similar in size to VEGF, FITC-Dextran (MW=40 kDa) was introduced to the source channel. Fluorescent images in the middle of the channel at the center and 1, 2 and 3 mm from the center were analyzed and intensity line profiles were plotted, see fig. 32. The generated gradient was linear and showed good correspondence between the four positions.

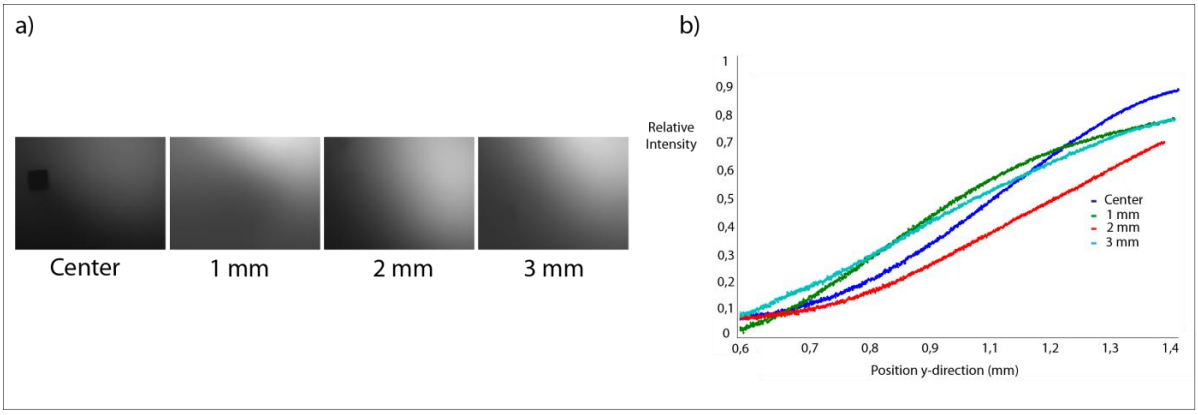

Figure 32. a) Fluorescence images of a concentration gradient of FITC –Dextran generated in the middle of the channel at the center and 1, 2 and 3 mm from the center. b) Intensity line profiles at the center and 1, 2 and 3 mm from center, from the fluorescent images in (a). The generated gradient was linear and showed good correspondence between the four positions.

The time it takes to clear a solution from the cell culture chamber was measured by filling the cell culture chamber with FITC-Dextran and introduce PBS to the source and sink channel at a flow rate of 1 µl/s. The flow rate (1 µl/s) was much higher than optimal flow rate for concentration gradient formation (4,8 nl/s) due to limit of time for conduction the experiment. Images were taken every second minute and the relative intensity of each image was plotted against time, fig. 33. The solution was cleared from the cell culture chamber after approximately 16 minutes.

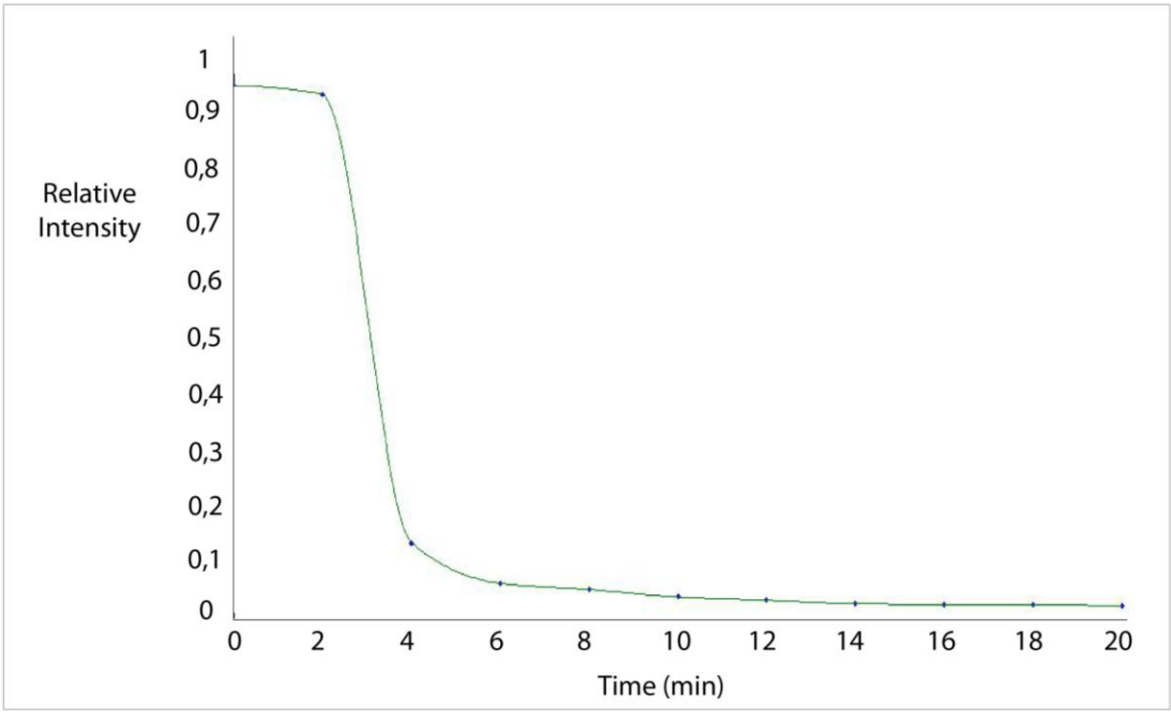

Figure 33. Time to clear a solution of FITC-Dextran from the cell culture chamber. The solution was cleared after approximately 16 minutes.

3.3. Au nano patterned surfaces

3.3.1. Surface characterization

Au nanopatterned surfaces were kindly provided by Joachim Spatz' group (Max Planch Institute for Intelligent Systems, Stuttgart, Germany). The surfaces had Au nanoparticles placed in a hexagonal pattern with inter-particle spacing ranging between 65-85 nm in a gradient manner as shown in fig. 34. Surfaces with inter-particle distance 85-125 nm were also provided and have been used in some experiments, but as the 65-85 nm spacing is most relevant for the proceeding of the project, only characterization data from those surfaces is shown. Fig. 35 below depicts SEM characterization of the surfaces at four distances from the dipping edge (edge of sample) in the gradient. The size of each Au nano-particle is approximately 5-8 nm, but as they are positioned onto the glass substrates they lose some of their circularity and the height of the nanoparticles is most likely below 5-8 nm.

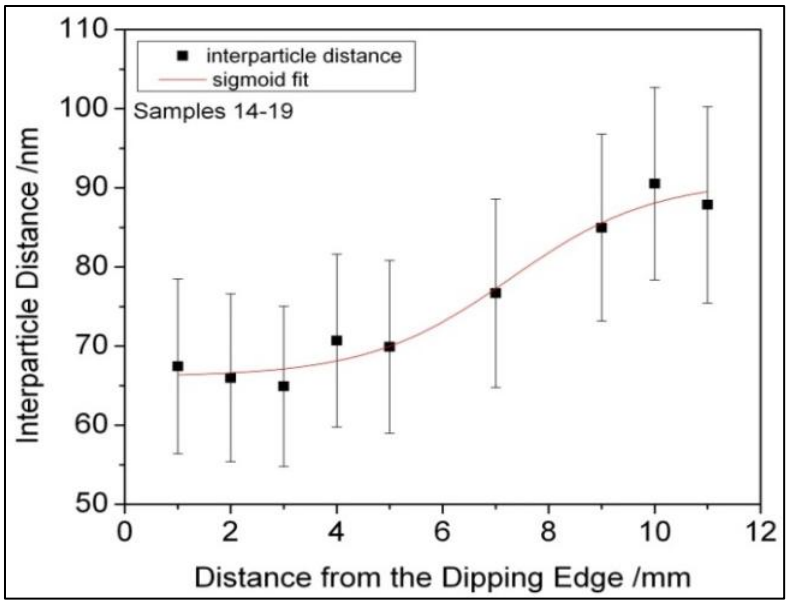

Figure 34. Inter-particle distance of Au nanoparticles at distance from dipping edge. The gradient is linear between approximately 4-10 mm from the dipping edge, generating a 6 mm wide linear gradient. Error bars show total error per image, while the standard error for each particle being 0,5–1 nm.

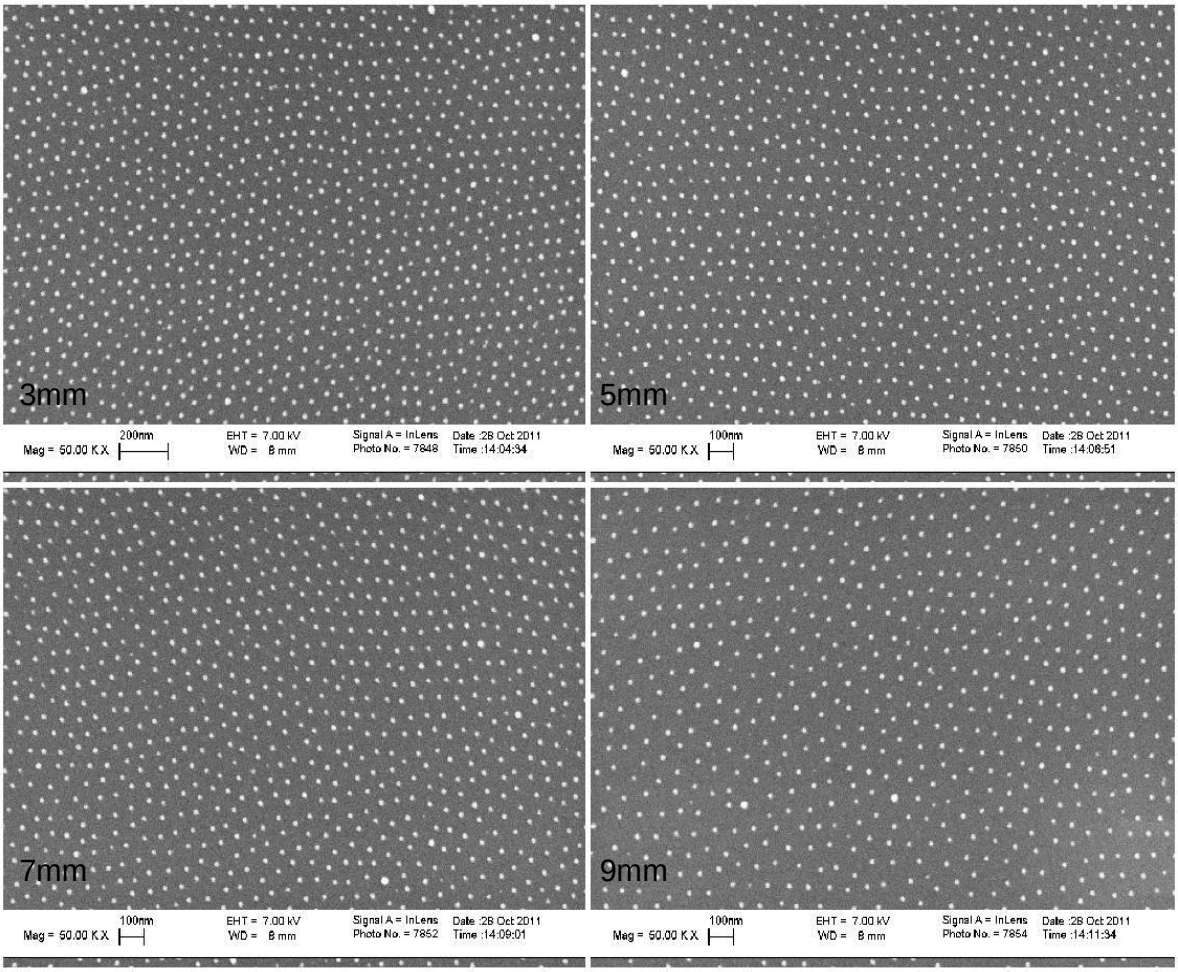

Figure 35. SEM images of an Au nanopatterned surface at 3, 5, 7 and 9 mm from the dipping edge.

3.3.2. Surface functionalization with cRGD

The Au nanopatterned surfaces were functionalized with c(RGDfK)-thiol, molecular structure shown in fig. 36. The thiol group (-SH) binds covalently to the Au atoms on the Au nano-particles. The molecule is built with a PEG spacer that separates the functional cRGD group from the surface binding –SH group, making it accessible to cell integrins.

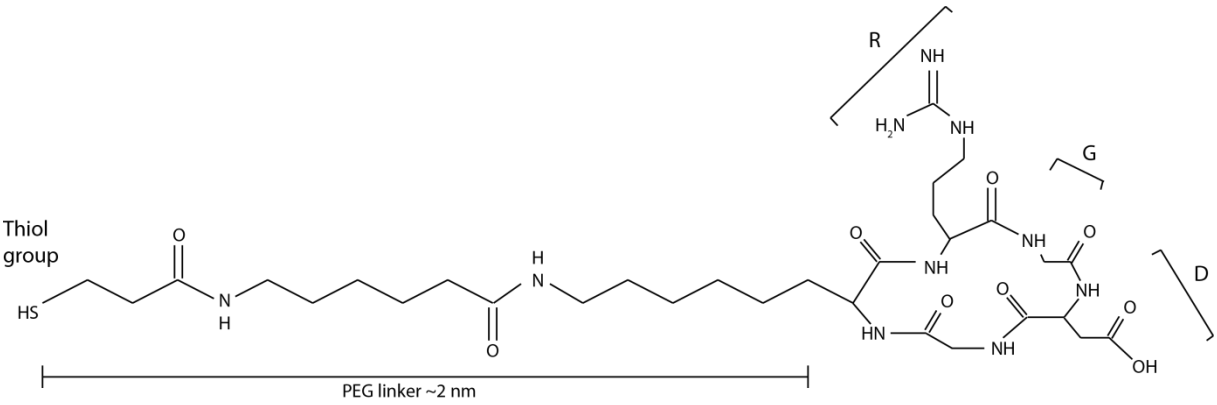

Figure 36. cRGDfK9-Thiol with the thiol group as the surface coupling site on one end and the functional cRGD peptide sequence at the other end. A PEG spacer is placed in between to separate the functional group from the surface.

3.3.3. Surface passivation with PLL-PEG

As cells can bind to glass, the surface in between the Au nano-particles had to be passivated to exclude non-specific cell attachment. This was done by electrostatically adsorb PLL-PEG molecules (fig. 37) to the surface by immersing the cRGD functionalized samples in PLL-PEG solution. The size of the PEG side chains was 2 kDa.

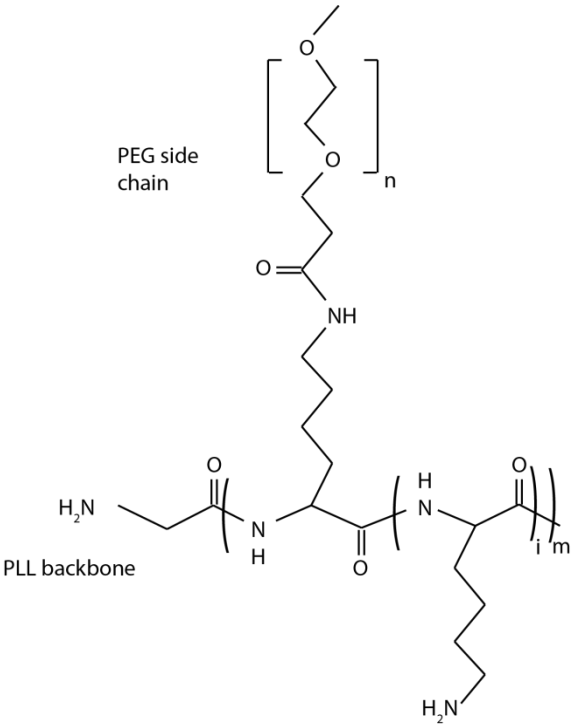

Figure 37. Molecular structure of PLL-PEG where PLL makes up the backbone from which PEG side chains are branched. *n* denotes the size of the PEG chain which was 2 kDa in this project, *i* the grafting ratio which was 3,5 and *m* the size of the PLL main chain which was 20 kDa.

The surface modification procedure where Au nanopatterned surfaces were first functionalized and then passivated is schematically outlined in fig. 38 below.

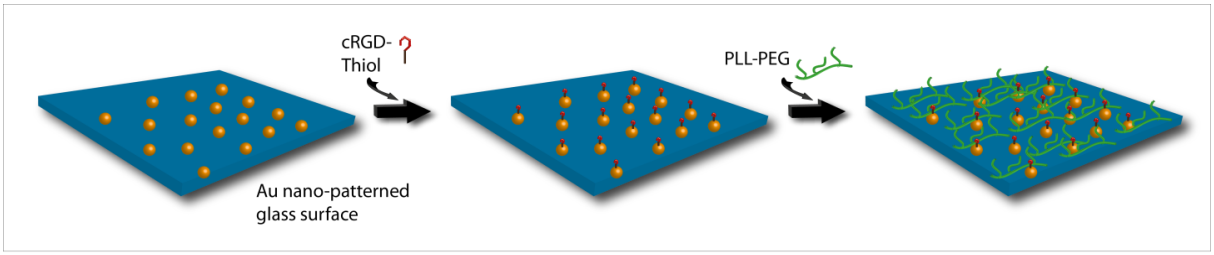

Figure 38. Schematically sketch of surface functionalization with cRGD-thiol and passivation with PLL-PEG of the Au nanopatterned surfaces.

3.3.4. Protein interaction studies by QCM-D

To investigate if PLL-PEG provided proper surface passivation, protein interaction studies were performed on PLL-PEG passivated surfaces by QCM-D. An Au nanopatterned surface (55 nm) was functionalized with cRGD. Untreated SiO2 and Au nanopatterned (55 nm spacing) surfaces and SiO_2 incubated in water for 2 days served as controls. First PLL-PEG was injected over the samples. To investigate passivation properties complete cell media including serum, containing several different kinds of proteins, was injected onto the samples. After injection, flow was turned off for 1 h and samples were subsequently rinsed with PBS. The large frequency shift that was observed after PLL-PEG injection (fig. 39), and the fact that the frequency did not shift back again after rinsing with PBS, showed that PLL-PEG was adsorbed onto all the samples. Upon injection of cell media a frequency shift was observed, indicating that some protein was adsorbed onto the surfaces. Further, as the frequency is shifted back again after rinsing with PBS, it can be concluded that the protein was rinsed off and that it was not adsorbed firmly. Fig. 37d) shows the QCM-D result for cRGD functionalized surface, where the frequency is shifted higher both after PBS rinsing, after PLL-PEG adsorption and after the flow was stopped, indicating a loss of mass from the surface at all time points.

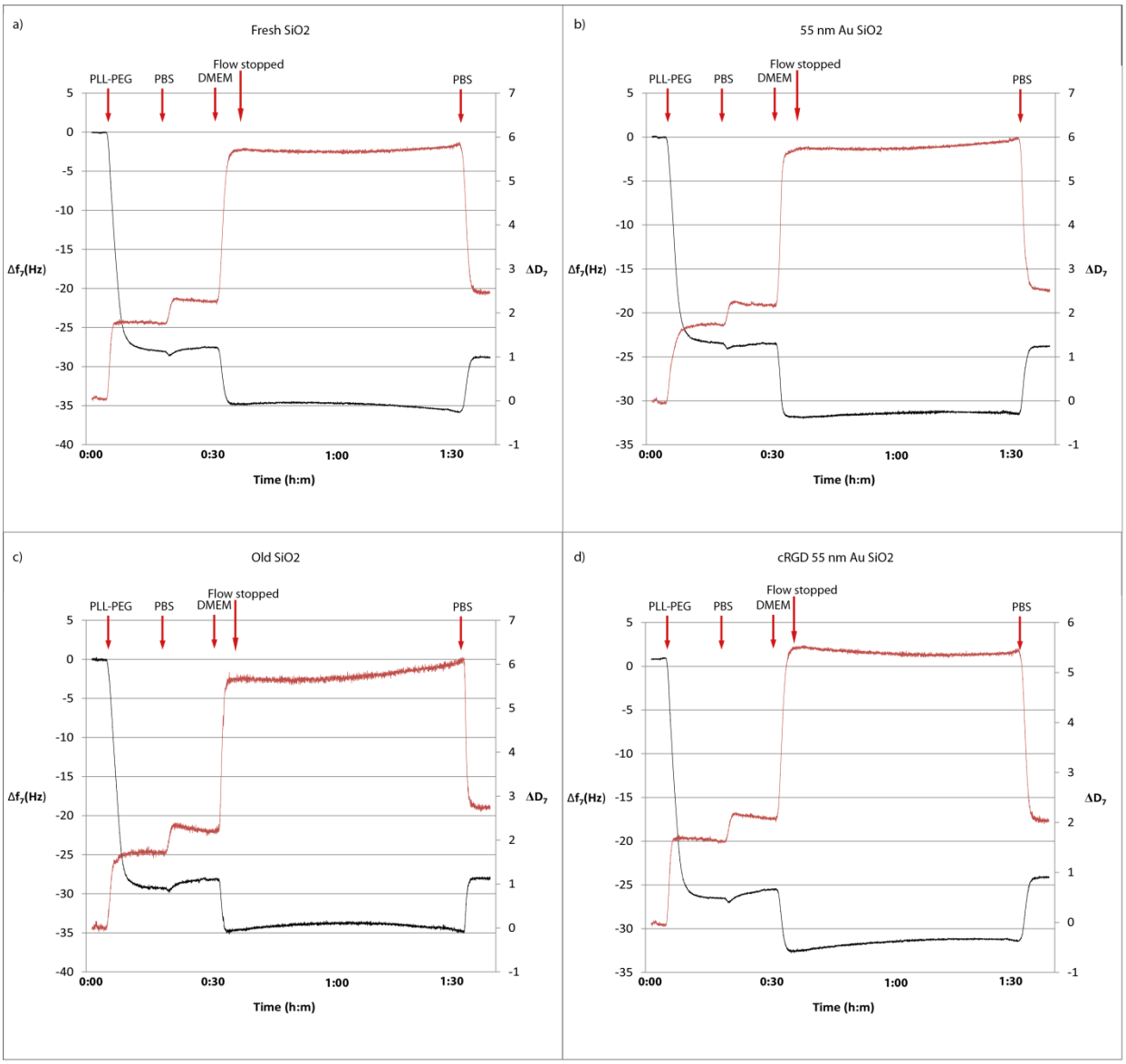

Figure 39. QCMD measurements of 4 surfaces with a) SiO2, b) 55 nm spaced Au particles on SiO2, c) SiO2 treated as (d) but with water and d) 55 nm spaced Au particle functionalized with cRGD. The graphs display frequency (red) and dissipation (black) as a function of time.

3.4. HUVEC culture

3.4.1. Cell culture in petri dishes

To evaluate surface modifications, HUVECs were seeded onto the studied surfaces in petri dishes. Comparison of cell attachment and spreading behavior was done between glass and Au nanopatterned surfaces, and functionalization and passivation methods were investigated.

3.4.2. Cell viability on Au nanopatterned surfaces

HUVECs were seeded onto non-treated and cRGD functionalized Au nanopatterned surfaces to investigate their viability and behavior to spread on these surfaces. Fig. 40 demonstrates that cells are viable, attached and spread on both non-treated and modified surfaces.

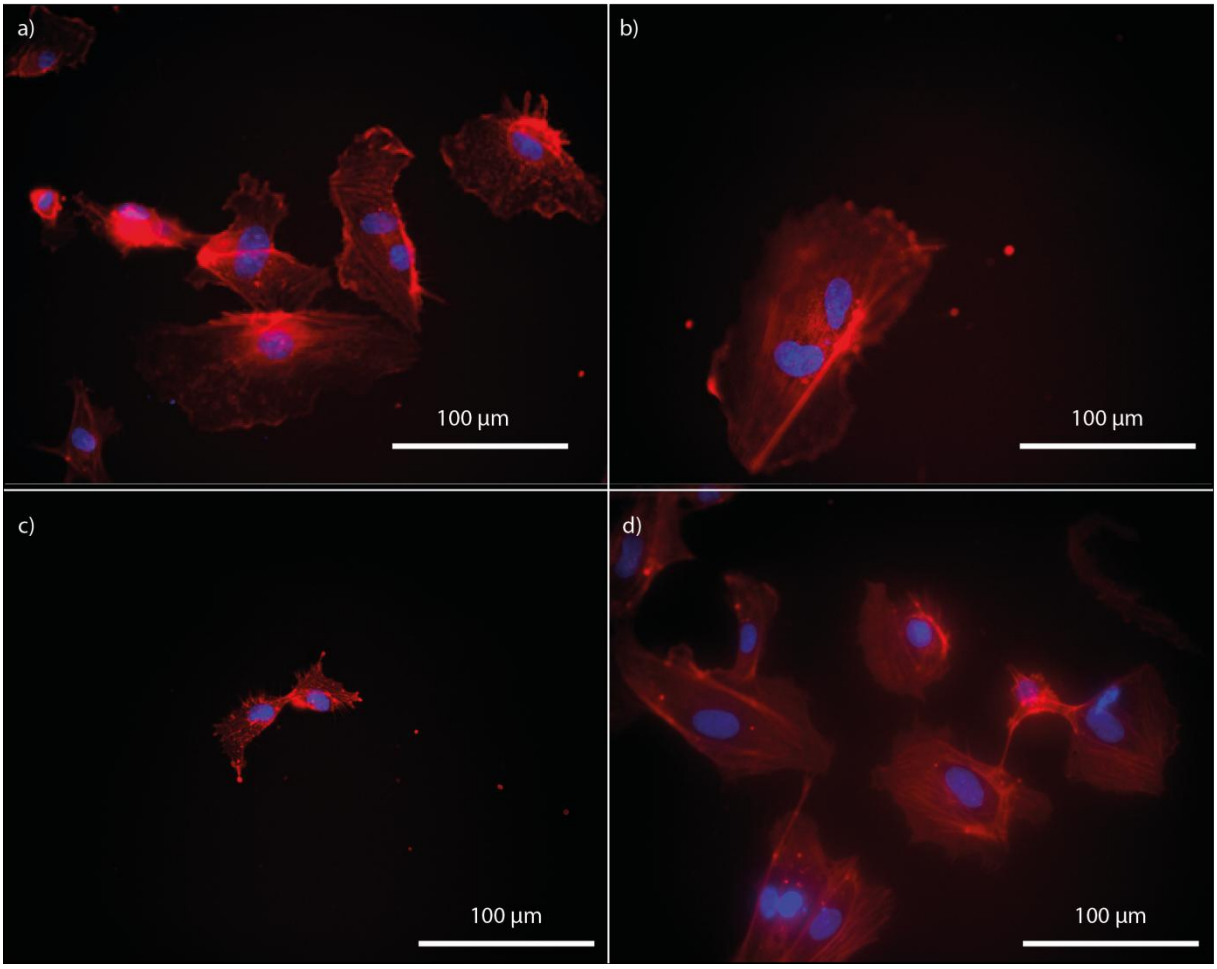

Figure 40. HUVECs on Au nanopatterned surfaces (85-125 nm spacing) a),b) Au particles functionalized with cRGD and c),d) non-modified surfaces. The cells have attached and spread on all surfaces, showing good viability. Cells stained with DAPI (blue) and Phalloidin (red), cultured for 24h.

3.4.3. PLL-PEG passivation

Passivation of surfaces with PLL-PEG was investigated by seeding cells on non-treated and PLL-PEG modified glass substrates and on PLL-PEG treated cRGD functionalized Au nanopatterned substrates. Results in fig. 41 indicate that PLL-PEG passivation works as a lower amount of cell attach to the PLL-PEG treated surfaces (fig. 41d)-f)) compared to controls (fig. 41a)-c)). Statistical analysis (fig. 42) of randomly taken images on the three different modifications demonstrates a significant decrease of cell attachment on PLL-PEG treated surfaces. The results also indicate a lower amount of attached cells on the cRGD functionalized Au nanopatterned substrates, which might be related to cRGD peptide being inaccessible for cells after PLL-PEG passivation.

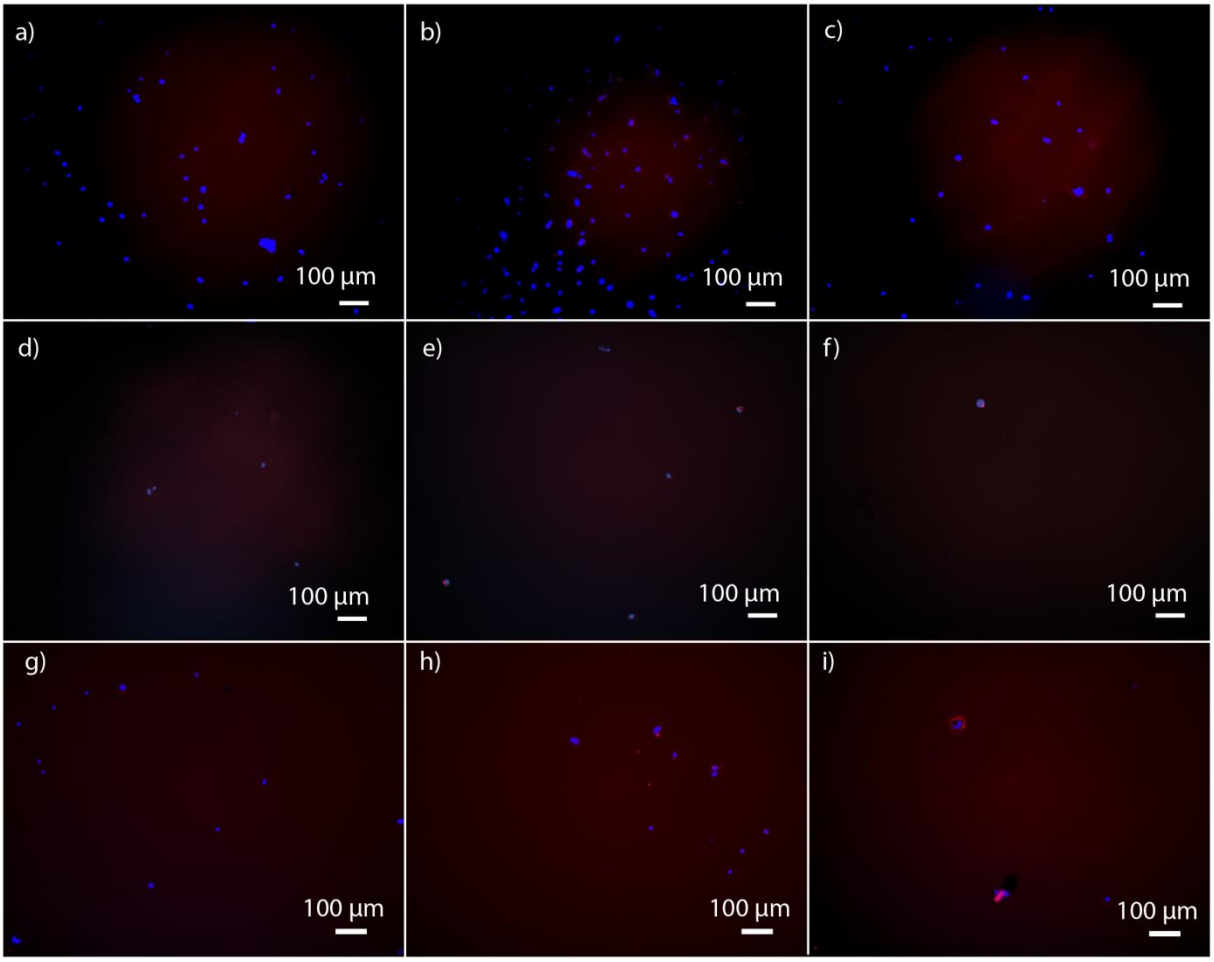

Figure 41. a), b), c) Non-treated glass surfaces with a high amount of cells attached. d), e), f) Glass surfaces passivated with PLL-PEG having a low amount of cells attached to them, indicating that the passivation was successful. g), h), i) cRGD functionalized Au nanopatterned surfaces passivated with PLL-PEG also show a low amount of cells attached onto them, indicating complete passivation of the surfaces. Cells stained with DAPI (blue) and Phalloidin (red), cultured for 24h.

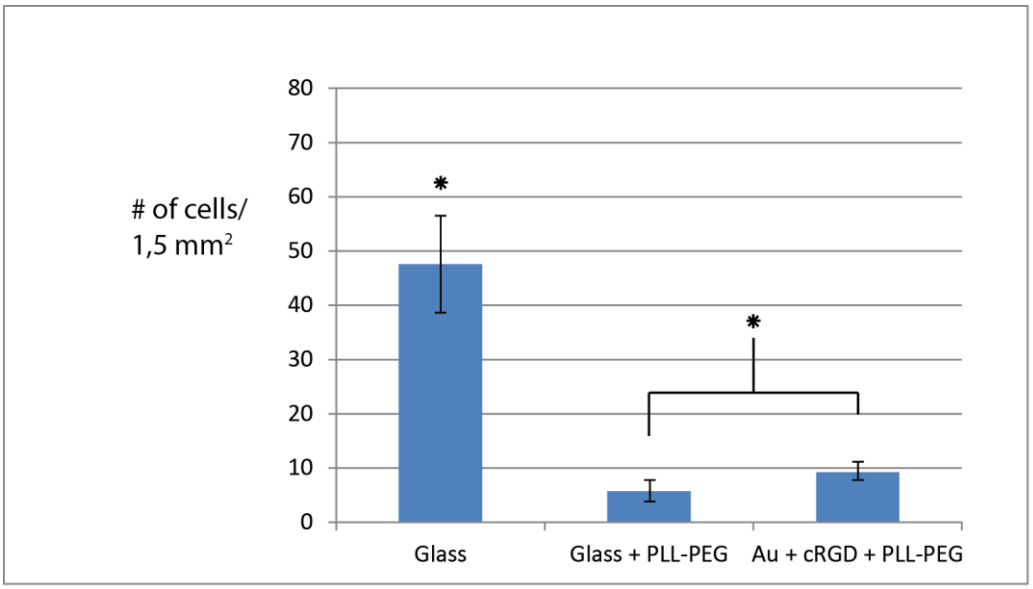

Figure 42. A significantly higher amount of cells are attached on the glass surface compared to PLL-PEG treated surfaces, indicating that PLL-PEG passivates the surfaces. The passivation of the PLL-PEG treated cRGD functionalized Au nanopatterned surface suggests that cells could not attach to the cRGD peptide. Asterix indicates significance, p=0,05, and error is calculated as standard error of the mean.

3.4.4. Cell culture in microfluidic system

To study cell survival inside the microfluidic chip, HUVECs were introduced to cell culture chamber and seeded for 24 h and 5 days respectively. The cells attached to the non-modified glass surface and showed good viability over the time of study (fig. 43).

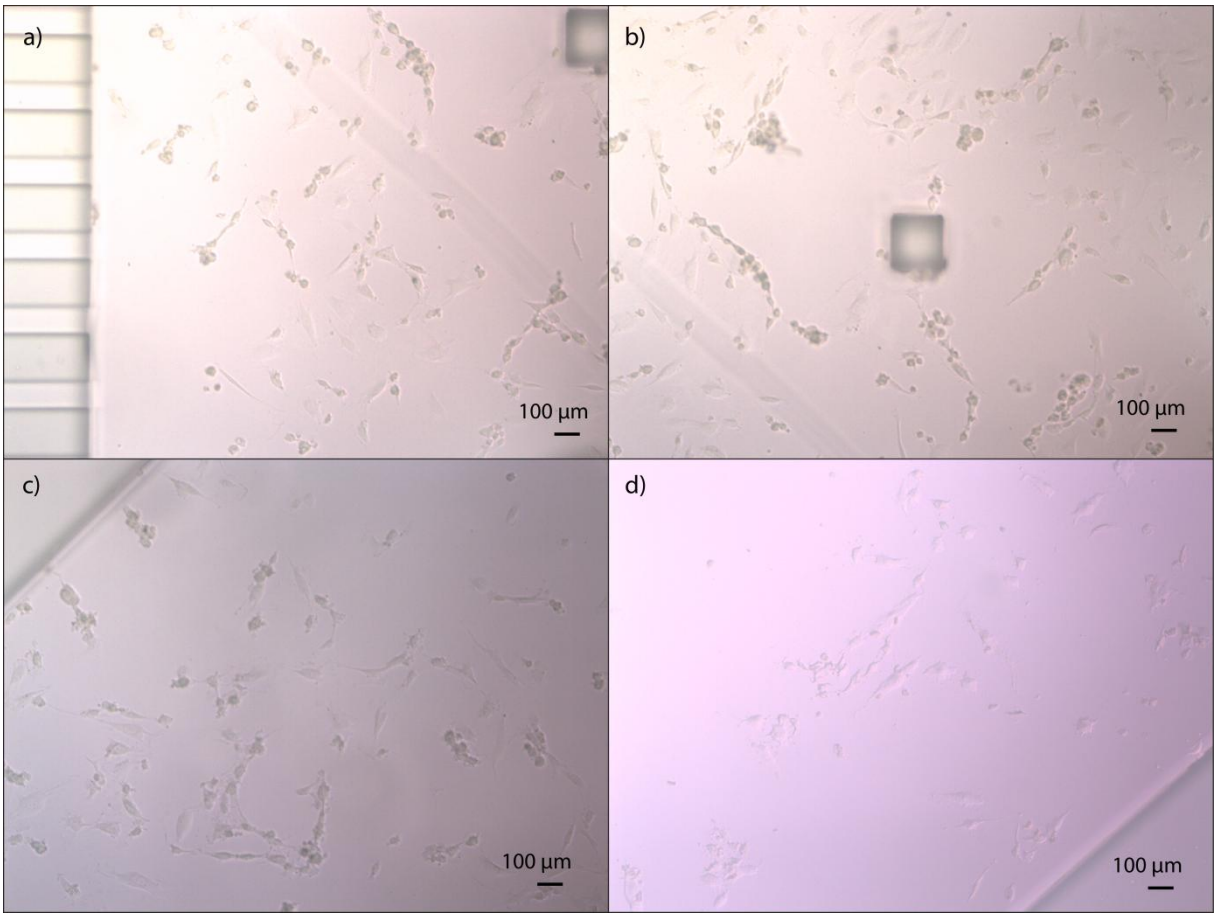

Figure 43. a), b) HUVECs on glass surface in the cell culture chamber after 24 h seeded under static conditions. c) Same as in (a) and (b) but after flow was applied trough the chamber. Cells were still present and were firmly attached as they were not flushed away. d) HUVECs in cell culture chamber after 5 days were still attached and showed good viability.

Cell viability and morphology was also studied on HUVECs cultured inside the microfluidic chip combined with a cRGD functionalized Au nanopatterned surface. Cells seeded for 24 h attached, spread and showed good viability (fig. 44).

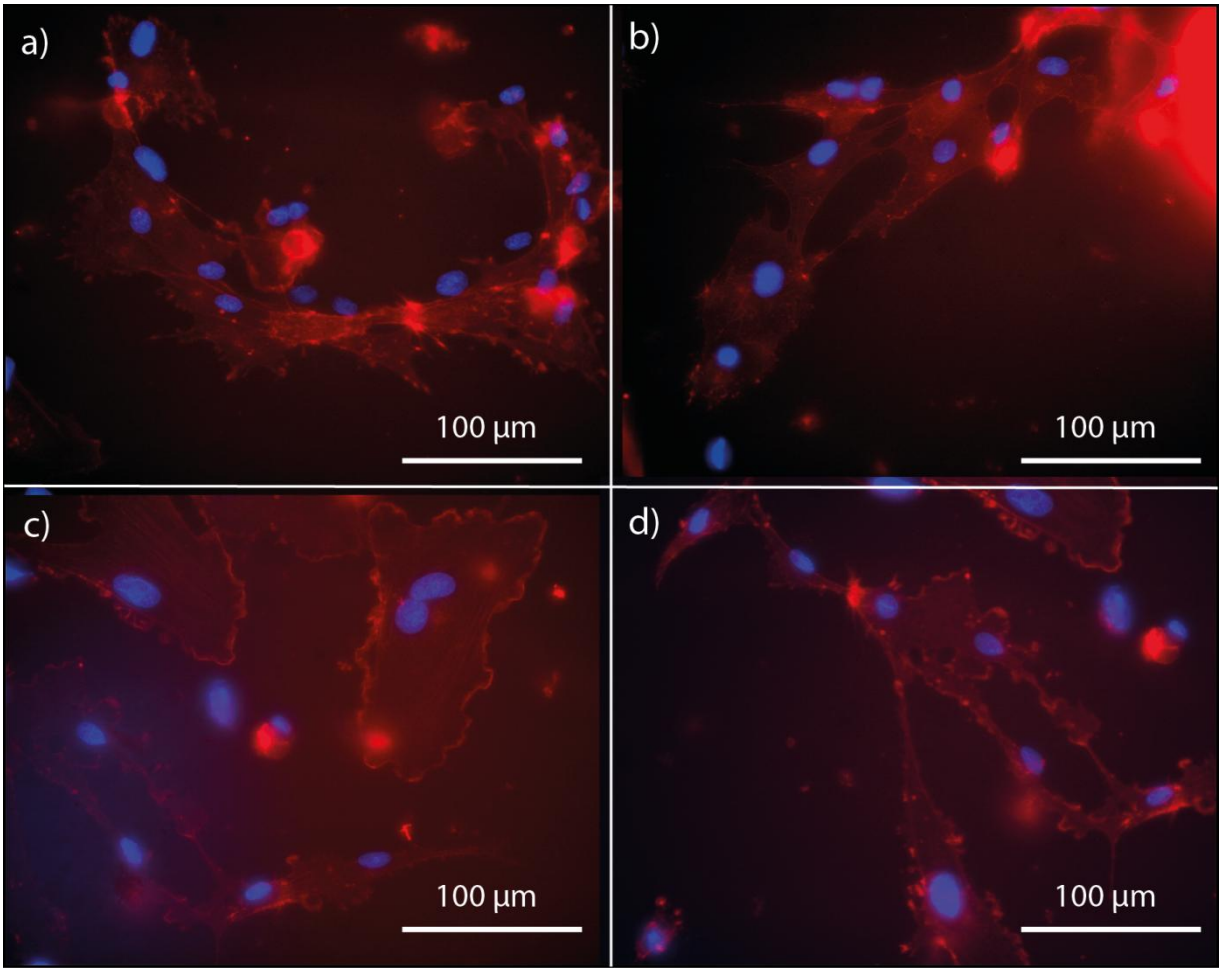

Figure 44. a), b) HUVECs seeded onto cRGD functionalized Au nanopatterned surface and c), d) glass surface inside the microfluidic cell culture chamber. Cells stained with DAPI (blue) and Phalloidin (red), cultured for 24 h.

4. Discussion

4.1. Microfluidic chip

With the vision to develop a microfluidic device in which endothelial cell migration could be investigated and to combine that device with a functionalized surface to study the effect of attachment peptide spacing on migration, certain requirements had to be fulfilled. HUVEC chemotaxis has previously been shown to be induced by VEGF concentration gradients with a steepness of at least 14 ng change in concentration per mm (3). This means that cells need a certain steepness of the concentration gradient in order to sense a difference in concentration between the leading and the retracting edge, and thereby actively migrate. It has also been shown by Chen *et al.* (2007) that saturation of the VEGF receptor occurs at concentrations of 40-100 ng/ml. A goal was therefore to develop a microfluidic device that generated a concentration gradient that was steep enough without having to use too high concentrations in the source channel. Calculations led to the first goal of having a gradient ranging over at least 60 % between the highest and lowest concentrations inside the cell culture chamber (relative concentration with 100 % in the source channel and 0 % in the sink channel, see fig. 45 for illustration). The gradient should also be as linear as possible throughout the cell culture chamber so that migration could be studied along the whole length of the chamber.

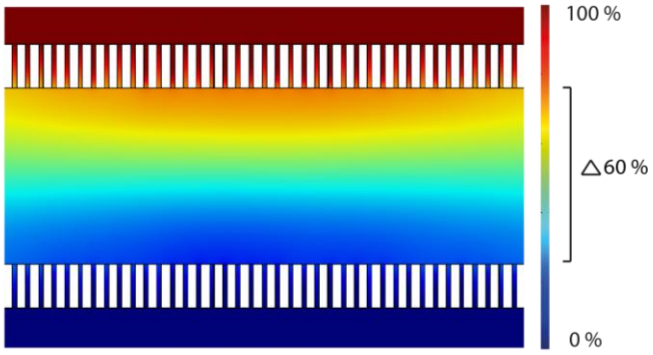

Figure 45. Percental concentration gradient in the source and sink channels and in the cell culture chamber.

To be able to study the effects of attachment peptide spacing, an Au nanopatterned surface functionalized with cRGD was used. The surface had nanoparticles placed in a hexagonal pattern with spacing ranging between 65-85 nm in a gradient manner. The cRGD gradient is placed perpendicular to the chemoattractant gradient, which makes it possible to study cell migration at different attachment peptide spacing in the same chemoattractant gradient (see fig. 46 for sketch of experimental set-up). The linear region of the spacing gradient on the Au nanopatterned surface is approximately 6 mm wide, thus this is the width in which cell migration should be studied. This generated the second goal of producing a concentration gradient that was uniform over at least 6 mm. To be able to study cell migration over a long enough distance, a third goal was to generate a concentration gradient over a length of 2 mm.

Upon these request the three main goals were to generate a concentration gradient inside a cell culture chamber that should be 2 mm long and at least 6 mm wide, and also be linear and at least 60 % steep.

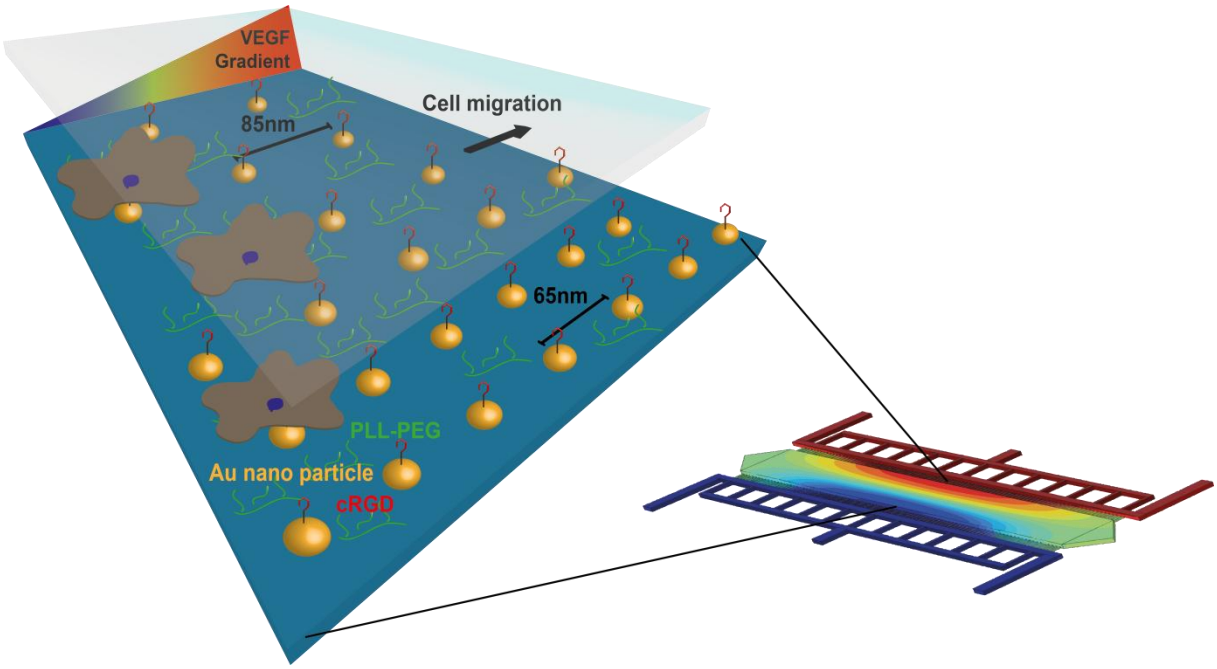

Figure 46. Sketch of the experimental plan. A cRGD pattern with precisely controlled spacing is presented to the cells in a gradient. A soluble gradient of VEGF is applied perpendicular to the cRGD gradient, inducing cell migration and the migration can be monitored as a function of attachment peptide spacing.

The design procedure of the microfluidic chip was an iterative process where designs were created in AutoCAD and simulations for fluid flow and transport of diluted species were performed in Comsol. The simulation data was evaluated and the layout of the design was improved in order to optimize concentration gradient formation. The initial design was based on a study by Shamloo *et al.* (2008), where a concentration gradient was generated within a 4 mm wide and 1 mm long microfluidic cell culture chamber (3). To fulfill the dimension goals, the initial design in this project had a much larger cell culture chamber with dimensions of 10 000 x 2 000 µm. From the initial design, parameters were investigated in order to reach the above mentioned goals.

The first parameter that was investigated was if it was possible to have a slow flow of cell media through the cell culture chamber, which would supply nutrients to the cells and remove waste products. The results show that even a very slow flow of 0,02 nl/s through the cell culture chamber completely disrupted the concentration gradient formation and the idea was discarded. Cell studies inside the microfluidic chamber have later shown that the volume of the cell culture chamber provides sufficient nourishment to cultured cells, and exchange of cell media based on diffusion will be sufficient for cell culturing.

Several models were designed and from the simulation data some conclusions could be drawn. It seemed like the concentration gradient formation at the site in the cell culture chamber that was placed in line with outlets was lost. This could be due to the formation of a zone with decreased velocity were the flow is turning in to the outlet, which could lead to less exchange of media and thereby a lower amount of diffusing molecules into the cell culture chamber. Splitting the inlets into several channels led to a more evenly distributed concentration inside the cell culture chamber and a wider model was also demonstrated to generate a wider concentration gradient.

The design of the source and sink channels where the inlets split into several channels and joined the source and sink channels at different points along the channels led to an increased flow rate in the channels after each inlet. A hypothesis was that if the velocity in the source and sink channels were more uniform along the channels, the resulting concentration gradient might be more uniform over a wider area. Triangular source and sink channels were designed to obtain a more uniform flow, however this approach did not result in more homogenous gradient formation as the concentration gradient was still lost at the ends of the cell culture chamber.

The size of the source and sink channel was a significant parameter that needed to be investigated. Narrower channels would lead to faster flow through the channels and source and sink channels that were half the length of the others generated a significantly steeper gradient. This also means that a slower flow rate could be used to generate a concentration gradient steep enough in the design with smaller source and sink channels. The flow rate is an important parameter as cell media and chemoattractants used, for example to induce cell migration, often are expensive and reducing reagent consumption is therefore advisable. The height of the capillaries determined the volume in which diffusion could take place from the source and sink channels into the cell culture chamber. Simulation data shows that a model with 50 µm high capillaries generates a steeper gradient than one with 25 µm high capillaries. Too high capillaries, on the other hand, would generate a too steep gradient (data not shown), and would also lead to less hydrodynamically decoupling of the source and sink channel and the cell culture chamber. Based in these results the capillary height was chosen as 50 µm. Simulation data from comparison of capillary length showed that shorter capillaries generated a steeper gradient. Even though a steep gradient is a goal of the design, it is important to consider that shorter capillaries would mean less hydrodynamically decoupling between the source and sink channel and the cell culture chamber. In the final model, a capillary length of 500 µm was chosen as that also allowed placing of source and sink channel, and thereby inlets and outlets, further away from the cell culture chamber, facilitating imaging of the cell culture chamber.

Diffusion of a molecule depends on its molecular weight where a larger molecule will diffuse slower than a small molecule. Cultured cells secrete a vast amount of compounds with molecular weights ranging from several Daltons up to M Daltons. To get an idea of how long time it would take to remove different secreted compounds under the flow conditions used in cell culturing experiments, simulations where performed on three different sized molecules; glucose, VEGF and hyaluronan. Glucose is a small molecule and was cleared faster from the cell culture chamber than VEGF, a larger compound. The very large glucosaminoglycan, hyaluronan, was never completely cleared from the system during the time of study (3,5 h). It is well known that cells produce their own ECM compounds in cultures and in specific that HUVECs produce hyaluronan, although it produce a much lower amount when not subjected to shear stress (26). As shown here, these large molecules are not removed by diffusion, a parameter that must be taken into account for longer cell culture studies. It could not least be a problem for the application of this project, as specific interactions with ECM attachment peptides are studied. Presence of ECM molecules produced by the cultured cells could lead to cell attachment and focal adhesion formation at these molecules, and it would not be possible to specifically control the attachment peptide environment. To overcome the problem, the plan in this project is to have the cells in the microfluidic cell culture chamber for only 24 h which is not sufficient time for endothelial cells to make enough of their own ECM to affect the experiment (26).

Based on the investigated parameters mentioned, one model was developed to best fit the goals. The figures that are shown in the simulation data do not include the design of inlets and outlets, as the structure would be more complex, unnecessarily increasing simulation time, due to the fact that they do not affect the concentration profile inside the channel system. The placing of inlets and outlets was done in a way that only one tube had to be connected to each inlet. The inlets and outlets were placed in line a bit away from the culture chamber which simplified imaging and gathered all the tubing at two places.

Flow rate is one of the most important parameters that can be controlled and adjusted to form desired concentration gradients. From the simulation data it can be concluded that higher flow rates generates steeper concentration gradients and that the steepness of the gradient increased rapidly with increasing flow rate until it tailed off after approximately 10 nl/s. The distance over which the gradient was linear decreased in an exponentially manner with an increasing flow rate, an indicative result as it can never be higher than the length of the length of the channel and never be below zero. The results mean that there has to be a balancing between the steepness and the length of the linear gradient when concerning what flow rate to use in an experiment. The gradient formed at a flow rate around 4,8 nl/s was selected as the optimal choice of flow rate for the purpose of this study as is generated a gradient that was linear over the whole length of the channel. The generated concentration gradient at flow rate 4,8 nl/s was uniform over 6 mm width, but it took approximately 7,5 h to reach a fully developed and stable gradient. The fact that it took a long time until the gradient was stable does not make a big difference in this project, as the study will go on for 24 h and the gradient will be stable for most of the time. To decrease the time to reach a stable gradient a higher flow rate could be applied during the initial state of the gradient formation, which would allow a faster gradient formation, and subsequently decrease it after some time.

A very low velocity (below 2,5e-6 m/s) is obtained in the cell culture chamber, a result also experienced by Shamloo *et al.* (2008) and should not affect the gradient formation or the cultured cells. Looking at the shear forces produced due to the velocity in the microfluidic channels in fig. 27c) it can be concluded that no shear force is applied surface of the cell culture chamber and that shear stress induced cell migration can be excluded in this experimental setup. Fig. 27d) illustrates the pressure drop and as can be seen it is evenly spread along the channels and there is no position in the model where the pressure drop is very large. This tells us that there will be a smooth flow through the channels.

As the model contains a high number of channels and thereby has a complex structure, some properties had to be taken care for in Comsol simulations in order to make the simulation to work and to shorten the solution times that otherwise can be very long (several days). Simulations can be performed either in stationary or time-dependent conditions. As for the fluid flow, only the stationary solution was interesting for this project as the fluid flow would not change over time. Therefore, fluid flow was always solved for using a stationary solver. For transport of diluted species, the solver was selected based on the specific question. At some simulations, only the stationary solution was of interest and a stationary solver was therefore used in order to shorten the solution time. A stationary solver returns a final stable, stationary, solution. In other cases, where the time dependency was important, a time dependent solver was used. To achieve quicker solution times in Comsol, simulations were divided and two separate solvers, one for fluid flow and the other for transport of diluted species, were used. In this way, one study with only fluid flow could be solved first. Then, a second study that used the

values from the first study could be used to solve for transport of diluted species. Another important aspect is discretization, a process in which a continuous system is divided into a finite number of elements with finite size, and solutions are obtained for each element. Depending on how the discretization is defined, solutions will be calculated in different nodes or points of the discrete elements. The model mesh was set to free triangular and to make the model function properly the discretization of the solution for transport of diluted species was set to quadratic. This discretization, in contrast to the default linear setting, calculates solution not only at the nodes of each triangle element but also at one point at each side of it.

As can be seen in some of the simulation data, the mesh (generation of discrete elements) that was used was quite coarse. The simulation software solves the physical equations for each element and therefore a finer mesh will generate a solution with higher resolution. When using a coarse mesh (element size 50,2-167 μm), it is therefore important to exclude that a finer mesh would generate a systematically different solution than the one obtained with the coarse mesh size. Simulations with finer mesh size (element size 2,5-38,5 μm) were performed and solutions for concentration gradient formation and velocity profile were compared. The model with the finer mesh size generated similar solutions as for the coarse mesh size, thus a so called mesh independency was achieved. With the purpose to decrease the solution time simulations with the coarse mesh were subsequently performed.

The production of the master for the microfluidic device met some problems. The height of the microfluidic design was 200 μm and to be able to produce a layer with that height, a less viscous SU-8 was used compared to what is normally used in the production process. As the capillaries were lower than the rest of the channels, the coating and developing was made in two steps. Due to the low viscosity of the SU-8, many bubbles were formed at the coating procedure with difficulties to degas. This was mainly a problem for the second layer as bubbles were trapped in the underlying structure. A next step to improve the procedure will be to only develop the sample when both layers are created, this to avoid bubble trapping structures. Cracking of the wafer when cooling down after the hard bake was another problem encountered, which was solved by a slower cooling down procedure.

The production of the PDMS microfluidic chip onto a glass slide was performed without major problems where one layer of PDMS was molded over the master. Attaching tubes for inlets and outlets demanded a PDMS layer that was thick enough to keep them in place. The one layer PDMS production generated a layer that was not thick enough for this purpose. Therefore, another layer of PDMS was bonded on top of inlets and outlets see fig. 47, a solution that gave better stability and held the tubing in place. One drawback with this design was observed later in the process when the thicker layer would not allow the objective to come close enough to the channel for cell imaging, and the 2nd PDMS layer had to be cut away. The production procedure needs to be improved further in order to both provide a chip stable enough for tube attachment and at the same time allow for microscopy studies. One solution could be to keep the 2nd layer of PDMS and image the samples from beneath instead by using inverted microscope (which was done) Another solution could be to develop a stand that keeps the tubes fixed and stable at one position.

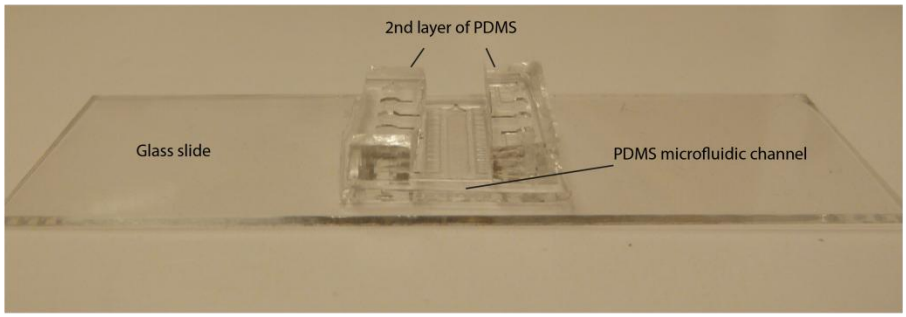

Figure 47. Glass slide with microfluidic PDMS channel. Two 2nd, thicker, PDMS layers are placed on top of the first PDMS layer to stabilize and support tubings attached to inlets and outlets.

Problems were encountered when the PDMS microfluidic chip should be combined with the Au nanopatterned surface. The surfaces were very thin and brittle and when the tubing was connected to inlets and outlets, they tore the sample in different directions leading to disruption of the surface. A production procedure were the surfaces are glued onto a more robust glass slide would be a solution to the problem in future applications.

It has to be noted that the concentration gradient formation is very easily disturbed by for example tube-movements and air bubbles, why these parameters are important to consider during experiments. Air bubble formation inside the microfluidic channels, as shown in fig. 48, has been a major issue in microfluidics for a long time and many suggestions and attempts have been done to get rid of the air bubble problem, as built-in bubble trappers, hydrophobic pores or hydrophilic coating of the microchannels (27). The PDMS is hydrophobic in its natural state and the PDMS walls inside the channels provide a surface where smaller bubbles can gather and form large bubbles. The bubbles can easily grow so large that they block the flow in a whole channel, see fig. 46 as an illustrative example. As the generated concentration gradient in the microfluidic design depends on flow in many channels it is very important that all of them are functioning. If an air bubble forms at one side of the source channel for example, there will not be any flow of the chemoattractant on that side, leading to a non-uniform concentration gradient inside the cell culture chamber. Or even worse; if the bubbles form inside the cell culture chamber they will cause cell death. Several improvements were made in this study to avoid bubble formation. Directly after activation and bonding of the PDMS onto the glass slide the PDMS is hydrophilic. This is due to the Si-OH groups that are formed onto the surface upon O_2 plasma activation. To keep the PDMS in a hydrophilic state, the channels were filled with water and stored in 4°C until use. If the channels had not been kept in water, one solution was to, prior to an experiment, flush the channel with ethanol. The ethanol filled the channels and made it easier to then switch the flow and fill the channels with the wanted solution. Another attempt was to first place the liquid to be used in the microfluidic channel in a sonicater with vacuum applied over to degas it, but the method did not seem to decrease the amount of bubbles formed inside the microfluidic chip. It was observed that more bubbles formed when a microfluidic chip had been used several times compared to if it came fresh from being stored in water. Fewer bubbles were also formed when the microfluidic chip was placed inside a cell culture incubator with water saturated atmosphere. The humidity of the surrounding environment could probably affect the diffusion of air and evaporation of water through the PDMS and thereby affect the amount of bubbles formed. Water evaporation from the channels probably leads to bubble formation since liquid is removed from the channel but not replaced fast enough. A more humid environment could generate lower water evaporation out from the PDMS and this is probably

what has happened in the incubator. A higher pressure in the outlet might also decrease the bubble formation as there would be less easy for bubbles to form if the pressure was higher. In future applications microfluidic PDMS channels should therefore be kept in as humid environments as possible for avoiding bubble formation.

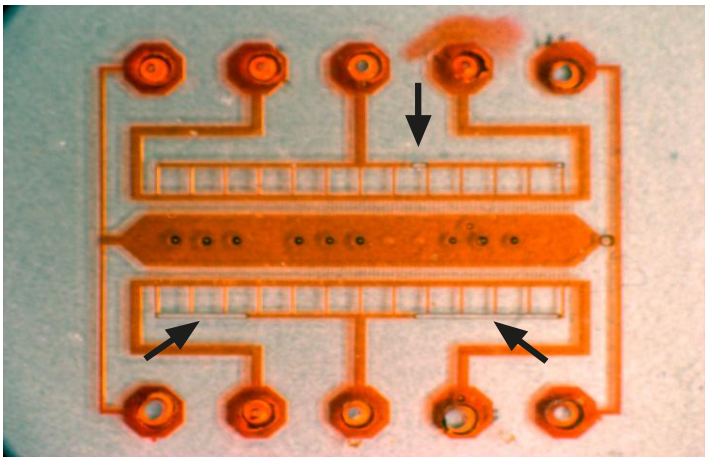

Figure 48. Air bubbles, marked with arrows, easily form inside the microfluidic PDMS channels. Air bubbles disturb the flow which in turn will disrupt the concentration gradient formation or lead to cell death.

To evaluate the microfluidic design gradient formation experiments were conducted by introducing a color dye into the source channel. The resulting gradient was compared to simulation data based on the diffusion coefficient for the color dye. The generated gradient formation had a steeper gradient formation in the middle of the cell culture chamber than simulation performed with diffusion coefficient for VEGF. This result is due to different diffusion coefficients and thereby different diffusion behavior between the molecules. The generated concentration gradient is clearly S-shaped. This behavior could also be seen in the experimental data, though the S-shape was not as distinct as in the simulation data. In experimentally analysis the absorbance of each molecule is spread out according to the point spread function, and the blur in the image results in a smeared intensity of the absorbing molecules, while simulations give the exact position of each molecule. This could be a reason for a more smeared and thereby more smooth gradient formation measured from the experimental data than the simulation data. Despite a small variance between simulation and experimental data, good correspondence was demonstrated as the analyzed gradients showed similar characteristics in behavior and the linear regression lines showed a similar steepness. Even though simulations can give a good idea about the experimental outcome, they do not include all physics. For example, the model did not include the property of diffusion through the PMDS. It might also be the case that the channel is not exactly 200 µm high but instead 250 or 300 µm, which would generate a different concentration gradient and the fact that the simulation and experimental data differ slightly is expected. As the color dye did not have the same diffusion coefficient as the chemoattractant VEGF, a gradient formation experiment was done with FITC-Dextran as well. The fluorescent labeled FITC-Dextran had a molecular weight similar to the one of VEGF. Imaging was done with 10x magnification which covered approximately one third of the length of the cell culture chamber. FITC photo-bleaches very fast and for each imaging event some fluorescence is lost. Due to that and uneven illumination, the intensity in the images could not be compared and stitching was not possible. Therefore only images from the middle of the channel were analyzed. The images show an uneven illumination as they have stronger intensity in the right corner

compared to the left, but should still generate sufficient data for gradient analysis. Plot of the line profiles showed that the gradient was linear over a 6 mm wide area in the cell culture chamber. FITC was used to experimentally measure the time it took to clear the cell culture chamber after it was filled with a high concentration. As the flow rate was much higher (1 µl/s) compared to simulation data, it is not surprising that the channel was cleared after a much shorter time, only 16 minutes, compared to almost 3 hours for a flow rate of 4 nl/s. Between each imaging event, the lamp was turned off, but there is still a small risk that the solution was photo-bleached during imaging leading to lower intensity measured for each image.

4.2. Surface modifications

Using PLL-PEG for surface passivation is simple and easy to use. Other approaches were investigated where PEG molecules could be covalently attached onto a glass surface. One possibility is to use the "PFPA" (perfluoro-phenyl Azide) where a promoter is bound to the surface and then activated by UV-light. The activation opens up the phenyl-rings on the now surface-bound molecule, creating a binding place for carbon atoms. Thus, they can be further bound to for example PEG molecules. This procedure would demand that the Au nanoparticles are covered by a thiol group, or something similar, to avoid binding of the PFPA onto them. The problem is that a cRGD-thiol molecule would probably not stand the UV treatment. Therefore, it would be necessary to have one protecting thiol group bound to the Au first, apply the PFPA and passivate the surface with PEG, before removing the protecting thiol from the Au with UV-Ozone exposure and bind the cRGD peptide via its thiol linker. This procedure would be difficult to perform inside the microfluidic chamber as it would demand having UV-ozone inside the microfluidic chip. It would also acquire having all the chemicals inside the microfluidic chip which could be difficult. The procedure demands extensively rinsing which can be difficult to obtain at the surface of the microfluidic channels as there are so called "dead zones", meaning zones with no flow, at the surface during laminar flow conditions. (Discussion with Laurent Feuz, SuSoS)

Due to the difficult procedure and limited experience in the area, covalently binding of PEG to a glass surface was not tested experimentally and instead the copolymer PLL-PEG was used for surface passivation of the glass surfaces. The PLL main chain is positively charged at neutral pH and binds electrostatically to the activated, negatively charged glass surface by Coulomb forces. The main chain is grafted with PEG side chains which forms an inert hydrated layer that shields proteins from the glass surface (23). At the starting point of this project, there was an uncertainty about whether electrostatic binding of PLL-PEG onto a glass surface would result in a sufficient passivation of the surface that is stable over the whole time span of cell experiments (at least 24h). Cell culture experiments were therefore performed to investigate if PLL-PEG provided sufficient surface passivation. In this project, a glass surface was first activated after which it was functionalized with a cRGD-thiol molecule. The functionalization procedure exposed the surface to a water-cRGD-solution for 2 days. As the binding of PLL-PEG onto the glass surface relied on electrostatically binding between a negatively charged glass surface and positively charged PLL main chains, the glass surface still had to be negative after the functionalization procedure with cRGD-thiol. It was questioned if the glass surface could be negatively charged after 2 days of water exposure. It must be noted that it was important to functionalize the Au nanoparticles before PLL-PEG was introduced, as PLL-PEG would have bonded onto the nanoparticles as well otherwise, and thereby blocked further modifications of these. Data from QCM-D measurements showed that PLL-PEG molecules were adsorbed onto all the examined surfaces and not washed away from them. No significant difference in the PLL-PEG

adsorption was observed between surfaces that had been exposed to water or water-cRGD-thiol solution for 2 days compared to freshly activated surfaces. QCD-M experiments further showed that no proteins were irreversibly adsorbed onto any of the PLL-PEG modified surfaces as the frequency shifted back to same value as is had before cell media was introduced. The QCM-D results hence demonstrate that PLL-PEG serves as a functional passivation method for protein adsorption. At the cRGD functionalized Au nanopatterned surface molecule desorption was observed as the frequency increased at all times. One explanation could be that the cRGD functionalized Au nanoparticles served as a platform for low adsorption forces but at rinsing with PBS the PLL-PEG molecules or proteins that had adsorbed were desorbed from the cRGD-Au nanoparticles. All the samples were normalized with respect to their frequency shifts and even though it could be argued that the drift in frequency in fig. 37d) could be due to a non-normalized shift, it should not be the case.

Statistical data from cell seeding experiments onto PLL-PEG modified and fresh glass surfaces indicate, in agreement with the QCM-D results, that PLL-PEG modification led to passivation of the surfaces, as a significant lower amount of cells were attached onto the PLL-PEG modified surfaces.

To be able to attach a cRGD peptide onto the Au nanoparticles, the peptide was coupled to a thiol group. The bonding of the molecule to the Au nanoparticles was produced when the S-H bond of the thiol group was broken and the sulfur atom bonded covalently to the Au atoms. It is important to notice that thiol groups can form covalent bonds with each other by breaking the S-H bonds and form covalent disulfide bonds instead. This can lead to problems if the molecules bind to each other in the thiol solution instead of to the Au nanoparticles. A way to get around this problem could be to use a linker molecule that can be activated in situ, thereby avoiding intermolecular interactions in solution prior to experiments.

Cell seeding experiments demonstrated a significant lower cell attachment on PLL-PEG passivated cRGD functionalized Au nanopatterned surfaces, something that was not seen in experiments without the PLL-PEG passivation. Cell integrin receptors have probably not been able to bind to the cRGD peptide, meaning that the peptide was not accessible to the cells. For the cRGD to be accessible it is not enough to just tangent the top layer of the PLL-PEG film, but it has to stick up long enough for the cell integrins to bind to it and form focal adhesions, see fig. 46 for an illustration of the mechanism. The height of a hydrated PLL-PEG layer is approximately 5 nm (28). The height of an Au nanoparticle is <5 nm and the length of the spacer on the cRGD-thiol molecule is approximately 2 nm. This means that if the spacer with the cRGD peptide does not stick straight up from the top of the Au nanoparticle, or if the cRGD-thiol molecule has bound onto the side of the particle, the peptide might not reach over the PLL-PEG layer. This would sterically hinder the cell integrins from binding to the cRGD peptide and the surface would thereby be passivated in spite of the presence cRGD peptide as illustrated in fig. 49. Blümmel *et al.* (2007) concluded that, for the purpose of passivating a surface in between 5 nm high Au nanoparticles, the optimal size of PEG molecules is 2kDa. The suggestion correlates with the size used for PEG in this project, and what needs to be considered is the length of the spacer on the cRGD-thiol molecule. A suggestion for future application is to use a molecule containing a longer spacer of approximately 15 PEG molecules, instead of 3 that was used in this project. The longer molecule would then allow cell accessibility of the cRGD peptide without it being sterically hindered by the PLL-PEG layer.

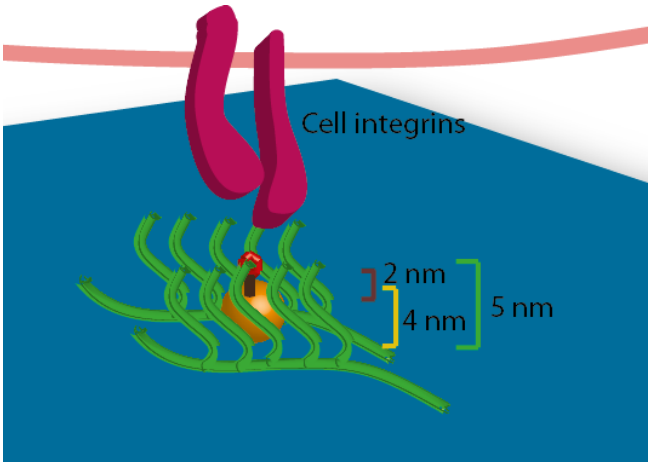

Figure 49. cRGD (red) attachment peptide attached to an Au nanoparticle (gold) with a spacer (brown) in between. The Au nanoparticle is approximately 4 nm and the spacer 2 nm. The cRGD might be covered by the PLL-PEG (green) layer, making the peptide inaccessible to the cell integrins (pink).

HUVECs seeded onto fresh or cRGD functionalized Au nanopatterned surfaces without PLL-PEG passivation showed good attachment and viability and were able to spread on the surfaces. Therefore, it does not appear a problem associated to the Au nanopatterned surfaces of the cRGD functionalization, which is an important result to keep in mind for future optimization.

As pointed out by Hersel *et al*. (2003) many attempts have been made to detect microdistributed RGD peptides on surfaces, but no one has yet solved the problem. Approaches have amongst other been to use X-ray photoelectron spectroscopy (XPS) to detect nitrogen as an indicator of RGD peptides, or incorporate a tag, e.g. fluorine, in the RGD peptide for detection and quantification with XPS (29). Lin *et al*. (1994) used a method where they hydrolyzed the sample and detected the free amino acids in the hydrolysate by a standard amino acid analyzer. (30)They also measured the contact angle at the RGD functionalized surface to prove the presence of the RGD peptides, as a surface with zwitterionic RGD peptide attached to it is more hydrophilic than non-functionalized surfaces (30). As the surfaces in this project were functionalized inside a microfluidic chamber the first three mentioned approaches were not possible to use. Confirming RGD peptides with ELISA or cell attachment assays can give a semiquantitative result as more cells might attach to a surface with RGD peptides (31). For the purpose of this project, cell attachment assays onto cRGD functionalized substrates would not yield any information of cRGD as cells showed attachment and spreading onto glass surfaces as well as on non-modified Au nanopatterned surfaces. PLL-PEG modification on Au nanopatterned surfaces, on the other hand, led to surface passivation. Successful incorporation of a cRGD peptide with the right spacer dimension could therefore be proven from a cell attachment assay. Further staining of vinculin, a protein present in focal adhesion complexes, would give information about focal adhesion formations between cell integrins and cRGD peptides. A future solution of the problem could also be to incorporate a small fluorescent molecule at the cRGD-thiol molecule by using a branched PEG chain at the thiol-PEG-cRGD molecule. The fluorophore could easily be detected in fluorescence microscopy trough the PDMS microchannel. But as the cRGD-PEG-thiol molecule is a complex compound to fabricate, this approach could reach problems.

4.3. HUVEC culture

Cell seeding experiments with HUVECs inside the microfluidic cell culture chamber demonstrated good viability of the cells and the ability for them to attach and spread at the bottom of the channel. As the seeding was done under static conditions (no media flow was applied) it can be concluded that the volume of the cell culture channel provided sufficient cell media for the HUVECs over a five day cell culture. The fact that cells survived on the media volume for 5 days means that the volume can be sufficient for cell cultures at higher concentrations for 24 h studies in the future.

HUVEC culture inside the microfluidic cell culture chamber combined with cRGD functionalized Au nanopatterned surfaces demonstrated attachment and spreading. The microfluidic channel together with the functionalized surface provides an environment supporting cell viability. The experiment did not include PLL-PEG modification of the surface as precedent experiments showed complete passivation of the surface, and hence no cell attachment results would have been able to obtain. Though, for future applications, it is important to show cell viability onto combined PLL-PEG and cRGD modified Au nanopatterned surfaces inside the cell culture chamber.

The introduction of cells into the microfluidic chamber was done through one cell culture chamber inlet (see appendix A). In the beginning of this project, an idea was to have the cells seeded at one of the long sides in the cell culture chamber. This was never done experimentally during the project, but by using two syringes and inject cells from one of them and cell free media with the other it might be possible to achieve a result like that. Having the cells on one side would be interesting for future migration studies as migration then could be studied as a bulk concentration of cells moving from one side of the cell culture chamber to the other.

Morphology studies of HUVECs cultured on glass surfaces and non-modified and functionalized Au nanopatterned surfaces shows that the cells behave very similar on the different surfaces. There is a tendency to more spreading and intercellular connections on the cRGD modified surfaces, which is an expected result as the attachment peptides should offer anchoring points for the cells.

4.4. Future work and challenges

With the goal to study cell migration as a function of attachment peptide spacing, which was the overall aim with the developed microfluidic platform, there are some important experiments that need to be performed prior to the “final” experiment. The combination of surface functionalization and passivation of the Au nanopatterned substrates has to provide sufficient cell attachment. Using a cRGD-thiol with a 15 molecule long PEG-spacer will hopefully result in cRGD accessibility to cell integrins where the cRGD attachment peptides can reach over the PLL-PEG passivation layer. To validate a new cRGD peptide, cell culturing should be done onto petri dishes as a first step. If cell attachment is confirmed onto the combined functionalized and passivated surfaces, cell culturing experiments inside the cell culture chamber should be performed. This experiment would verify that the system still provides an environment that promotes cell attachment. If the new cRGD peptide does not provide any cell attachment in combination with the passivation method, a new surface modification protocol might be necessary. For example, passivation can be performed by covalently bind PEG molecules to the glass surface using a silanization method (21). The drawback with this method is that the silanization can be difficult to control. As silanes would also react with Au nanoparticles, the

particles first have to be functionalized with the cRGD if the method would be used. To verify focal adhesion formation at the cell-surface interface, staining of vinculin could be used. Vinculin is present in the cytosol and present at a high concentration in the focal adhesion complex formed intracellular. For imaging of vinculin-stained focal adhesions, total internal reflection fluorescence (TIRF) would be suitable. In the technique the object is imaged from below and only focuses at points very close to surface. As focal adhesion are formed close to the surface it means that they would be imaged while at the same time the noise from the free vinculin in the cytosol would not be imaged.

To verify gradient formation inside the microfluidic cell culture chamber, new experiments with FITC-Dextran should be performed. The fast photo-bleaching of FITC makes it difficult to take several images in a row and still maintain the same intensity of the FITC fluorescence. An objective that makes it possible to image the whole length of the channel would therefore be appropriate to use. The magnification of this objective would have to be approximately 2,5x, which would be sufficient for studying the gradient formation.

In a study made by Hischfeld-Warneken *et al.* (2008) cell migration of Mc3t3 osteoblasts was observed in the direction of a cRGD gradient (21), when the gradient had a steepness of at least 15 nm change of spacing per 1 mm steep. This process where cells migrate as a function of an adhesive molecular cue is called haptotaxis. The Au nanopatterned surfaces used in this project has a gradient steepness of approximately 5 nm change in spacing per 1 mm, and even though the gradient is not as steep as 15 nm/mm haptotaxis should not be excluded. Future cell seeding experiments should therefore be performed to investigate the event of cell migration along the cRGD gradient.

Cell culture experiments inside the cell culture chamber showed cell viability under static conditions. Next step will be to seed cells inside the microfluidic chip under flow conditions. First this should be done with cell media introduced though the source and sink channels. After confirming cell viability, initial cell migration experiments should be performed. To supply the cells with a surface to migrate on, the bottom of the cell culture chamber could be coated with collagen, an ECM molecule commonly used for endothelial cell cultures (3). After cell seeding and imaging of the initial cell state, a VEGF gradient would be applied by introducing cell media with additional VEGF in through the source channel (to the sink channel only cell media should be introduced). After 24 h, imaging would be done again and cell migration investigated by comparing of number cells in different zones of the cell culture chamber at times t=0 and t=24 h. This experiment would also tell if 24 h is an appropriate time interval for cell migration studies. If not, the time interval might have to be changed to either shorter or longer culturing time.

Only after these experiments have been performed successfully, the final experiment with the combined microfluidic channel, the VEGF gradient and the functionalized and passivated Au nanopatterned surface could be used to study the effect of attachment peptide spacing in directed cell migration.

5. Conclusion

From an initial design, a new model was created in which a concentration gradient was generated over a 6 mm wide and 2 mm long area in a microfluidic cell culture chamber, making it possible to study cell migration in uniform conditions over a 6 mm wide area. The model was hence compatible with the 6 mm wide functionalized Au nanopatterned surfaces and could be used to study attachment peptide spacing effect on endothelial cell migration. Further, the model had a concentration gradient ranging over almost 90 % over the length of the cell culture chamber. This fulfilled the goals that were set up at the start point of the design procedure. The model contained a cell culture chamber in which no shear stress was applied, excluding shear stress induced cell migration. The chamber also provided an environment where cells could be cultured for at least five days. From experimental results it was concluded that simulation data gives a good idea of the experimental results and that it is reliant.

To be able to precisely control attachment peptide spacing, Au nanopatterned surfaces were biofunctionalized with a cRGD-thiol molecule. Cell showed viability onto both non-modified and functionalized surfaces. Protein and cell passivation was achieved by PLL-PEG modification, evaluated by QCM-D measurements and cell adhesion assay. The combination of these two modifications needs a modified cRGD molecule in order to provide a specific cell attachment surface.

In conclusion, a microfluidic platform has been developed in which the effect of cell attachment peptide spacing on directed cell migration can be studied.

6. References

1. Carlson, B.M. *Principles of regenerative biology.* Michigan : Academic Press, 2007.

2. Blitterswijk, van. *Tissue Engineering.* 1st ed. : Academic Press, 2008.

3. Shamloo, A., Ma, N., Poo, M., Sohn, L.L., Heilshorn, S.C. *Endothelial cell polarization and chemotaxis in a microfluidic device.* Lab on a chip, 2008; 8: 1292-1299.

4. Hersel. U., Dahmen, C., Kessler, H. *RGD modified polymers: biomaterials for stimulated cell adhesion and beyond.* Biomaterials, 2003; 24: 4385-4415.

5. Gerhardt, H., Golding, M., Fruttiger, M., Ruhrberg, C., Lundkvist, A., Abramsson, A., Jeltsch, M., Mitchell, C., Alitalo, K., Shima, D., Betsholtz, C. *VEGF guides angiogenic sprouting utilizing endothelial tip cell filopodia.* Journal of Cell Biology, 2003; 161: 1163-1177.

6. Shamloo, A., Heilshorn, S.C. *Matrix density mediates polarization and lumen formation of endothelial sprouts in VEGF gradients.* Lab on a Chip, 2010; 10: 3061-3068.

7. Ngalim, S.H., agenau, A., Le Saux, G., Gooding, J.J., Gaus, K. *How do cells make decisions: Engineering micro- and nanoenvironments for cell migration.* Journal of Oncology, 2010, Article ID 363106, 7 pages.

8. Byzova, T.V., Goldman, C.K., Pampori, N., Thomas, K.A., Bett, A., Shattil, A.J., Plow, E.F. *A mechanism for modulation of cellular responses to VEGF: Acitvation of the integrins.* Molecular Cell, 2000; 6: 851-860.

9. Maheshwari, G., Brown, G., Lauffenburger, D.A., Wells, A., Griffith, L.G. *Cell adhesion and motility depend on nanoscale RGD clustering.* Journal of Cell Science, 2000; 113: 1677-1686.

10. Baranska, P., Jerczynska, H., Pawlowska, Z., Koziolkiewicz, W., Cierniewski, C.S. *Expression of integrins and adhesive properties of human endothelial cell line EA.hy 926.* Cancer Genomics & Proteomics, 2005; 2: 265-270.

11. Whitesides, G.M. *The origins and the future of microfluidics.* Nature, 2006; 442: 368-373.

12. Velve-Casquillas, G., Le Berre, M., Piel, M., Tran, P.T. *Microfluidic tools for cell biological resaerch.* Nano Today, 2010; 5: 28-47.

13. Welty, J.R., Wicks, C.E., Wilson, R.E., Rorrer, G. *Fundamentals of Momentum, Heat, and Mass Transfer.* 4th Ed. Oregon : John Wiley & Sons, Inc., 2001.

14. White, F.M. *Viscous Fluid Flow.* [ed.] 2nd Ed. Rhode Island : McGraw-Hill, 1991.

15. Hsu, S., Thakar, R., Liepmann, D., Li, S. *Effects of shear stress on endothelial cell haptotaxis on micropatterned surfaces.* Biochem. Biophys. Res. Commun., 2005; 337: 401-409.

16. Gross, P.G., Kartalov, E.P., Scherer, A., Weiner, L.P. *Applications of microlfuidics for neuronal studies.* Journal of the Neurological Sciences, 2007; 252: 135-143.

17. Mac Gabhann, F., Popel, A.S. *Differential binding of VEGF isoforms to VEGF receptor 2 in the presence of neuropilin-1: a computational model.* Am. J. Physiol. Heart Circ. Physiol., 2005; 288: H2851-H2860.

18. Zimmerman, W.B.J. *Multiphysics Modelling with Finite Element Methods.* [ed.] Ardéshir Guran. University of Sheffield : World Scientific, 2006.

19. Arnold, M., Cavalcanti-Adam, E.A., Glass, R., Blümmel, J., Eck, W., Kantlehner, M., Kessler, H., Spatz, J. *Activation of Integrin Function by Nanopatterned Adhesive Interfaces.* ChemPhysChem, 2004; 5: 383-388.

20. Cavalcanti-Adam, E.A., Micoulet, A., Blümmel, J., Auernheimer, J., Kessler, H., Spatz, J. *Lateral spacing of integrin ligands influences cell spreading and focal adhesion assembly.* European Journal of Cell Biology, 2006; 85: 219-224.

21. Hirschfeld-Warneken, V.C., Arnold, M., Cavalcanti-Adam, A., López-García, M., Kessler, H., Spatz, J.P. *Cell adhesion and polarisation on molecularly defined spacing gradient surfaces of cyclic RGDfK peptide patches.* European Journal of Cell Biology, 2008; 87: 743-750.

22. Glass, R., Arnold, M., Cavalcanti-Adam, E.A., Blümmel, J., Haferkemper, C., Dodd, C., Spatz, J.P. *Block copolymer micelle nanolithography on non-conductive substrates.* New Journal of Physics, 2004; 6: 101-119.

23. Feuz, L., Leermakers, F.A.M., Textor, M., Borisov, O. *Adsorption of Molecular Brushes with Polyelectrolyte Backbones onto Oppositely Charged Surfaces: A Self-Consistent Field Theory.* Langmuir, 2008; 24: 7232-7244.

24. Nimeri, G., Fredriksson, C., Elwing, H., Liu, L., Rodahl, M., Kasemo, B. *Neutrophil interaction with protein-coated surfaces studied by an extended quartz crystal microbalance technique.* Colloids and Surfaces B-Biointerfaces, 1998; 11(5): 255-264.

25. Lord, M.S., Modin, C., Foss, M., Duch, M., Simmons, A., Pedersen, F.S., Besenbacher, F., Milthorpe, B.K. *Extracellular matrix modelling during cell adhesion monitored by the quartz crystal microbalance.* Biomaterials, 2008; 29(17): 2581-2587.

26. Gouverneur, M., Spaan, J.A.E., Pannekoek, H., Fontijn, R.D., Vink, H. *Fluid shear sress stimulates incorporation of hyaluronan into endothelial cell glycocalyx.* Am J Physiol Heart Circ Physiol, 2006; 290: H458-H462.

27. Lochovsky, C., Yasotharan, S., Günther, A. *Bubbles no more: in-plane trapping and removal of bubbles in microfluidic devices* .Lab Chip, 2012; 12: 595-601.

28. Blümmel, J., Perschmann, N., Aydin, D., Drinjakovic, J., Surrey, T., Lopez-Garcia, M., Kessler, H., Spatz, J.P. *Protein repellent properties of covalently attached PEG coatings on nanostrustured SiO2-based interfaces.* Biomaterials, 2007; 28: 4739-4747.

29. Cook, A.D., Hrkach, J.S., Gao, N.N., Johnson, I.M., Pajvani, U.B., Cannizzaro, S.M., Langer, R. *Characterization and development of RGD-peptide-modified poly(lactic acid-co-lysine) as an interactive, resorbable biomaterial.* Journal of Biomedical Materials Research, 1998; 35(4): 513-523.

30. Lin, H.B., Sun, W., Mosher, D.F., García-Echeverría, C., Schaufelberger, K., Lelkes, P.I., Cooper, S.L. *Synthesis, surface, and cell-adhesion properties of polyurethanes containing covalently grafted RGD-peptides.* Journal of Biomedical Materials Research, 1994; 28(3): 329-342.

31. Kantlehner, M., Schaffner, P., Finsinger, D. Dr., Jonczyk, A. Dr., Diefenbach, B., Nies, B. Dr., Hözlemann, G. Dr., Goodman, S.L. Dr., Kessler, H. Prof. Dr. *Surface coating with cyclic RGD peptides stimulates osteoblast adhesion and proliferation as well as bone formation.* ChemBioChem, 2000; 1(2): 107-114.

Appendix A – Microfluidic chip design

CAD drawing with complete inlets and outlets. The dimensions of the different channels are marked in the drawing.

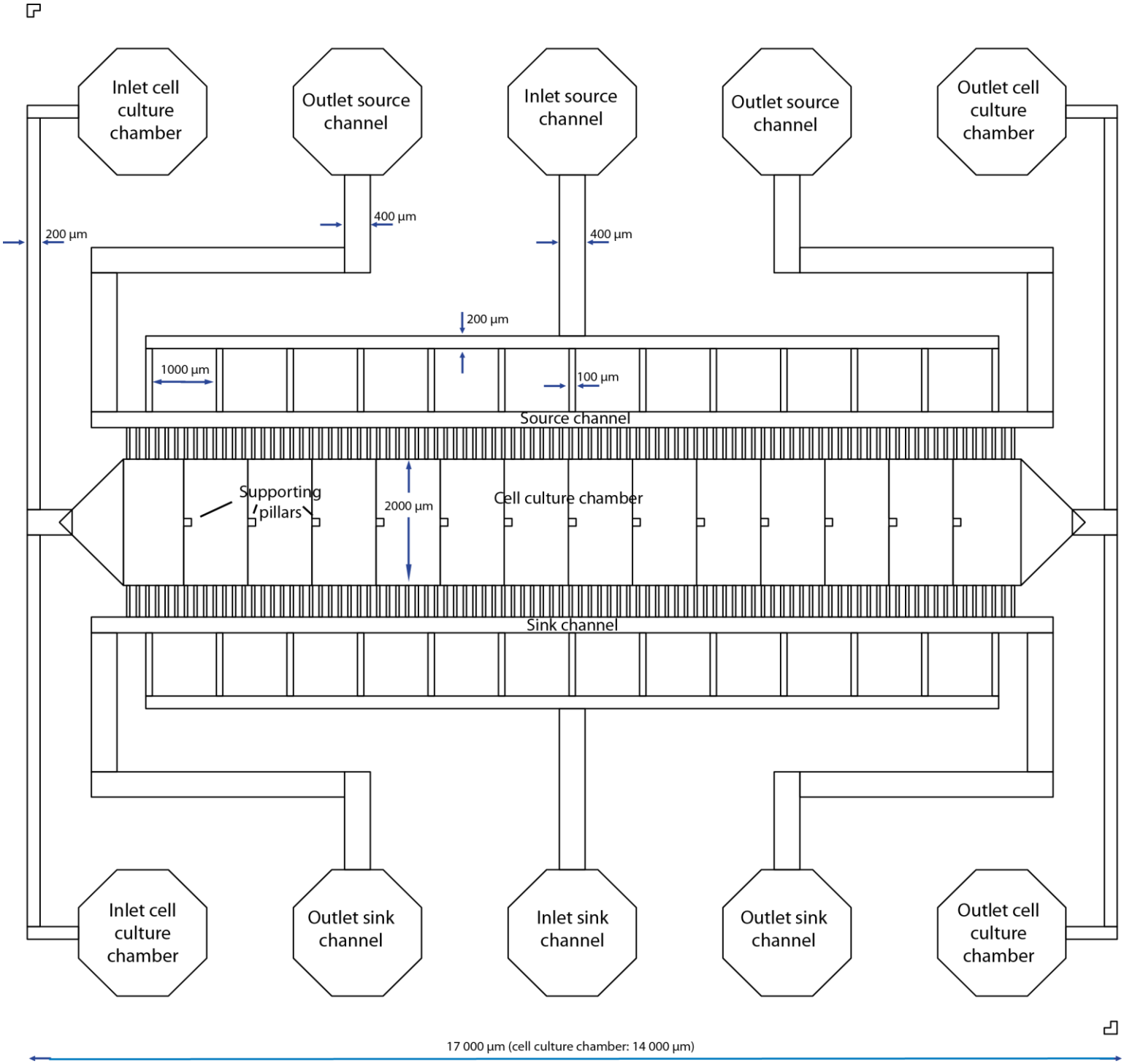

Appendix B – Poster

The Poster was presented at Lab-on-a-chip Workshop: Reaching new horizons with nanotechnology, Nanoconnect Scandinavia, February 2, 2012 and Science and Technology day 2012 at the Department of Chemical and Biological engineering, Chalmers University of Technology and Department of Chemistry and Molecular Biology, Gothenburg University, March 23-30.

A Microfluidic Platform for Cell Migration Studies

Elin Bernson, Patric Wallin, Francesco Mazzotta, Julie Gold

Division of Biological Physics, Chalmers University of technology, Sweden

bernson@student.chalmers.se

wallinp@chalmers.se

Cell microenvironment

Cell migration is a cellular fate process essential for embryogenesis, tissue regeneration and wound healing. *In vivo* cell migration is promoted by soluble chemotractant concentration gradients which are sensed by the cells and stimulate cell movement, a process called chemotaxis. Migration is also controlled by cell surface interactions where focal adhesions are formed between cell integrins and RGD attachment peptides in the extra cellular matrix. The ability to study these processes *in vitro* brings new possibilities in controlling and directing cell cultures in areas as tissue engineering. The experimental system that was developed in this study makes it possible to precisely control both the surface spacing of attachment peptides and the chemical environment around cells, and to simultaneously study their effect on cell migration.

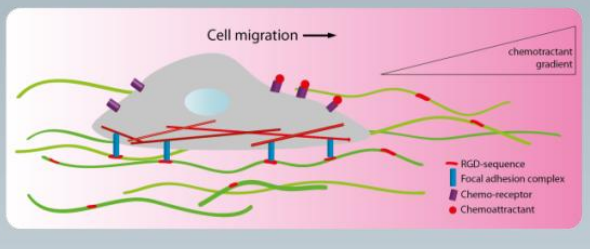

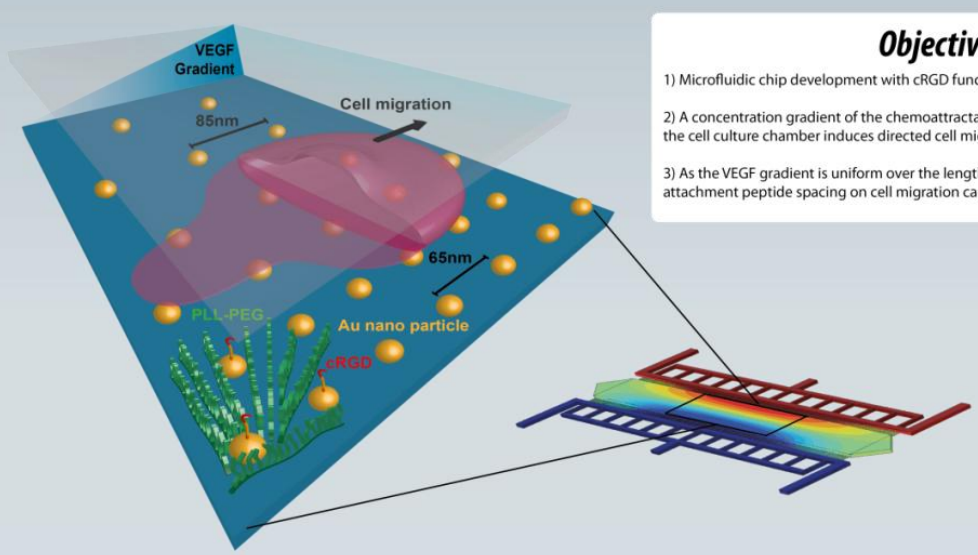

Objective

1) Microfluidic chip development with cRGD functionalized surfaces

2) A concentration gradient of the chemoattractant VEGF applied over HUEVCs in the cell culture chamber induces directed cell migration

3) As the VEGF gradient is uniform over the length of the chamber, the effect of attachment peptide spacing on cell migration can be studied

Microfluidic generated chemotractant gradient*

1) Gradient formation inside a cell culture chamber (2x14 mm) was studied by COMSOL Multiphysics simulations to optimize the microfluidic chip design and test different design and flow parameters

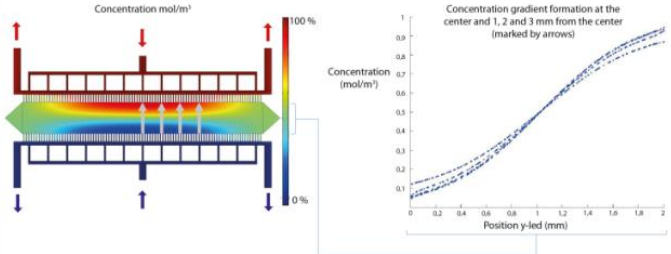

2) Gradient formation was also studied experimentally with a color dye. Images were taken and gradient formation was evaluated by measuring intensity values of line profile plots at the same positions in the channel as for the simulation

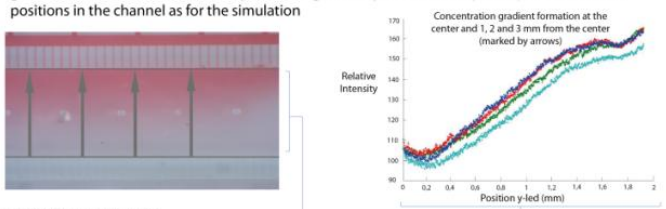

* E. Shamloo *et al.* Lab on a Cip, 2008

cRGD functionalized Au nano-patterned surface gradients*

1) Au nano dots placed with increasing spacing (65-90 nm) in a gradient manner

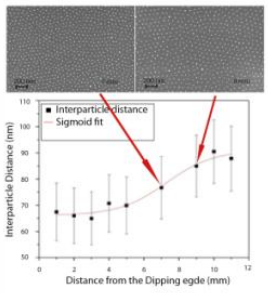

2) Surfaces were functionalized with cyclic RGD to promote cell attachment and focal adhesion formation

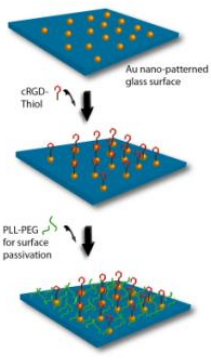

3) Endothelial cells that were seeded onto the functionalized surfaces attached and spread. Furthermore good viability of the cells could be observed

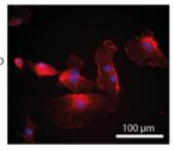

HUVECs on a cRGD functionilized Au nanopatterned surface stained with DAPI (blue) and Phalloidin (red), (24 hr).

*V. Hirschfeld-Warneken, J. Spatz, Max Planck Institute for Metal Research, Stuttgart, Germany.
E. Cavalcanti-Adam *et al.* European Journal of Cell Biology, 2006.

Acknowledgements

The research leading to these results has received funding from the European Union Seveth Framework Program (FP7/2007-2013) under grant agreement n° NMP3-SL-2009-229294 NanoCARD, from Vinnova contract n° :2009-00227 "Scaffolding nanomaterials for stem cell proliferation, migration and neural differentiation".